PROFILE ANALYSIS OF X-RAY POWDER DIFFRACTION DATA

by

Vishnu Visvanathan Naicker

Submitted in partial fulfilment of the requirements for the Degree of Master of Science in the Department of Physics in the Faculty of Science at the University of Durban-Westville

Supervisor : Professor D W Engel

Date submitted: December 1988

To my parents, Grace and Krish Naicker

ACKNOWLEDGEMENTS

I would like to thank the following people for their assistance:

Professor D W Engel, Department of Physics, University of Durban-Westville, under whose direction this research was done, for his keen interest, encouragement and guidance throughout this project.

Ms V Naidoo, Computer Services Division, University of Durban-Westville, for her help with the computational problems on the Mainframe.

Mr H Edwards and Mr D Johnstone, Department of Physics, University of Durban-Westville for their help with the computing and plotting routines.

Professor R Bharuthram, Department of Physics, University of Durban-Westville, for his help with numerical problems.

The University of Durban-Westville for the use of the library and computer facilities.

All my colleagues in the Department of Physics, University of Durban-Westville, for their assistance and concern.

My parents for their constant support and encouragement.

SUMMARY

Various strategies have been tested for obtaining integrated intensities from x-ray powder diffractometer data. An asymmetric pseudo-Voigt profile function was used to fit the pattern in the region above $2\Theta = 35°$ (Cu-Kα radiation). At lower angles where the asymmetry was strongest and the profile function not suitable the peaks were integrated numerically. A smooth background function was estimated from the regions of minimum intensity of the pattern. The profile parameters were initially refined in small ranges of about 10° 2Θ in order to determine their 2Θ-dependence. Thereafter final refinements of peak intensities were undertaken using the profile parameters thus determined.

Analysis of data from the mineral Fe-akermanite, $Ca_2Mg_{0.4}Fe_{0.6}Si_2O_7$, generated 173 integrated intensities with $I > 2\sigma(I)$ out of 187 positions separated in 2Θ by more than 0,02°. Of the total of 213 reflections in the range, those overlapping exactly or separated by < 0,02° were treated as single peaks. The structure was refined using an overall isotropic temperature parameter and a parameter to compensate for preferred orientation, giving an unweighted residual of 10,4% for 14 parameters.

CONTENTS

Chapter 1 INTRODUCTION

The atomic structure of crystalline materials can be studied by analysing the diffraction pattern produced by some radiation such as x-rays, neutrons or electrons. This diffraction analysis can be done using a sample which is either a single crystal or a powder consisting of many small crystals of different orientations.

Single crystal diffraction is the more powerful technique because each reflection (off a crystal plane) can be measured individually from the others. In the powder diffraction pattern reflections overlap because of the random orientation of the powder grains. This leads to difficulty in the assignment of the intensities of individual reflections. Therefore, special attention has to be given to fitting the observed pattern with suitable profile functions.

Since in many applications materials are only available in powder form, x-ray powder diffraction techniques have to be exploited and optimised. Two main strategies in analysing powder diffraction patterns can be used, the two step strategy and the Rietveld strategy.

In the two step strategy, the lattice cell parameters are determined first. In analysing the diffraction pattern, the diffraction angles 2Θ for reflections are thus considered fixed, and a careful analysis and fitting of the diffraction pattern is conducted to obtain "integrated" intensities of the individual reflections. The second step is the refinement of the structural parameters to give the best agreement between the observed and calculated integrated intensities I_o and I_c.

In the Rietveld strategy, good starting values for the cell parameters, profile parameters and structural parameters are first obtained. Refinement of all these parameters in one step is conducted to get the best possible fit between Y_o and Y_c, the intensities at each 2Θ point in the pattern.

The two step procedure has two main problems. Firstly, the distribution of intensities in a cluster of overlapping reflections cannot be automatically revised during structure refinement if not done optimally in the profile fitting step. Secondly, if the profile fitting of the pattern is done in small ranges of the

spectrum, it would be difficult to automate.

In the Rietveld procedure, it is difficult to find an analytic profile function suitable for the entire 2θ range. Also, problems can arise with peaks shifts due to instrumental aberrations.

In this investigation the feasibility of the two-step strategy was studied for patterns with a large number of peaks. The main effort was concentrated on developing strategies for optimising the first step, namely, the determination of integrated intensities. A standard program was implemented to perform the second step, namely, the refinement of the structural parameters.

Chapter 2 THEORY OF CRYSTAL STRUCTURE AND CRYSTAL DIFFRACTION

The theory of crystal structure and crystal diffraction is discussed in various standard texts (eg Kittel, 1976) and a brief summary will be given here.

2.1 Crystal lattices and symmetry

A structure is called crystalline if it is based on a lattice. A 3-D lattice is a periodic arrangement of points based on 3 unit translations $\underline{a}$, $\underline{b}$ and $\underline{c}$. All lattice points are described by

$$\underline{r} = u\underline{a} + v\underline{b} + w\underline{c}$$

where u, v and w are integers.

In the crystal, each lattice point has an identical structural unit called the basis (Kittel, 1976, p4) composed of one or more atoms associated with it. Every lattice point therefore has an identical arrangement of atoms around it.

The vectors $\underline{a}$, $\underline{b}$ and $\underline{c}$ form a parallelepiped, called the unit cell of the lattice. The shape of the unit cell is defined completely by the magnitudes of these vectors and the angles α, β and γ between them. These six parameters are called the lattice parameters. A lattice can have various types of symmetries, eg, axial lengths may be equal or interaxial angles may have the special values 90° or 120° leading to the seven so called crystal systems.

If lattice points occur only at the corners of the unit cell, ie, there exists one lattice point per unit cell, such a cell is called a primitive cell. Non-primitive cells can also be chosen in a lattice. These have a larger volume than the primitive cell and extra lattice points at the face or body centres. Such centring is sometimes required in order that the unit cell may exhibit the symmetry that is inherent in the lattice. The various types of lattice symmetry and lattice centring lead to the 14 Bravais lattice types (see Kittel, 1976, p14 & 15).

An object has a certain symmetry if it appears unchanged when a certain transformation is performed on it. The transformation is

then called a symmetry operation. All lattices have translational symmetry (the 3 unit translations) and a centre of inversion (the operation [x, y, z] → [-x, -y, -z]). Lattices can further exhibit rotational symmetry (2- , 3- , 4- or 6-fold) and "rotation inversion" symmetry. When these symmetry elements (ie, those which a lattice can exhibit) are combined in different ways, 32 distinct combinations arise. These are the so called point groups. When these symmetries are extended by elements which combine translation with reflection or rotation and are applied to the 14 Bravais lattices, 230 combinations called space groups result for the symmetry of a crystal structure.

2.2 Lattice Planes

A family of lattice planes is a set of parallel planes such that any lattice point lies on some member of this family. (See Stout and Jensen, 1968, p19). These sets of planes are indentified by three indices, h, k and l corresponding to the axes a, b and c of the unit cell. From the periodic nature of the lattice, when any set of planes cuts an axis (say a) of the unit cell, the axis will be divided into n equal parts of length a/n where n is an integer. The index h for this particular axis will then be n. The plane can be similarly indexed along the b and c axes. Fig 2.1 shows some families of planes with their corresponding indices.

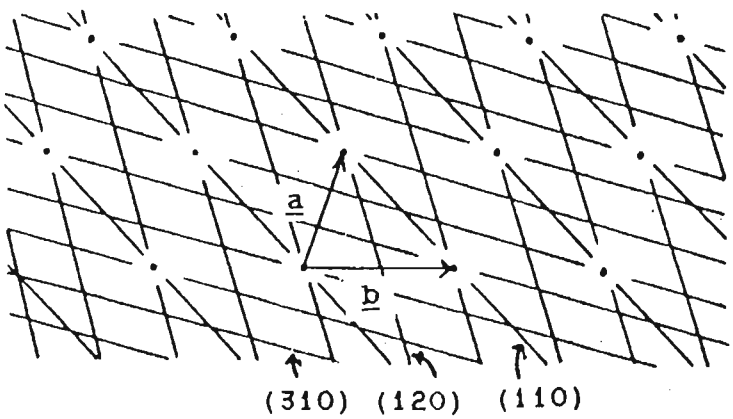

Fig 2.1 A representation of three sets of lattice planes. The planes are parallel to the c axis.

The perpendicular distance d between adjacent planes in a family of planes depends upon the unit cell parameters and the corresponding hkl-values. The d-values decrease with increasing values of the indices h, k and l. For example, the expression for the tetragonal system ($a = b$, $\alpha = \beta = \gamma = 90°$) is:

$$d = [(h^2+k^2)/a^2 + (l/c)^2]^{-\frac{1}{2}}$$

A full list of expressions for d for the various crystal systems is given by Klug and Alexander, 1974 (p37).

2.3 X-ray diffraction from lattices

For any two lattice points A_1 and A_2 the phase difference between two waves scattered by these points will be $\kappa \underline{r}.\underline{S}$ where $\kappa = 2\pi/\lambda$, $\underline{r}$ is the vector joining A_1 and A_2, and $\underline{S} = \underline{s} - \underline{s}_o$, $\underline{s}_o$ being the unit incident wave, and $\underline{s}$ the unit scattered wave. (See James, 1967, p1). $\underline{S}$ is normal to a plane which can be thought of as scattering $\underline{s}_o$ into $\underline{s}$ through an angle 2θ, ie, $\underline{s}_o$ and $\underline{s}$ are at an angle θ to the reflecting plane with normal $\underline{S}$.

Thus for a point Q a distance R from the lattice, the displacement of a wave scattered by a lattice point at a vector distance $\underline{r}$ from the origin is

$$Y = (\bar{Q}_o/R)\exp(i\omega t + i\kappa \underline{r}.\underline{S}) \qquad [2.1]$$

where $\underline{r} = u\underline{a} + v\underline{b} + w\underline{c}$ and $\bar{Q}_o$ is the amplitude of the scattered wave at unit distance from the scattering point in direction $\underline{S}$. The total displacement Y due to all the lattice points will be

$$Y = (\bar{Q}_o/R)\exp(i\omega t)\ \Sigma\exp(i\kappa \underline{a}.\underline{S})\ \Sigma\exp(i\kappa \underline{b}.\underline{S})\ \Sigma\exp(i\kappa \underline{c}.\underline{S}) \qquad [2.2]$$

Each summation involves the total number of lattice points in each unit translation direction.

From equation 2.2, the intensity I of the total displacement is

$$I = |Y^2|$$
$$= (\sin N_1\phi_1/\sin\phi_1)^2(\sin N_2\phi_2/\sin\phi_2)^2(\sin N_3\phi_3/\sin\phi_3)^2 \qquad [2.3]$$

where $\phi_1 = \frac{1}{2}\kappa\underline{S}.\underline{a} = \kappa a \sin\theta \cos\alpha$

$\phi_2 = \frac{1}{2}\kappa\underline{S}.\underline{b} = \kappa b \sin\theta \cos\beta$

$\phi_3 = \frac{1}{2}\kappa\underline{S}.\underline{c} = \kappa c \sin\theta \cos\tau$

$\cos\alpha$, $\cos\beta$ and $\cos\tau$ are the direction cosines of $\underline{S}$ with respect to $\underline{a}$, $\underline{b}$ and $\underline{c}$. The intensity I will be a maximum when $\phi_1 = h\pi$, $\phi_2 = k\pi$ and $\phi_3 = l\pi$, where h, K and l are integers. Substituting $\kappa = 2\pi/\lambda$ gives

$$\cos\alpha = h\lambda/2a \sin\theta$$
$$\cos\beta = k\lambda/2b \sin\theta$$
$$\cos\tau = l\lambda/2c \sin\theta \qquad [2.4]$$

The direction cosines of the normal to the hkl plane are

$$\cos\alpha = hd_{hkl}/a$$
$$\cos\beta = kd_{hkl}/b$$
$$\cos\tau = ld_{hkl}/c \qquad [2.5]$$

where d_{hkl} is the interplanar spacing of the hkl set of planes, see fig 2.2.

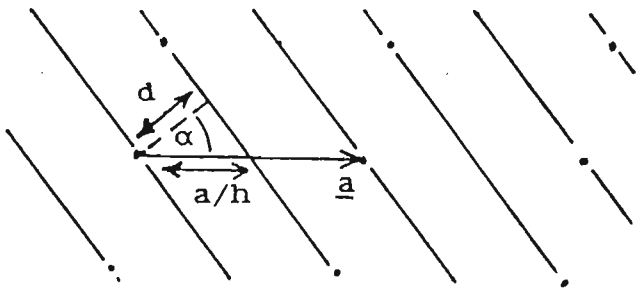

Fig 2.2 Direction cosine of d_{hkl}

This normal will thus be parallel to the normal $\underline{S}$ of the reflecting plane, implying that the hkl plane will be parallel to the reflecting plane. Equations 2.4 and 2.5 imply

$$\lambda = 2d_{hkl}\sin\theta \qquad [2.6]$$

This is Bragg's law.

If the h, K and l values of equation 2.4 have a common multiple n, equation 2.6 becomes

$$n\lambda = 2d_{hkl}\sin\theta \qquad [2.7]$$

Crystal diffraction can thus be thought of as reflection from planes of the lattice, each set of planes producing a reflection at some angle θ, where θ must satisfy equation 2.7. When discussing diffraction from a lattice it is usual to consider the angle 2θ between the incident and reflected beam, rather than θ. Equation 2.6 implies that the larger the interplanar spacing, the smaller the diffraction angle 2θ.

2.4 The reciprocal lattice and the Ewald Sphere

The reciprocal lattice is of great value in understanding single crystal or powder diffraction.

From the unit cell translation vectors $\underline{a}$, $\underline{b}$ and $\underline{c}$, a reciprocal lattice can be constructed with unit translation vectors $\underline{a}^*$, $\underline{b}^*$ and $\underline{c}^*$ such that

$$\underline{a}^* = (\underline{b} \times \underline{c})/V$$
$$\underline{b}^* = (\underline{c} \times \underline{a})/V$$
$$\underline{c}^* = (\underline{a} \times \underline{b})/V$$

where $V = \underline{c}.(\underline{a} \times \underline{b})$ is the volume of the unit cell.
A lattice vector $\underline{r}^*$ in the reciprocal space will be

$$\underline{r}^* = h\underline{a}^* + k\underline{b}^* + l\underline{c}^*$$

where h, k and l are integers. The reciprocal lattice vector $\underline{r}^*(h,k,l)$ is normal to the real lattice plane hkl, and has magnitude $1/d_{hkl}$.

The Ewald sphere is a construction in reciprocal space equivalent to the Bragg reflection condition. A sphere is constructed (see Fig 2.3) with the origin O of the reciprocal lattice on the surface of the sphere with radius $1/\lambda$ and with centre P, such that $\underline{PO}$ is in the direction of the primary beam (unit vector $\underline{s}_0$). The scattered wave (unit vector $\underline{s}$) will be in the direction $\underline{PQ}$.

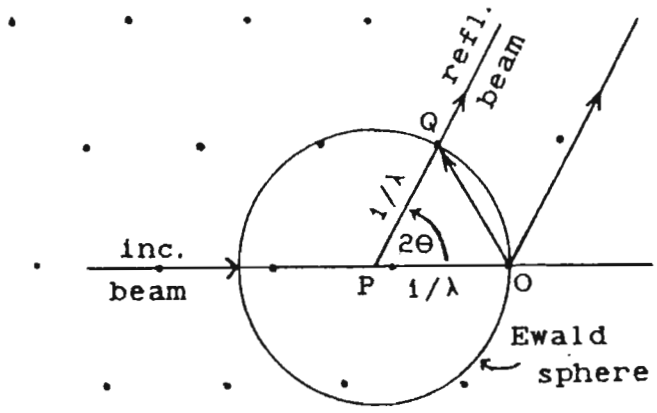

Fig 2.3 The Ewald Sphere

From the figure vector $\underline{OQ}$, which is in the direction of $\underline{S} = \underline{s} - \underline{s}_0$, ie normal to the reflecting plane, has magnitude $2\sin\theta/\lambda$. By Bragg's equation, this must equal an integral multiple of $1/d_{hkl}$ for reflections to occur. Thus, if $\underline{OQ}$ is a reciprocal vector, and its end-point lies on the Ewald sphere, then only will a reflection occur, with scattered wave vector in the direction of $\underline{PQ}$.

When the crystal is stationary, only a few reciprocal lattice points will lie on the Ewald sphere, resulting in a limited number of reflections. If the crystal is rotated about some point, then the lattice and the reciprocal lattice will also rotate and more reciprocal lattice points will come into reflecting position.

In single crystal work the intensities of the reflections are recorded individually on a film or measured by a counting device and the crystal structure can be determined by analysing the intensities of the reflections.

2.5 X-ray diffraction using powders.

A crystal powder is a polycrystalline specimen characterised by random orientations of very small crystals or crystallites. Thus the reciprocal lattice vector $\underline{r}^*(hkl)$ corresponding to the set of planes hkl assumes all directions with equal probability, with the consequence that the point Q of Fig 2.3 is dispersed over all positions on the surface of a sphere of radius $r^*(hkl) = 1/d_{hkl}$, with origin at the reciprocal lattice origin, as indicated in fig 2.4.

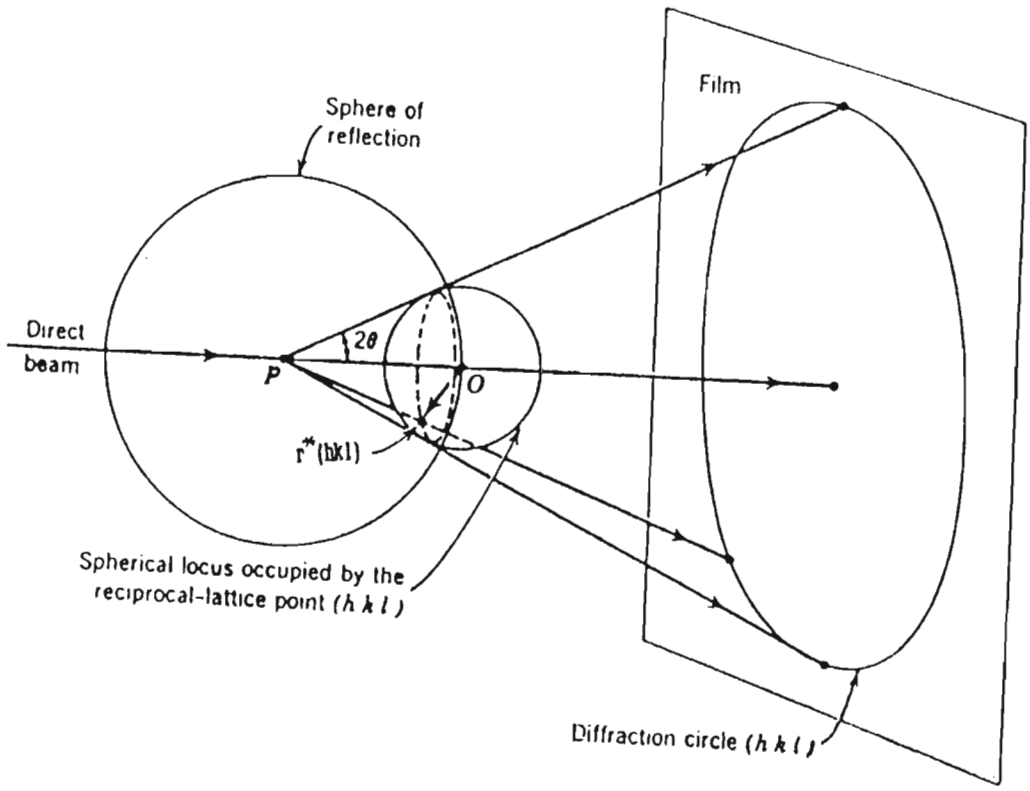

Fig 2.4 The reflection circle from a powder sample (See Klug and Alexander, 1974, p176)

This sphere intersects the sphere of reflection in a circular zone, which shown in perspective, is the dotted ellipse in Fig 2.4. Reflections from the planes (hkl) therefore take place in all directions defined by this zone in reciprocal space, and the diffracted rays, which can be thought of as originating from P, lie on the cone of semiapex angle 2θ with the direct beam as its axis. A film placed perpendicular to the incident beam will record the diffracted rays as a circle. Another plane (h'K'l') will generate a cone of angle 2θ', leading to a different diffraction circle. Larger hkl-values give smaller d-values and larger 2θ-values, ie, circles with larger radii.

Often, many different sets of planes will have equal interplanar spacing, eg, (-1, k, l) and (1, K, l) for a monoclinic system and (5, 0, l) and (4, 3, l) for a tetragonal system. This means that the diffraction circles formed from different sets of hkl planes with equal interplanar spacing will be identical.

2.6 The intensities of diffraction.

For powder specimens the intensity of a reflection is given by the following expression

$$I = Sc.Mu(hkl).Lp(hkl).Po(hkl).|F_{hkl}|^2 \qquad [2.8]$$

where Sc ≡ scale factor
Mu ≡ multiplicity factor
Lp ≡ Lorentz-polarisation factor
Po ≡ preferred orientation factor
F ≡ structure factor

In general the absorption of the beam in the sample influences the intensities of the refections. As the effect does not vary with 2Θ for the geometry used in this study, the absorption factor can be neglected here.

2.6.1 Multiplicity factor

Depending on the crystal symmetry certain reflections have equal structure factors and occur at the same 2Θ-values. The observed intensity is thus enhanced by a factor equal to the number of such equivalent reflections.

2.6.2 Lorentz or velocity factor

This factor depends on the rate at which the reflecting planes of the crystal pass through the reflecting position. Planes parallel to the axis of rotation of the sample will remain in the reflecting position for a shorter period of time than planes which are not parallel to the axis of rotation.

The form of this factor for a powder sample is (Klug and Alexander, 1974, p144)

$$L = [\ \sin 2\Theta \sin\Theta\ ]^{-1}$$

2.6.3 Polarisation factor (see Klug and Alexander, 1974, p142)

If the primary beam is polarised so that the electric vector is oscillating parallel to the plane containing the incident and scattered beam, there is a reduction in the scattered amplitude by a factor cos2θ. If the primary beam is polarised perpendicular to the plane there is no such reduction in scattered amplitude. If the primary beam is unpolarised the polarisation reduction factor for the intensity is the average

$$p = \tfrac{1}{2}\,(1 + \cos^2 2\theta)$$

If the radiation is monochromatised, then the primary beam is itself polarised, and the polarisation factor will then have the form

$$p = [1 + \cos^2 2\theta \cos^2 2\theta_m]/[1 + \cos^2 2\theta_m]$$

where θ_m is the diffraction angle of the monochromator crystal. This is the form used in the present study.

2.6.4 Preferred orientation factor

Sometimes the orientation of the crystallites in the powder sample is not completely random. The crystallites will tend to line up in certain directions when the sample is being prepared, so that for a particular reflection some regions of the diffraction cone are enhanced. The preferred orientation factor takes this effect into account (See Dent Glasser, 1977, p125).

If the crystallites are platelets, one could imagine that the platelet normal is a preferred orientation vector and that these vectors are distributed preferentially about the normal to the sample surface, ie, the scattering vector for the diffractometer geometry. In this case the preferred orientation factor is

$$Po = \exp\{-P[\pi/2 - \alpha(\underline{r}^*(hkl))]\}$$

where P is the preferred orientation parameter and α the angle

between the scattering vector $\underline{r}^*(hkl)$ and the platelet normal.

If the crystallites are needles, the needle axis is the preferred orientation vector and this vector would be distributed preferentially in the plane of the sample surface. The preferred orientation factor is (see Will, Jansen and Schäfer, 1983, p6)

$$Po = \exp\{-P\ \alpha(\underline{r}^*(hkl))\}$$

2.6.5 The Structure Factor

F_{hkl} is the amplitude of the wave scattered by one unit cell of a crystal in units of the scattering power of a free electron. This is the factor (in the expression for the intensity of a reflection) which depends on the structure of the crystal and from which the structure can be refined. The general form of F is

$$F_{hkl} = \Sigma\ f_j \exp(i\phi_j)$$
$$= \Sigma\ f_j \exp\ 2\pi i(hx_j + ky_j + lz_j)$$

ϕ_j is the phase difference of a wave scattered from point (x_j, y_j, z_j) with respect to one scattered from the origin of the unit cell for the hkl-reflection. The sum is taken over the j atoms in the unit cell. (x_j, y_j, z_j) are the fractional coordinates of atom j relative to the origin of the unit cell. f_j is the form factor of the atom j. For reflections with $\Theta = 0°$, f is equal to Z, the number of electrons in the atom (atomic number).

The atom is not a mathematical point but the electrons are spread throughout the volume of the atom. Thus for reflections at Θ greater than zero, the contributions from different points in the atom will be out of phase, leading to partial interference. f thus decreases with Θ, (see eg, Klug and Alexander, 1974, p149 and International Tables for X-ray Crystallagraphy, 1974, p72).

These values are calculated under the assumption that the binding energy of the electrons are small compared with the energy of the x-ray photon being scattered. When an atom has an absorption edge close to the wavelength of the x-ray photon, this is no longer true, and the scattering amplitude shows a sharp change with wavelength. This phenomenon is known as anomalous

dispersion. The atomic scattering factor can thus be expressed as a complex number

$$f(\text{total}) = f + f' + if''$$

where f' and f'' are the real and imaginary anomalous terms. Values of f' and f'' as functions of $\sin\Theta/\lambda$ are listed in the International Tables for X-ray Crystallography, 1974, p149.

Atoms in a crystal undergo thermal motions which are small vibrations about the equilibrium positions in the lattice. Recalling the effect that increasing Θ has on the atomic scattering factors, a similiar situation arises as the temperature increases. The amplitude of vibrations will increase and the phase difference of the waves scattered from different parts of the electron cloud will increase. This results in a decrease of the scattering power of the atom by a factor $\exp(-M)$, where $M = B(\sin\Theta/\lambda)^2$ and B is called the temperature factor of the atom.

In the above form, all directions of vibration are assumed equivalent, which is often the case for lattices with high symmetry. For lower symmetry, all directions are not equivalent, resulting in an anisotropic vibration tensor B_{ij}, (Klug and Alexander, 1974, p146) The exponent M becomes

$$M = \tfrac{1}{4}(h^2a^{*2}B_{11} + k^2b^{*2}B_{22} + l^2c^{*2}B_{33} + 2hka^*b^*B_{12} + 2hla^*c^*B_{13} + 2klb^*c^*B_{23})$$

Chapter 3 THE PROFILE OF THE INDIVIDUAL REFLECTIONS

3.1 Recording of the x-ray diffraction spectrum

Fig 3.1 is a representation of the diffraction circles produced by the hkl planes with different interplanar spacing.

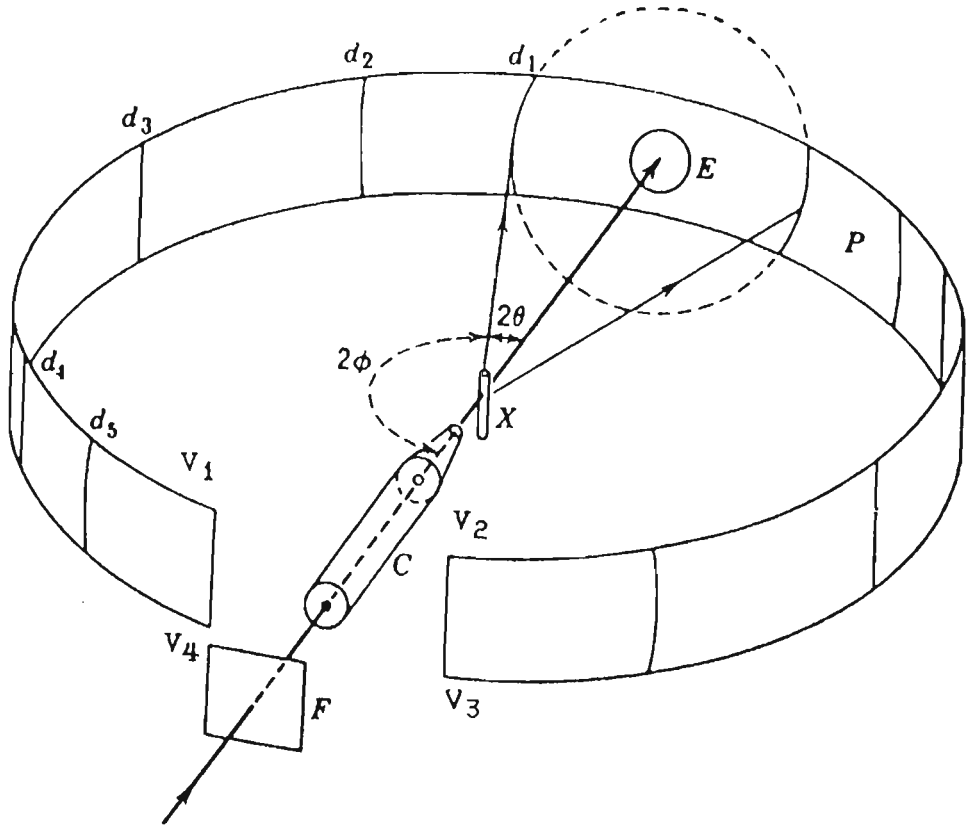

Fig 3.1 Geometrical features of the Debye-Scherrer technique (Klug and Alexander, 1974, p178).

Normally, only a section through these circles, as shown in fig 3.1 by the cylindrical strip $V_1V_2V_3V_4$ are recorded by various methods. Two standard techniques are described below.

1) Debye-Scherrer camera. Intensities are recorded on a cylindrical photographic film which is placed in the position of the strip $V_1V_2V_3V_4$. The sample to film distance is constant for all 2θ and is equal to the source to sample distance.

2) Bragg-Brentano parafocussing diffractometer. Consider rays diverging from a point source S striking an extended powder sample AA'. The construction in Fig 3.2 illustrates that if the sample is shaped to lie on a circle passing through S then the

rays scattered from each point in the sample through some angle 2θ will all pass through a point D lying on the same circle. The circle is therefore called the focussing circle. For different 2θ-values the points D will lie at different distances from the centre of the sample P.

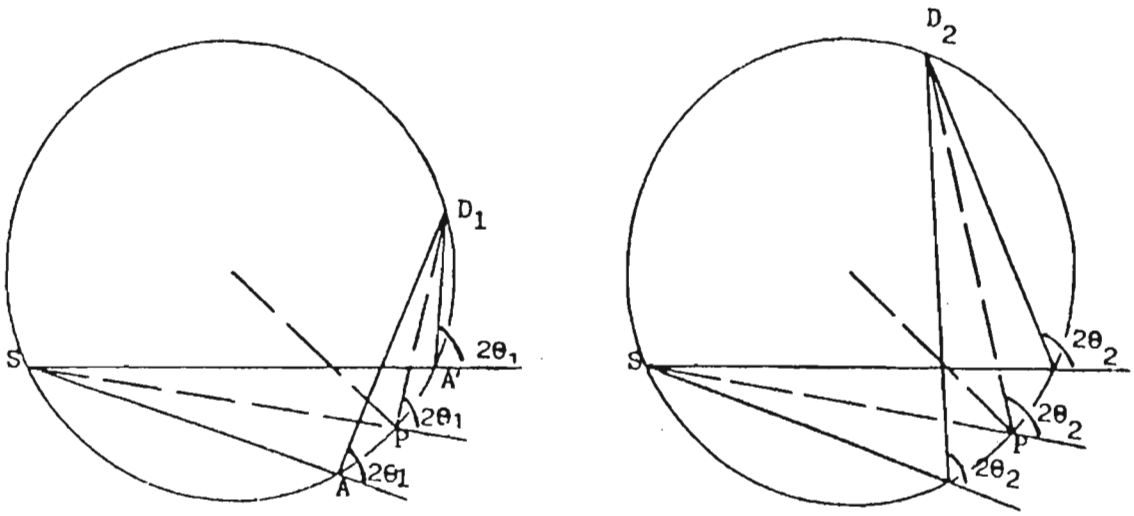

Fig 3.2 Focussing of diffracted rays - fixed sample and focussing circle and variable detector distance.

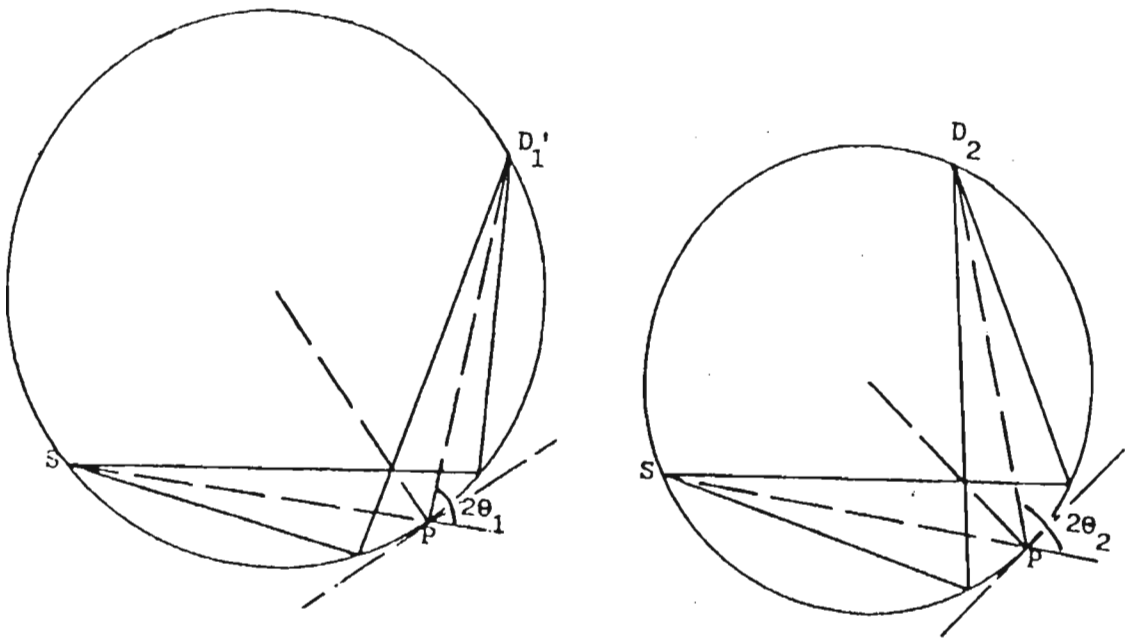

Fig 3.3 Focussing of diffracted rays - rotating sample and fixed detector distance.

If the tangent at P (sample plane) makes equal angles θ with

the primary and diffracted rays (Fig 3.2, right diagram) then the source-sample distance SP and sample-dectector distance PD are equal. The geometry of the Bragg-Brentano diffractometer is as follows. In order to record intensity as a function of 2θ the detector is rotated about the sample and the symmetrical geometry is maintained by letting the sample rotate at half the speed of the detector (θ, 2θ mode). Thus the sample-detector distance remains constant (for different 2θ) and equal to the source-sample distance. The focussing circle changes in size. (Fig 3.3).

In practise the sample is not a line but extends vertically out of the plane of the diagram. Further the sample is flat rather than curved and the geometry is called "parafocussing". The sample has a finite thickness and all these factors lead to a broadening of the angular range over which a certain hkl-reflection occurs.

The plane of figures 3.2 and 3.3 is normally referred to as the equatorial plane, and the normal to this plane as the axial direction.

The spectrum of intensity against 2θ can be recorded in the continuous scan or the step scan mode. In the former case the detector travels at a fixed angular speed, the impulses are passed to a ratemeter and the time-averaged count rate is recorded on a chart recorder. In the step scan mode the detector remains stationary at each angular position chosen, while impulses are collected for a short time. The step scan mode was used throughout in this work.

Fig 3.4 shows the optical arrangement of the diffractometer. The x-ray source F is the line focus of an x-ray tube. The equatorial divergence of the primary and reflected beams are limited by the dimensions x and x' of the apertures X and G. The axial divergence is limited by so-called Soller slits s_1 and s_2.

The spectrum exhibits peaks due to the various Bragg reflections hkl, superimposed on a background due to effects such as thermal diffuse scattering, Compton scattering, air scattering, etc. The integrated intensities of the reflections are the areas under the peaks and special techniques are required to obtain these from the spectrum so that they can be used further in the analysis of the crystal structure.

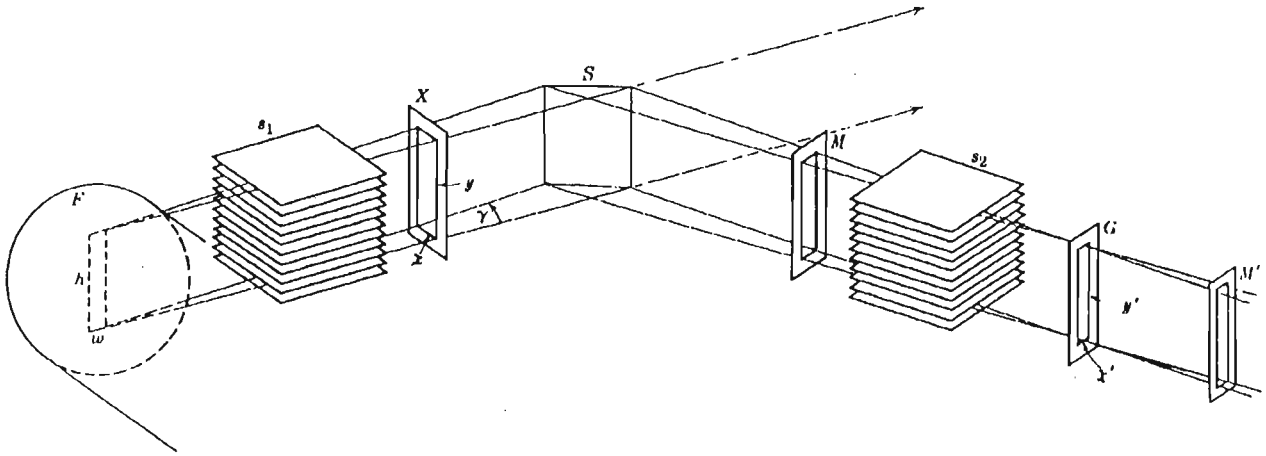

Fig 3.4 Optical arrangement of the diffractometer (Klug and Alexander, 1974, p277).

Often, the peaks in the spectrum overlap, and analytical expressions (line profile functions) to describe the peaks must be obtained to assign the correct intensities to peaks which overlap and much work in obtaining these expressions has been done by many researchers.

Before mention is made of the expressions of the line profiles, the factors that influence these profiles will be discussed. These factors can be expressed as mathematical functions and as will be discussed in the next section, the expression for the line profile can be directly obtained by a convolution of these functions.

3.2 Factors that affect the line profile

An ideal powder diffraction line should occur exactly at the 2θ position for that reflection and it should be infinitesimally narrow. However, the geometry of the diffractometer and the physical nature of the x-rays and the specimen cause the diffraction lines to be broadened asymmetrically, and to be displaced from the theoretical 2θ positions to lower angles (see Klug and Alexander, 1974, p290ff).

The following "physical" factors affect the line profile.

1) The incident x-ray beam is composed of α_1 and α_2 components, each with its own wavelength and spectral width. The spectral

distribution of the incident radiation can be approximated by a Gaussian function.

2) The small size of the crystallites in the specimen and the nature and magnitude of the distortions of the crystal lattice can cause the line to be broadened.

The "geometrical" factors can be attributed to

1) the size of the source (effective focus of the x-ray tube).
2) the flat specimen surface since the displacement of the different portions of the flat specimen surface from the focussing circle varies,
3) the axial divergence of the beam which will depend upon the distance between the individual plates of the Soller slits and the length of the plates,
4) the specimen transparency since the incident beam penetrates a certain distance into the specimen, the extent depending upon the absorption coefficient of the sample,
5) the width of the receiving slit,
6) the $\Theta/2\Theta$ misalignment of the diffractometer, ie the sample plane not being exactly tangent to the focussing circle.

Fig 3.5 illustrates the effect of the various factors on the line shape. The geometrical factors are discussed in detail by Wilson (1963). Retief and Engel (1985) have dealt in particular with the transparency correction.

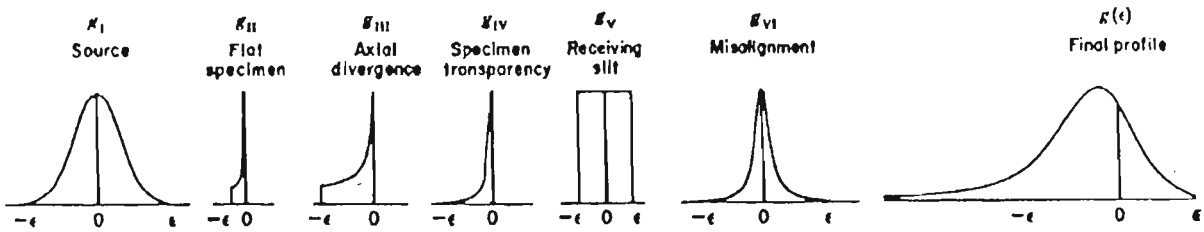

Fig 3.5 The factors causing instrumental (geometrical) line broadening (Klug and Alexander, 1974, p292).

3.3 Mathematical representation of the line profile

The above factors can be represented by mathematical functions and a convolution of these functions will result in the theoretical line profile function. The form of the individual functions calculated for certain instrumental parameters are

shown in fig 3.5 together with the final convoluted function of these functions.

It is customary to refer to the profile function as the W*G*S-function, ie the convolution of Wavelength, Geometrical and Specimen line broadening effects. The convolution W*G is called the instrument function and S the specimen function.

3.4 Approximations of the profile functions

The determination of the above individual line-broadening functions for a particular diffractometer, radiation and sample is very difficult. Therefore instead of convoluting the individual functions to obtain a profile function, it is preferable to fit a suitable mathematical profile function to the diffraction spectrum itself. Functions that have been used in the literature are now discussed.

1. The Gaussian function $G = I_0 \exp[-\ln 2 (D/w)^2]$

where D is $2\theta - 2\theta_0$, $2\theta_0$ the position of the peak maximum, I_0 the height of the maximum and w the peak halfwidth at half maximum.

2. The Lorentzian function $L = I_0[1 + (D/w)^2]^{-1}$

3. The Voigt function is the convolution of a Gaussian function with a Lorentzian function (see Ahtee et al., 1984).

4. The pseudo-Voigt function V is the sum of a Gaussian and a Lorentzian function with an adjustable mixing parameter n, called the shape parameter:

$$V = nL + (1 - n)G$$

It is a close approximation to the Voigt function but easier to work with than a convolution.

5. The Pearson VII function P (see Hall, 1977):

$$P = I_0[1 + D^2/ma^2]^{-m}$$

Some of the work done using the above profile functions is now mentioned briefly. Will, Parrish and Huang (1983) used a sum of seven Lorentzian functions to fit the instrument function of the diffractometer, and convoluted this with a single Lorentzian as the specimen function S to fit the diffraction pattern. Ahtee et al. (1984) used the Voigt function as a profile function. The Gaussian was used to give the main shape of the peak, and the Lorentzian to describe the tail of the peak. Toraya et al. (1983) give a discussion of the use of the Pearson VII function and refer to other recent work.

The pseudo-Voigt function has been used in the present work.

3.5 The asymmetric pseudo-Voigt function

The pseudo-Voigt function is

$$V = nL + (1 - n)G \qquad [3.1]$$

Since L and G are given the same values of the parameters I_o, $2\theta_o$ and w, the function V also has the same parameter values and is also symmetric about $2\theta_o$.

Fig 3.6 shows the pseudo-Voigt function calculated using values of -1, 0, 1, 2, 3 for the shape parameter n. A value of 0 gives the Gaussian function and a value of 1 the Lorentzian. Beyond the halfwidth the Gaussian drops off to zero faster than the Lorentzian. Within the halfwidth the Gaussian is broader than the Lorentzian. For shape parameter values less than 0, the pseudo-Voigt function attains negative values at around two halfwidths away from the peak. For values greater than 1,79, the function will have three points of inflection on each side instead of only one. Thus, suitable values of the shape parameter for the pseudo-Voigt function lie between 0 and 1,79. In practice a maximum value of around 1,5 is more satisfactory.

The actual line profile (fig 3.5) is unsymmetrical and the maximum is shifted. Therefore, the pseudo-Voigt function was made asymmetric by defining different values of n and w for the left and right flanks. Since the incident beam contains a pair of lines, the α_1/α_2 doublet, which cannot be separated by the

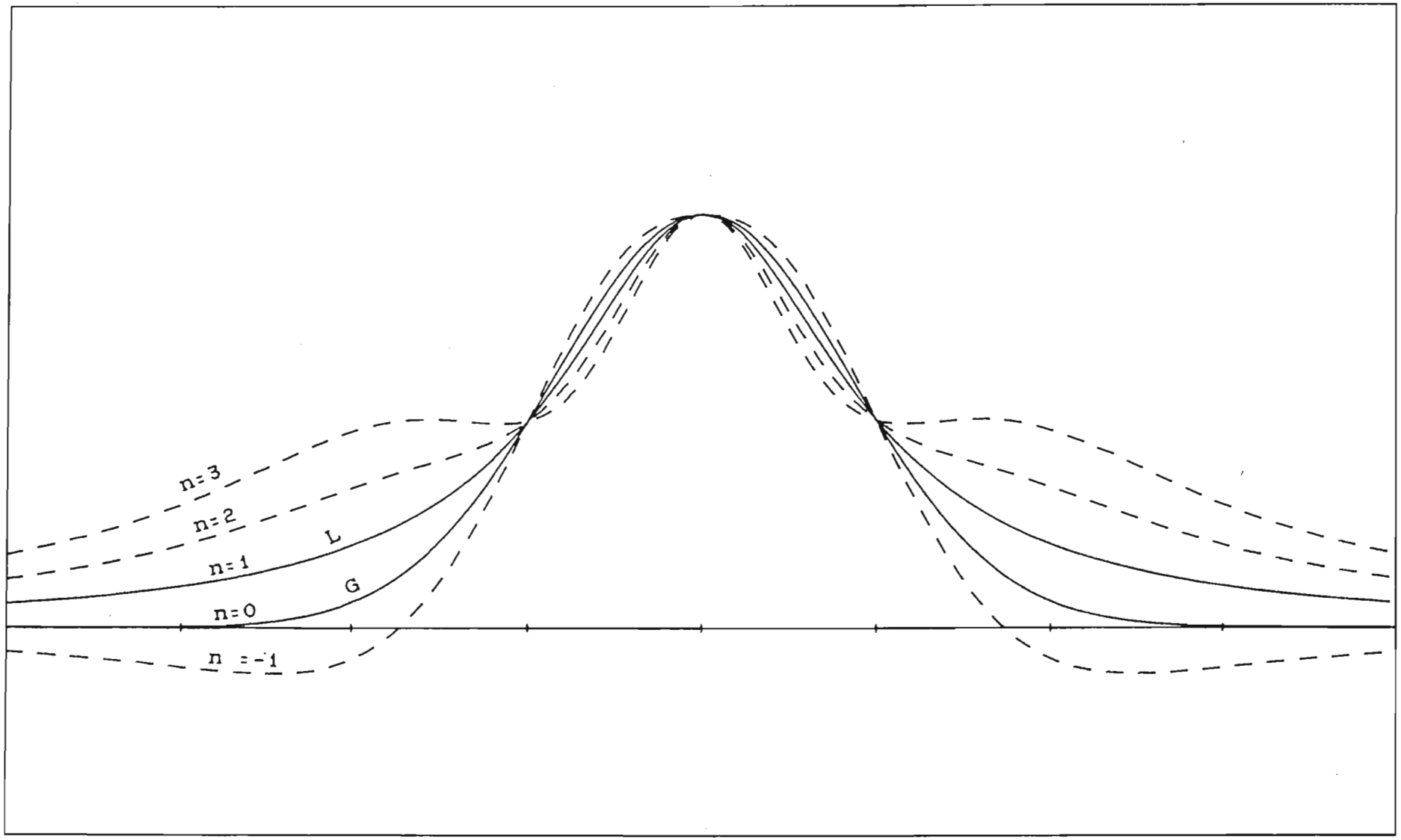

Fig 3.6 The pseudo-Voigt function with shape parameters -1, 0, 1, 2, 3

diffracted-beam monochromator, a function consisting of two components with a certain intensity ratio r_{21} is required. The total profile function is therefore

$$
\begin{aligned}
V_{tot} &= V_1 + r_{21}V_2 \\
V_1 &= V(I_o,\ w_{L1},\ n_{L1},\ 2\theta_1) \text{ for } 2\theta < 2\theta_1 \\
&\quad\ V(I_o,\ w_{R1},\ n_{R1},\ 2\theta_1) \text{ for } 2\theta > 2\theta_1 \\
V_2 &= V(I_o,\ w_{L2},\ n_{L2},\ 2\theta_2) \text{ for } 2\theta < 2\theta_2 \\
&= V(I_o,\ w_{R2},\ n_{R2},\ 2\theta_2) \text{ for } 2\theta > 2\theta_2
\end{aligned}
$$

$2\theta_1$ is the position of the α_1 maximum. w_{L1} and w_{R1} are the left and right halfwidths and n_{L1} and n_{R1} the left and right shape parameters for the α_1 peak. $2\theta_2$ is the position of the α_2 maximum calculated using

$$\sin(2\theta_2) = \lambda_2/\lambda_1 \sin(2\theta_1)$$

where λ_1 and λ_2 are the wavelengths of the α_1 and α_2 components respectively. w_{L2} and w_{R2}, n_{L2} and n_{R2} are the parameters of the α_2 peak. Fig 3.7 illustrates these parameters.

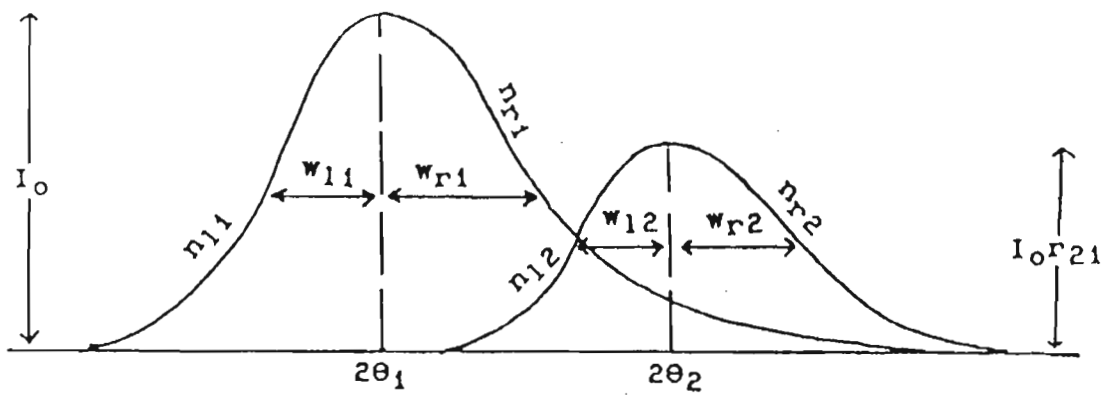

Fig 3.7 Parameters of the asymmetric pseudo-Voigt function for the α_1/α_2 doublet.

In our procedure the profile parameters of the α_2 peak were usually kept the same as those of the α_1 peak in order to keep the number of profile parameters small.

Using the integrals

$$\int_0^\infty \exp(-y^2)\,dy = \tfrac{1}{2}\sqrt{\pi} \qquad \text{and} \qquad \int_0^\infty dy/(1 + y^2) = \tfrac{1}{2}\pi$$

the area under a symmetric Gaussian of halfwidth w and peak maximum I_0 is

$$I_{int} = \sqrt{\pi/\ln 2}\; w\; I_0$$

The area under a symmetric Lorentzian of halfwidth w and peak maximum I_0 is

$$I_{int} = \pi\; w\; I_0$$

The area under the asymmetric pseudo-Voigt function including α_1 and α_2 components (ie the integrated intensity) is therefore

$$\begin{aligned} I_{int} = \tfrac{1}{2}\, I_0 \sqrt{\pi/\ln 2}\{&[(1 - n_{l1})w_{l1} + (1 - n_{r1})w_{r1}] \\ &+ r_{21}[(1 - n_{l2})w_{l2} + (1 - n_{r2})w_{r2}]\} \qquad [3.2] \\ + \tfrac{1}{2}\, I_0\, \pi \quad &\{(n_{l1}w_{l1} + n_{r1}w_{r1}) + r_{21}(n_{l2}w_{l2} + n_{r2}w_{r2})\} \end{aligned}$$

Chapter 4 EXPERIMENTAL DETAILS

The data sets evaluated were obtained using a Philips PW 1730/10 powder diffractometer (with the Bragg-Brentano parafocussing geometry) at the Mineralogical Institute of the University of Bonn. A fine-focus Cu X-ray tube was used and the radiation was monochromated by placing a graphite monochromator crystal (reflection off the (0002)-planes with $2\Theta_m$ = 26,62°) in the diffracted beam. The wavelengths of the α_1 and the α_2 components of the beam were taken as 1.540568 and 1.544438 Å respectively. The beam path was evacuated to about 0,1 torr in order to reduce the background due to air scattering and to increase the peak intensities by reducing air absorption.

The spectrum was recorded as a step scan travelling from high to low angles in equal steps, usually 0,02° 2Θ, the accessible range being 10-144° 2Θ. A sample spinner was used in order to reduce the effect of preferred orientation. The detector was a scintillation counter.

The diffraction spectra of two samples were obtained. One was a standard sample of silicon and another the mineral Fe-akermanite. For silicon, scans of each diffraction peak were taken individually, producing the 13 small data sets. For akermanite, the entire spectrum was recorded in 5 scans. Details of the angular ranges and increments used for these scans are shown in table 4.1.

The data sets were collected by Dr B Bolzenius and Prof D W Engel, to whom thanks are due for making them available for further analysis.

Table 4.1 Data sets of silicon and Fe-akermanite.

specimen	scan no.	2θ range	step increment	no. of observations
Si	1507	134,50 - 139,00	0,02	226
Si	1508	125,00 - 129,60	0,02	211
Si	1509	111,90 - 116,10	0,02	211
Si	1510	104,80 - 108,40	0,02	181
Si	1511	93,60 - 96,60	0,02	151
Si	1512	86,60 - 89,40	0,02	141
Si	1513	74,90 - 77,80	0,01	291
Si	1514	67,90 - 70,40	0,01	251
Si	1515	55,10 - 57,10	0,01	201
Si	1516	46,30 - 48,30	0,01	201
Si	1517	27,50 - 29,50	0,01	201
Si	1518	25,70 - 27,70	0,01	201
Si	1519	19,80 - 21,80	0,01	201
Ak	1553	135,00 - 144,00	0,02	451
Ak	1554	95,00 - 135,00	0,02	2001
Ak	1535	55,00 - 95,00	0,02	2001
Ak	1533	42,00 - 55,00	0,02	651
Ak	1534	10,00 - 42,00	0,02	1601

Chapter 5 PROGRAMS USED FOR DETERMINING INTEGRATED INTENSITIES

5.1 Peak fitting procedure

In order to obtain the integrated intensities of the many reflections present in a spectrum, the profile peak fitting program PPP, initially developed by Bolzenius et al. (1985), was implemented and further modified. The profile function used to model the peaks was the pseudo-Voigt function. The data is a set of n observed point intensities Yo(i) measured at angles 2θ(i). The program PPP fits a calculated set of values Yc(i) to the observations Yo(i), using a non-linear least squares fitting procedure. If there are a number of peaks in the range, then each peak contributes to the intensity at any position 2θ(i) in the range. Each value Yc(i) is thus calculated using the equation

$$Yc(i) = \Sigma_j V(j,i) + bg(i)$$

where V(j,i) is the contribution of the j'th peak to the intensity at the position 2θ(i) and bg(i) is the background contribution at this position.

The calculated intensities Yc(i) thus depend upon the following parameters:

1) the positions and heights of the peaks
2) the widths, shapes and α_2/α_1-ratio of the peaks
3) the parameters defining the background.

It is these parameters which are adjusted to optimum values (ie refined) during the least squares fitting procedure to obtain the best agreement between the experimental and calculated values. From these optimum parameter values, the integrated intensities of the individual reflections can be calculated.

Before the program PPP is discussed further, a brief discussion of the theory of the least squares procedure will be presented.

5.2 The Least Squares Procedure

For a detailed discussion of the procedure see eg:
Will, Jansen and Schäfer (1983) p2, Martin (1971) p85, Pugh E M

and Winslow G H (1966) p91. A brief summary is given here.

The set of observations is represented by a vector $\underline{Yo}$ of n elements, where n is the number of observations, the calculated values by a vector $\underline{Yc}$ also of n elements, and the parameters used to calculate $\underline{Yc}$ by a vector $\underline{P}$ of m elements, where m is the number of parameters.

In our case $\underline{Yc}$ has non-linear dependence upon the parameter set $\underline{P}$. If $\underline{Yc}$ did have a linear dependence upon the parameters, then we could write $\underline{Yc}$ as

$$Yc_i = \Sigma_{K=1,m} P_K \phi_K(2\Theta_i)$$

where $\phi_K(2\Theta)$ are linearly independent functions which depend only upon 2Θ.

We define $\underset{\sim}{Q}$ to be a matrix with elements

$$Q_{iK} = \phi_K(2\Theta_i)$$

Then

$$\underline{Yc} = \underset{\sim}{Q}\ \underline{P}$$

The optimum fit of $\underline{Yo}$ by $\underline{Yc}$ will be obtained by minimising the quantity

$$S = (\underline{Yo} - \underset{\sim}{Q}\ \underline{P})^T\ \underset{\sim}{W}\ (\underline{Yo} - \underset{\sim}{Q}\ \underline{P}) \qquad [5.1]$$

$\underset{\sim}{W}$ is a weighting matrix whose elements are obtainable from the variances of the $\underline{Yo}$ vector elements. Minimising S by using

$$\partial S/\partial P_K = 0$$

the set of normal equations for the parameters is obtained

$$\underline{P} = (\underset{\sim}{Q}^T\ \underset{\sim}{W}\ \underset{\sim}{Q})^{-1}\underset{\sim}{Q}^T\ \underset{\sim}{W}\ \underline{Yo} \qquad [5.2]$$

(Martin, 1971, p88, equation 8.13)

For the non-linear case such as ours an iterative procedure can be used based on the small deviations from a "good" set of starting parameters $\underline{P}_o$. A Taylor expansion of Yc_i about $\underline{P}_o$ (two terms only) yields

$$Yc_i = Yc_i\Big|_{P=Po} + \Sigma_{K=1,m}(\partial Yc_i/\partial P_K)\Big|_{P=Po}\delta_K$$

ie, $$\underline{Yc} = \underline{Yc}_o + \underset{\sim}{A}\,\underline{\delta} \qquad [5.3]$$

where $\underset{\sim}{A}$ is a matrix with elements

$$A_{ij} = \partial Yc_i/\partial P_j\Big|_{P=Po}$$

and $\underline{\delta}$ is a vector whose element δ_j is a small increment of the parameter P_j. Substitution of 5.3 into 5.1 yields

$$S = (\underline{Yo} - \underline{Yc}_o - \underset{\sim}{A}\,\underline{\delta})^T\,\underset{\sim}{W}\,(\underline{Yo} - \underline{Yc}_o - \underset{\sim}{A}\,\underline{\delta}) \qquad [5.4]$$

and, using $\underline{\Delta} = \underline{Yo} - \underline{Yc}_o$ as the new observable, equation 5.4 becomes

$$S = (\underline{\Delta} - \underset{\sim}{A}\,\underline{\delta})^T\,\underset{\sim}{W}\,(\underline{\Delta} - \underset{\sim}{A}\,\underline{\delta})$$

This is now a linear equation with respect to $\underline{\delta}$, and has the form of equation 5.1. Hence the normal equation analogous to 5.2 is

$$\underline{\delta} = (\underset{\sim}{A}^T\underset{\sim}{W}\,\underset{\sim}{A})^{-1}\underset{\sim}{A}^T\underset{\sim}{W}\,\underline{\Delta} \qquad [5.5]$$

Solving equation 5.5 yields increments δ_j by which the starting parameters Po_j must be changed to yield a better fit. Since equation 5.3 is an approximation, the solution for the optimum parameters can only be obtained by solving equation 5.5 iteratively. Each successive iteration will use as a starting set of parameters, the previous set modified by the increments calculated in the previous iteration. The procedure is stopped either after a fixed number of iterations (cycles) or when the set of parameter values converges, ie the increments drop below set limits.

5.3 Structure of program PPP

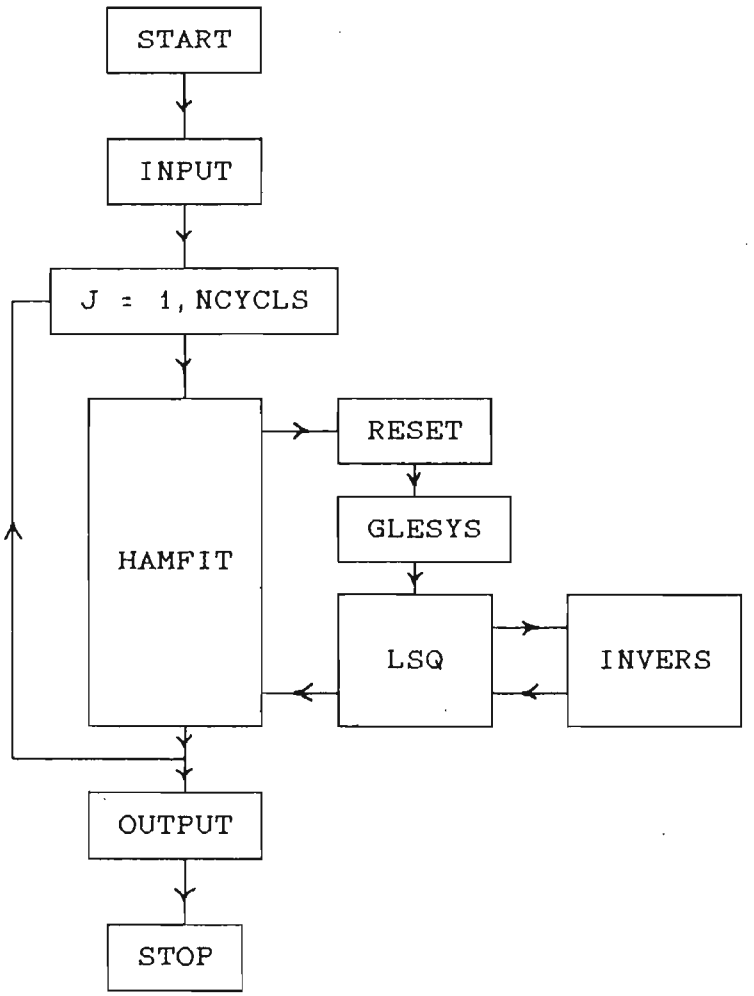

Fig 5.1 Flow diagram of program PPP

A simple flow diagram of PPP is shown in fig 5.1. On an IBM PC with 640 kilobytes of memory the program can fit a maximum of 500 observations and 57 parameters and for this and other reasons the set of observations is broken up into ranges of 5-10° 2θ. Good starting values of the parameters are read in subroutine INPUT, together with the array of observations. The program refines the parameter values following the iterative scheme of section 5.2, stopping after a given number of iterations. These iterations are controlled in subroutine HAMFIT where equation 5.5 is solved by calling the subroutines RESET, GLESYS and LSQ. RESET contains the options which can set certain parameters equal to others. GLESYS calculates the matrix $\underset{\sim}{A}$ of equation 5.5 ie, the matrix of

derivatives. LSQ then solves equation 5.5, which involves inverting the matrix ($\underset{\sim}{A}^T \underset{\sim}{W} \underset{\sim}{A}$). This inversion is done in subroutine INVERS. The weighting matrix used is a diagonal matrix, where the i'th diagonal element is the inverse of the square root of the i'th observation. Each iteration (in HAMFIT) generates the changes in values (shifts) that the parameters must undergo to produce a better fit. The change is reduced by a damping factor (which can be set by reading in the value in INPUT). The damping factor is aimed at ensuring the convergence of the refinement even if the starting parameters are rather poor. However, it is still important that good starting estimates of the parameters should be made.

After all the iterations have been completed, the final parameter values together with their errors and the Yc-values are produced in OUTPUT. This subroutine also generates the correlation matrix of the parameters. The R-values, residuals which are a measure of the quality of the fit, are calculated by the following equations:

$$R = \left[\frac{\Sigma\, [Yo(i) - Yc(i)]^2}{\Sigma\, Yo(i)^2} \right]^{1/2}$$

$$R_w = \left[\frac{\Sigma\, W(i,i)\,[Yo(i) - Yc(i)]^2}{\Sigma\, W(i,i)\, Yo(i)^2} \right]^{1/2}$$

$$R_a = \left[\frac{\Sigma\, \left| Yo(i) - Yc(i) \right|}{\Sigma\, Yo(i)} \right]$$

As can be seen from these equations, when the fit between the calculated and experimental values is good, then the R-values will be low, since Yo(i)-Yc(i) will be close to zero. These refinement R-values should be compared with statistical R-values calculated solely from the counting statistics of the observations by the equations

$$R_s = \left[\frac{\Sigma\ Yo(i)}{\Sigma\ Yo(i)^2} \right]^{\frac{1}{2}}$$

$$R_{ws} = \left[\frac{\Sigma\ W(i,i)\ Yo(i)}{\Sigma\ W(i,i)\ Yo(i)^2} \right]^{\frac{1}{2}}$$

$$R_{as} = \left[\frac{\Sigma\ Yo(i)^{\frac{1}{2}}}{\Sigma\ Yo(i)} \right]$$

These "statistical" R-values represent the lower limit to be expected for the refinement R-values. A good refinement will generate R-values only slightly greater than the statistical ones. When, however, the number of observations being fitted is not much larger than the number of parameters being refined, it is possible that the refinement R-values become smaller than the statistical R-values. This is not satisfactory, since the statistical R-values indicate the limit of the experimental accuracy.

Apart from the inspection of the R-values two further checks on the quality of the refinement are carried out. Firstly, the parameters should refine to acceptable values and secondly a plot of Yo and Yc as functions of 2Θ should look reasonably good, ie there should not be certain regions where the deviations are exceptionally large.

5.4 Parameters of refinement

The parameters used to calculate the intensities Yc(i) can be grouped into three main classes.

1) Two background parameters bgl and sl. The background is assumed to be linear throughout the range, usually 5-10° 2Θ, and background values at any position 2Θ(i) in the range are calculated from the value of the background at the left endpoint of the range being analysed (bgl), and the slope (sl) of the

background function by the equation

$$bg(i) = bg1 + s1\ [2\theta(i) - 2\theta(1)]$$

where $2\theta(1)$ is the position of the left endpoint of the range.

2) 9 profile parameters. These are the left and right halfwidths and shapes of the two components of the α_1/α_2 doublet (w_{1l}, w_{1r}, n_{1l}, n_{1r}, w_{2l}, w_{2r}, n_{2l}, n_{2r}) and their height ratio r_{21}. The parameters are assumed to be the same for all the peaks in the range.

3) The positions $2\theta_o$ and integrated intensities I of the peaks present in the range. The intensities, rather than the heights of the peaks are refined, since it is the intensities and their errors which are required for the refinement of the crystal structure.

5.5 Refinement options

The program PPP has various options available for use in refining the peaks in a certain range.

1) Certain of the parameters listed in section 5.4 can be held constant during the refinement. Examples of parameters held constant in certain cases to produce satisfactory fits were background parameters and positions of certain peaks.

2) A certain region of the range of observations can be left out of the refinement. This is useful if there is spurious background in the spectrum (eg, from impurities in the sample or stray radiation in the diffractometer geometry. The bad fit in this region could influence the refinement adversely if the region were not excluded.

3) The values of certain parameters can be constrained to remain equal to each other during the refinement. In this way, the form of the α_2 peak could be constrained to remain the same as that of the α_1 peak by fixing the values of w_{l2}, w_{r2}, s_{l2}, and s_{r2} to those of w_{l1}, w_{r1}, s_{l1} and s_{r1} respectively. Also the peaks could be made symmetric about the $2\theta_o$ position by setting the parameters w_{r1}, s_{r1}, w_{r2}, and s_{r2} to w_{l1}, s_{l1}, w_{l2} and s_{l2} respectively.

Options 1 and 3 have the further advantage of reducing the number of parameters refined.

5.6 Error estimates of the parameters

The errors of the parameters are estimated from the least squares fitting procedure. This vector set of errors $\underline{\sigma}$ is

$$\underline{\sigma} = \left[\frac{(\underline{A}\ \underline{\underline{W}}\ \underline{A})^T\ S}{N - NP} \right]^{\frac{1}{2}}$$

where S is the quantity minimised, defined by equation 5.4. N is the number of observations and NP the number of parameters refined.

5.7 Correlations of the parameters

When changes in two different parameters produce similar types of improvement in the fit then the two parameters are said to be correlated. Often refinements with highly correlated parameters produce unsatisfactory fits or do not converge. The matrix of correlation coefficients is calculated by the program and can be inspected for these features. Where correlation is high it is sometimes possible to fix one of the parameters at a suitable value and thus produce a satisfactory refinement.

5.8 Modifications of program PPP

5.8.1 Non-linear background.

The background in any particular 5-10° range was calculated as a linear function in the program PPP. It was found necessary to modify the program to accommodate marked non-linearity within individual ranges. This was achieved simply by subdividing the range into small enough sub-ranges, so that in each sub-range the background could still be considered to be quite accurately linear. Values of the background at the left of each sub-range and the slopes of the background in each sub-range were supplied

as input. The program then calculated an array of background values, the i'th element of the array being the background contribution to the i'th observation. In this modified version, the background could not be refined, since the number of parameters to be refined would increase tremendously. Suitable values of the background parameters were obtained in a manner to be described later.

5.8.2 Extra shape parameters.

As the Gaussian and Lorentzian components were always given identical halfwidths the pseudo-Voigt function has the same halfwidth no matter what the value of n is (see fig 3.6). In an attempt to improve the quality of the profile function, each peak half (eg the left half) was given two shape parameters, one for the inner (upper) part of the peak and one for the tail (lower) part. This causes the derivative of the function to have a slight discontinuity at the halfwidth, which is, however, considered acceptable. For the α_1 component the function is therefore defined (compare section 3.5):

$$V_1 = V(n_{l1l}, w_{l1});\ 0° < 2\theta < 2\theta_o - w_{l1}$$

$$= V(n_{lu1}, w_{l1});\ 2\theta_o - w_{l1} < 2\theta < 2\theta_o$$

$$= V(n_{ru1}, w_{r1});\ 2\theta_o < 2\theta < 2\theta_o + w_{r1}$$

$$= V(n_{rl1}, w_{r1});\ 2\theta_o + w_{r1} < 2\theta < 180°$$

n_{l1l} and n_{lu1} are the lower and upper left-hand shapes and n_{ru1} and n_{rl1} the upper and lower right-hand shapes of the α_1 peak.

In fig 5.2 the four ranges in which the various shape parameters are valid are shown.

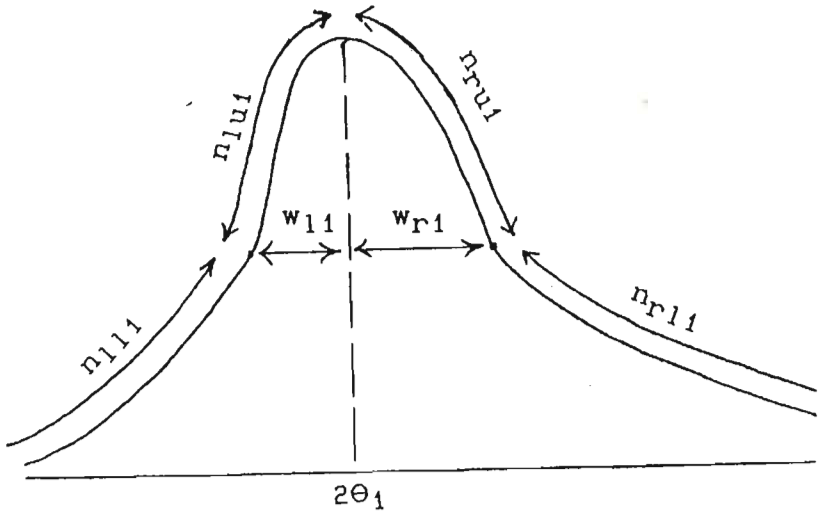

Fig 5.2 The upper and lower shape parameters.

The integrated intensity is determined by the following considerations. For the Lorentzian, half of the area under the curve is contained in the range between the peak maximum and the halfwidth. For the Gaussian this factor is 0,7610 (refer to Abramowitz and Stegun, 1972). The integrated intensity for the α_1 peak is therefore (compare equation 3.2):

$$I_{int} = \tfrac{1}{2} I_o \sqrt{\pi/\ln 2}\,[[(1 - n_{ll1})\ 0,3390 + (1 - n_{lu1})\ 0,7610]\ w_{l1}$$
$$+[(1 - n_{rl1})\ 0,3390 + (1 - n_{ru1})\ 0,7610]\ w_{r1}]$$
$$+\tfrac{1}{2} I_o \pi\ [[n_{ll1}\ 0,5 + n_{lu1}\ 0,5]\ w_{l1}$$
$$+[n_{rl1}\ 0,5 + n_{ru1}\ 0,5]\ w_{r1}]$$

The contribution of the α_2 component has the same form. In chapter 6 tests using this modification are discussed. However, the modification was not implemented further.

5.8.3 Change of subroutine GLESYS.

As mentioned in section 5.5 the program PPP has the option of fixing certain parameters to be equal to others, eg, the form of the α_2 peak could be set to that of the α_1 peak by setting the α_2

widths and shapes equal to those of α_1. In this case, only the α_1 widths and shapes will be refined and at the beginning of each refinement cycle, the α_2 parameters are set to those of the α_1 parameters in subroutine RESET. Then, the matrix $\underset{\sim}{A}$ in equation 5.6, ie, the matrix of derivatives, is calculated in GLESYS, each element of the matrix being calculated by the equation

$$A_{ij} = \left[\frac{\partial Y_i}{\partial P_j} \right]_{2\Theta(i)}$$

$$= \left[\frac{Yc[par(j)+delpar(j)]-Yc[par(j)-delpar(j)]}{2\ delpar(j)} \right]_{2\Theta(i)} \qquad [5.6]$$

where par(j) is the parameter value and delpar(j) is the increment with which par(j) is changed in order to calculate the derivative. The value of delpar used is 0,1 of the error of the parameter value from the previous cycle.

In the original program, subroutine GLESYS was not written correctly for the case in which the form of the α_2 peak was set to that of α_1. To understand this let us consider the parameters influencing the right half of the peaks, say w_{r1} and w_{r2}. The parameter w_{r1} is defined as a parameter to be refined while w_{r2} is "not refined". At the beginning of each cycle w_{r2} is simply set equal to w_{r1} in subroutine RESET. However, in calculating the elements A_{ij} of the derivative matrix using equation 5.6, when j refers to the parameter w_{r1} the derivative was calculated by changing the value of w_{r1} only and not w_{r2}. Thus the observations on the right half of the α_2 peak were not able to influence the refinement of the parameter w_{r1}/w_{r2} correctly.

Fig 5.3a shows the result of seven cycles of refinement of the akermanite reflection at 57,54° 2Θ. It is clear that the fit on the right flank of the α_2 peak is very poor. The residual R dropped to 0,0437 after 3 cycles and then rose to 0,0606 after the seventh cycle with oscillating behaviour in between.

The subroutine GLESYS was therefore modified in such a way that when the option is used that sets the form of the α_2 peak equal

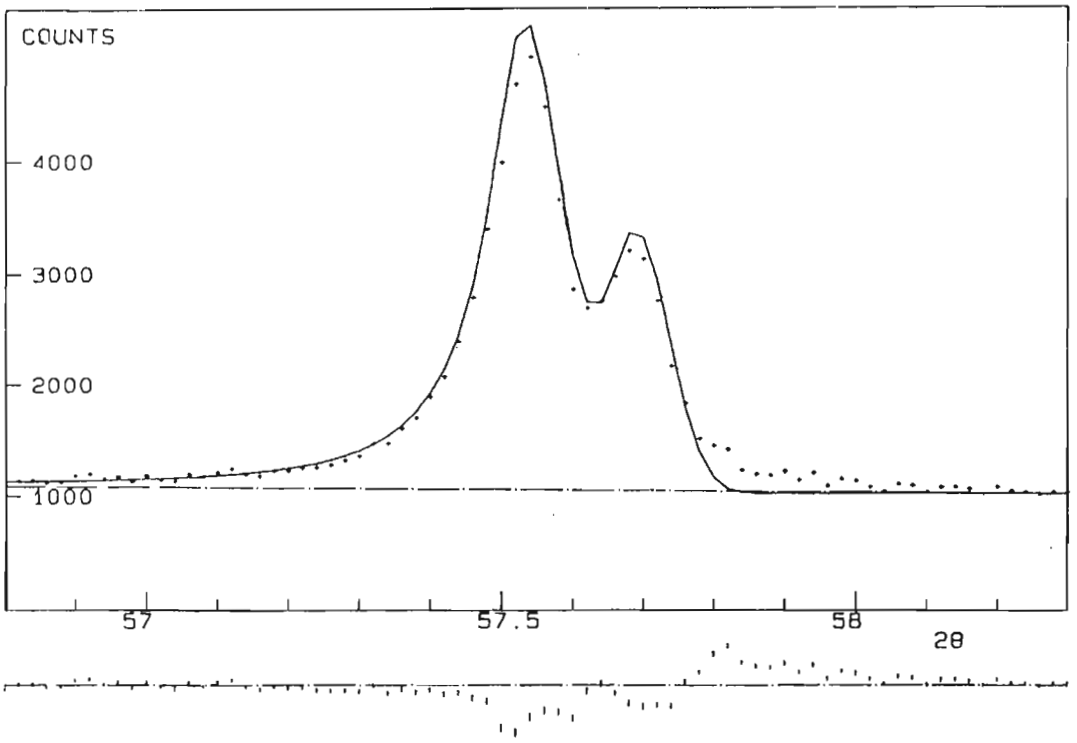

Fig 5.3a Fit after 7 refinement cycles with incorrect version of GLESYS, sample AK, R = 0,0606

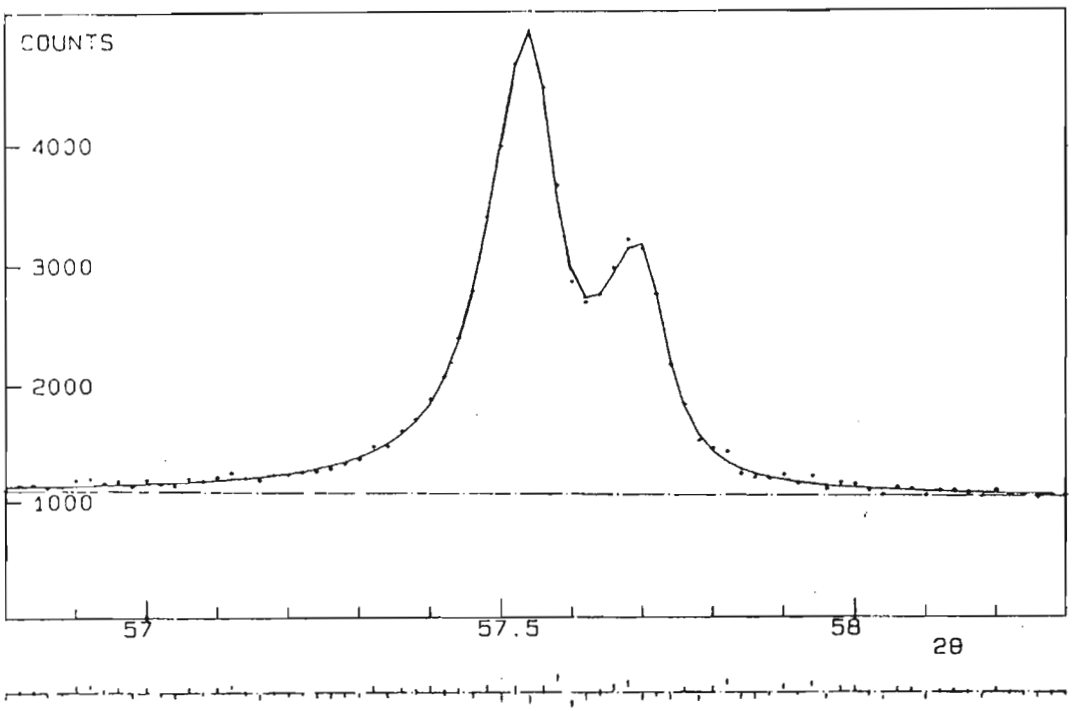

Fig 5.3b Fit after 4 refinement cycles with modified version of GLESYS, sample AK, R = 0,0190

to that of the α_1 peak, the α_2 parameters do influence the fit. The matrix element A_{ij} involving parameter w_{r1} (say) was calculated by changing not only the value of w_{r1} but also that of w_{r2}. Fig 5.3b shows the refinement using the modified GLESYS. As can be seen the fit is greatly improved on the right flank of the α_2 peak. The residual is now 0,0190.

5.8.4 The weight matrix.

PPP was originally designed for mainframe operation. It was also implemented and modified on the ICL mainframe at UDW. It was then modified to run on personal computers. One of the disadvantages of the PC is that its memory is limited to 640 kB. The program PPP uses several arrays of large dimensions, and it was found that a maximum of about 300 observations could be fit and a maximum of 29 parameters could be refined using the original program. Since 11 of the parameters were the profile parameters, this meant that the positions and intensities of only 9 peaks could be refined. Also, for an increment of 0,02° 2θ between observations the maximum range of the refinement is 6° 2θ. Since the form of the weighting matrix used was always diagonal, this matrix ($\underset{\sim}{W}$ in equation 5.5) was replaced by a simple vector array. In order to do this, the form of the equations in subroutine LSQ which evaluates equation 5.5 was changed. With this modification, it was found possible to fit 500 observations and refine 57 parameters. This means that 23 peaks in a range of 10° 2θ can be refined on a 640 kB PC.

5.9 Numerical step program

For peaks which are well separated (no overlap), the area of the peak can be calculated simply by using the trapezoidal approximation

$$I = \Sigma_{i=1,n-1}[Yo(i+1)+Yo(i)]*XINC/2 \qquad [5.7]$$

XINC is the 2θ separation between observations (which is constant) and the sum is taken over all the observations which

define the peak. This method just calculates the area of the peak as the sum of the strip areas under the straight lines joining adjacent observations. From this area, the area due the background intensity must be subtracted.

Chapter 6 PROCEDURES AND STRATEGIES OF PROFILE REFINEMENT

6.1 Division of the spectrum into ranges

Two powder data sets were analysed, a standard sample of silicon (Si) and the mineral akermanite (AK). The peaks of Si were well separated and therefore could be refined individually. However, for akermanite, the peaks were not well separated and there was severe overlapping at high angles. It was therefore not feasible to refine the akermanite peaks separately. However, the entire spectrum of the akermanite data was not analysed in one refinement but was split into small ranges for the following three main reasons.

1) The profile parameters are known to be functions of 2θ. It was decided to determine this functional dependence experimentally without attempting to describe it analytically. If the entire spectrum was analysed in one refinement using PPP, this would generate only average values of the profile parameters for the entire spectrum. The spectrum was therefore divided into several smaller ranges, and each range analysed individually, assuming that the profile parameters were approximately constant within one range.

2) The background curve should be continuous and smooth but is not linear over the entire spectrum. However, if the spectrum is split up into small enough ranges, then the background curve could be taken to be approximated by a linear function in each range. In our program PPP, the background was calculated linearly using the slope of the background (parameter sl) and the value of the background at the left edge of the refinement range, (parameter bgl).

3) The progam PPP, being compiled and run on personal computers, could only use a maximum of about 420 Kb of memory. This led to a limitation on the number of observations that could be fitted to 500 points and the number of parameters that could be refined to a maximum of 57. Since the akermanite pattern had about 6700 observations and 200 peaks, the analysis of the data had to be carried out on smaller ranges which could be accommodated by the program on the PC.

The spectrum of akermanite was split up into the smaller ranges shown in table 6.1.

Table 6.1 Refinement ranges of akermanite spectrum.
R - residual from refinement, R_S - minimum residual from counting statistics (see section 5.3).

Range (2Θ)	No of peaks	final run ref. no.	R	R_S
35,04 - 43,00	9	102	0,0323	0,0103
43,40 - 48,20	4	90	0,0330	0,0138
48,20 - 53,00	8	91	0,0272	0,0089
54,60 - 59,00	6	107	0,0306	0,0211
59,10 - 64,06	10	122	0,0330	0,0189
64,10 - 68,10	6	94	0,0301	0,0170
68,80 - 73,60	8	95	0,0334	0,0233
73,60 - 79,90	13	116	0,0275	0,0224
79,90 - 83,65	5	117	0,0309	0,0257
83,65 - 89,30	11	100	0,0315	0,0254
89,50 - 97,00	13	103	0,0424	0,0326
97,10 - 100,10	6	101	0,0322	0,0333
100,10 - 109,00	20	99	0,0417	0,0312
109,00 - 113,00	9	104	0,0336	0,0333
113,20 - 118,50	11	96	0,0390	0,0312
118,50 - 123,60	8	125	0,0403	0,0330
123,60 - 129,60	10	97	0,0401	0,0348
129,80 - 137,80	16	106	0,0398	0,0314
137,80 - 144,00	7	124	0,0379	0,0285

The end points of the ranges were chosen to lie in regions of the spectrum where there was as large a gap as possible between neighbouring peaks.

6.2 Determination of the background

The choice of the values of the background can influence the other parameters in the refinement systematically. Therefore when the background parameters are refined together with the profile parameters and peak positions and intensities the parameters will be correlated. Such a refinement of all parameters was carried out on akermanite in the range 59,10 - 64,06° 2Θ containing 8 peaks. The final background and profile parameters are shown in table 6.2a (run R1). In this table the widths listed are $2w_l$ and $2w_r$ ie not halfwidths but twice these values, ie the full width

at half maximum (FWHM) of the equivalent symmetrical peak.

Table 6.2a Background and profile parameters with errors in parentheses. Akermanite, range 59,10 - 64,06° 2Θ (Runs defined in the text). Widths listed are $2w_l$ and $2w_r$, ie equivalent full width.

parameter	R1	R2	R3
bg1	923 (10)	924 (9)	924 (-)
s1	14,8 (3,7)	14,8 (-)	14,8 (2,9)
r_{21}	0,498 (0,009)	0,498 (0,009)	0,498 (0,009)
$2w_l$	0,135 (0,004)	0,135 (0,004)	0,135 (0,004)
$2w_r$	0,098 (0,004)	0,098 (0,004)	0,098 (0,004)
n_l	0,94 (0,05)	0,94 (0,05)	0,94 (0,05)
n_r	0,94 (0,08)	0,94 (0,07)	0,94 (0,07)

Table 6.2b Correlations of background parameters with other parameters. a_1 and i_1 are the position and integrated intensity of peak 1.

	bg1	s1	r21	w_l	w_r	n_l	n_r	a_1	i_1	a_2	i_2	a_3	i_3	a_4	i_4	a_5	i_5	a_6	i_6	a_7	i_7	a_8	i_8
r1 bg1	1.0	-.61	.00	-.03	.05	-.19	-.14	.07	-.36	-.08	-.43	.07	-.25	-.05	-.32	-.05	-.10	.00	-.19	-.05	-.21	-.02	-.04
s1	-.61	1.00	.08	.04	-.00	-.10	-.15	-.06	.17	.04	.05	-.00	.02	.00	-.16	-.06	.03	-.02	-.27	.01	-.37	-.05	-.51
r2 bg1	1.0	--	.07	-.01	.06	-.31	-.30	.04	-.33	-.07	-.50	.09	-.30	-.07	-.53	-.11	-.11	-.01	-.46	-.06	-.59	-.06	-.52
r3 s1	--	1.00	.11	.03	.03	-.27	-.30	-.02	-.07	-.01	-.29	.05	-.17	-.04	-.47	-.12	-.04	-.03	-.49	-.03	-.64	-.07	-.68

It is interesting to understand qualitatively the nature of the correlation. The correlation coefficients between the background parameters and other parameters are shown in table 6.2b. The correlation of bg1 with the intensities is quite strong (coefficients -0,36 -0,43 -0,25 -0,32 -0,10 -0,19 -0,21 -0,04). The correlation coefficients are all negative as an increase in background causes a decrease in intensity of the peaks to fit the observations. The background parameter bg1 has negative correlation with the shape parameters n_l and n_r (coefficients -0,19 and -0,14). This can be understood as an increase in background would cause the pseudo-Voigt function to become more Gaussian (ie fall off more quickly to zero) and cause the shape parameters to decrease towards 0, in an attempt to fit the observations. The bg1 parameter does not correlate much with the

widths (coefficients -0,03 and 0,05) nor with the peak positions (coefficients 0,07 -0,08 0,07 -0,05 -0,05 0,00 -0,05 -0,02). The correlation of the background slope parameter s1 with the other parameters is similar. It correlates negatively with the shapes and not with the widths. It does not correlate with the peak positions. s1 does correlate with intensities (coefficients 0,17 0,05 0,02 -0,16 0,03 -0,27 -0,37 -0,51). This trend in coefficients is due to the fact that the slope increases the background value towards the right hand part of the range.

When both bg1 and s1 are refined the correlation effect with background is shared between the two parameters. This can be seen from the refinements R2 and R3. These refinements are similar to refinement R1 but in R2 s1 was kept constant and in R3 bg1 was kept constant. The correlation coefficients are also shown in table 6.2b. It can be seen that in general the correlation coefficients are roughly equal to the sum of the two correlation coefficients obtained when both background parameters were refined (R1). These strong correlations of the background with the intensities show that the choice of a suitable background is very important for obtaining accurate integrated intensities for crystal structure refinement. However, in refining the background in ranges, although the fit between Yo and Yc would be very good, the background at endpoints of the adjacent ranges would not be continuous. Fig 6.1 shows the refinements of the background together with the other parameters in the two neighbouring ranges (59,10 - 64,04) and (64,10 - 68,10) of akermanite. The discontinuity shows that the background determined in such a manner would not be satisfactory.

To obtain a fairly smooth background, two methods can be suggested.

1) The entire spectrum is analysed by refining the background for each individual range. Each refinement will produce background values for the left and right endpoints of the range. At a common endpoint of two adjacent ranges, the "correct" background value can be defined as the average of the values obtained in the two ranges. The refinements can now be repeated defining the background by linear interpolation between the endpoint values.

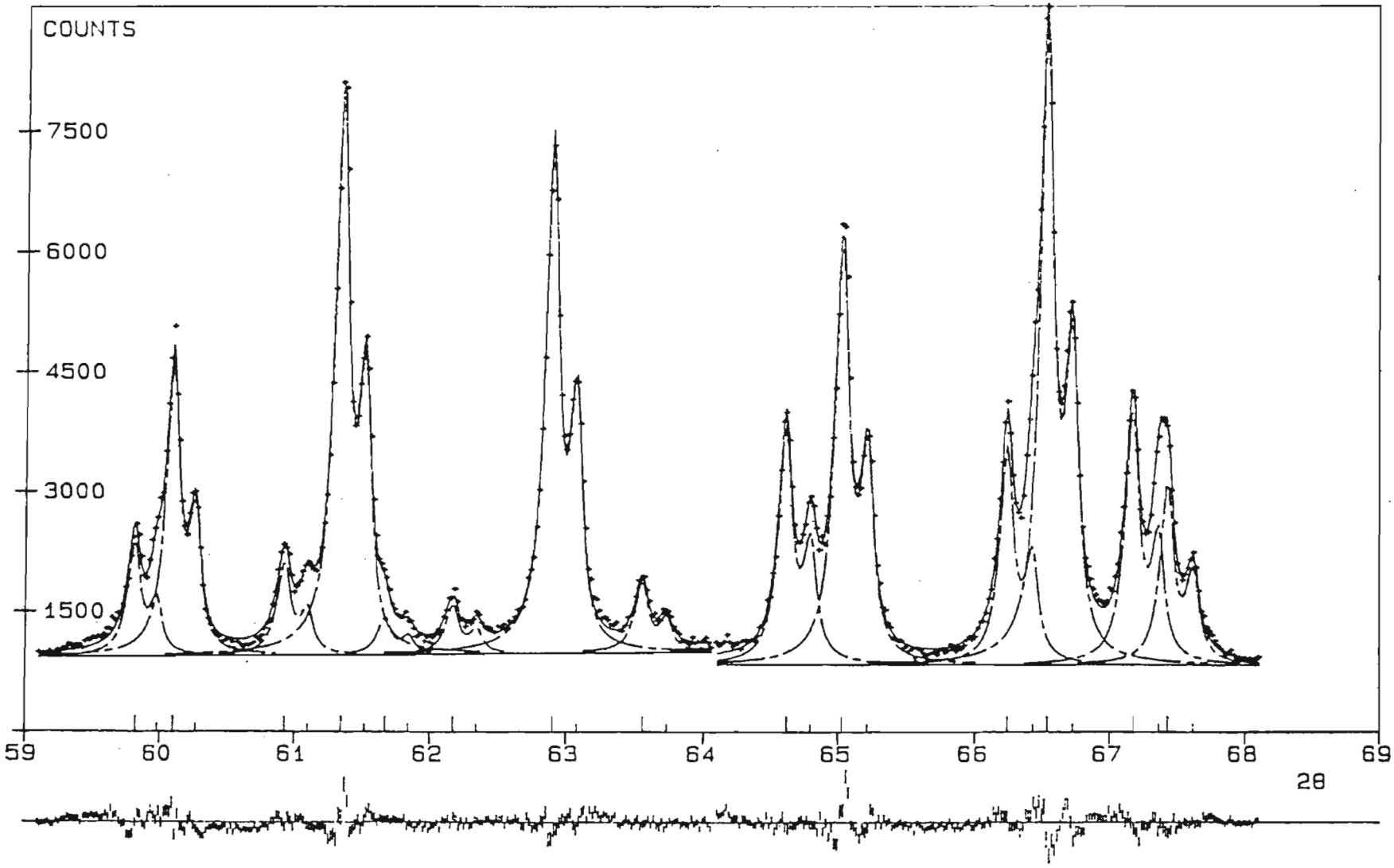

Fig 6.1 Refinement of background in the two ranges 59,10 - 64,06 and 64,10 - 68,10.

2) The background is initially determined for the entire spectrum by inspection without refining the other parameters (ie determine a global background). These background values (global background) are then used in analysing the spectrum, and if need be, they are adjusted by trial and error to obtain a better fit. This method is able to cope with a highly non-linear background. In our work, we have used this method and it is discussed in the next section.

6.3 Estimation of the global background function

The determination of a smooth (global) background function was based on the identification of regions of lowest intensity in the diffraction pattern in gaps between clusters of peaks. It was assumed that in these regions the contributions of the Bragg reflections was zero or very low. The regions identified are listed in table 6.3. The observations Yo(i) in these regions were smoothed, the smoothed intensities So(i) being calculated as running averages of nine points using the equation

$$So(i) = [\Sigma_{K=i-4,\, i+4} Yo(K)]/9$$

A candidate for a background value in a low level region was taken to be the minimum smoothed value in that region. These minimum values are also shown in table 6.3. Fig 6.2 shows a plot of the smoothed observations in one such region. Fig 6.3 shows a plot of all the minima chosen and the first attempt at passing a global background curve through (below) these points. It is clear that in many of the low level regions considered, the minima cannot be accepted as actual background values. The following factors may have contributed to raising many of the minima above the background level.

1) In regions far from Bragg peaks the background exhibits several broad areas of enhanced intensity (due, eg to impurities). If such an enhanced background happens to occur in a low level region between clusters of peaks, it would not be noticed as such.

2) Some low level regions were narrow and had large peaks close to them. The tails of these peaks could contribute appreciably to the intensity minimum.

Hence many of the minima are considered to be above the actual background and the background curve had to be taken below them.

The further modification of this background function during the profile analysis is discussed later.

Table 6.3 Intensity minima in low level regions of the diffraction pattern

low level region 2θ range	position of minimum	minimum smoothed background
10,22 - 11,40	10,78	723,00
12,22 - 13,80	12,96	820,11
18,02 - 19,00	18,60	1200,00
21,02 - 22,40	21,88	1173,00
25,42 - 26,40	25,90	1007,00
27,02 - 27,80	27,78	1224,00
29,22 - 29,80	29,56	1603,00
34,42 - 35,40	34,72	960,80
39,42 - 41,20	39,96	1003,30
	41,02	1027,00
42,02 - 43,80	42,20	1005,00
	43,56	1085,00
45,42 - 46,00	45,62	1098,22
46,22 - 47,20	46,74	1050,00
47,82 - 48,60	48,08	1216,00
52,62 - 55,00	54,32	1022,70
58,66 - 59,40	59,17	975,44
63,62 - 64,60	64,14	1106,44
73,22 - 74,40	73,58	765,11
79,42 - 80,20	79,76	921,56
83,42 - 84,00	83,60	811,11
87,82 - 88,40	88,06	722,33
91,02 - 92,00	91,70	599,33
96,62 - 97,20	97,04	716,00
99,82 - 100,80	100,20	673,33
108,02 - 109,00	108,84	640,22
112,82 - 113,80	113,18	741,56
123,22 - 124,00	123,52	684,87
129,22 - 130,00	129,60	697,67
134,42 - 135,20	134,88	771,89
136,62 - 138,60	137,84	857,00
141,22 - 142,20	141,72	892,33

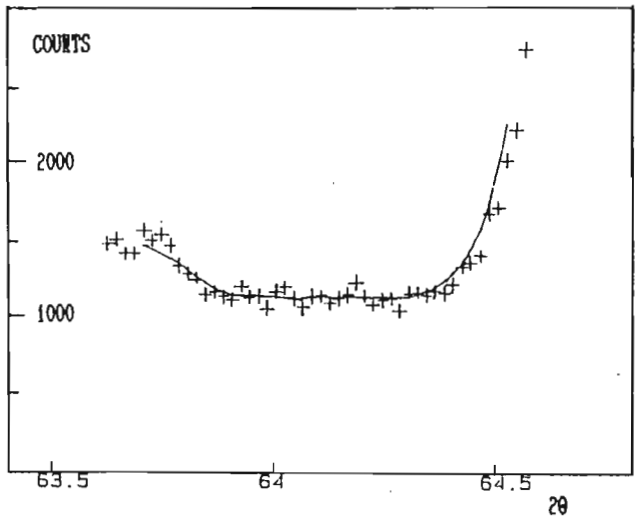

Fig 6.2 Plot of intensities in a low level region. The observations are shown as crosses and the the smoothed values as a continuous curve.

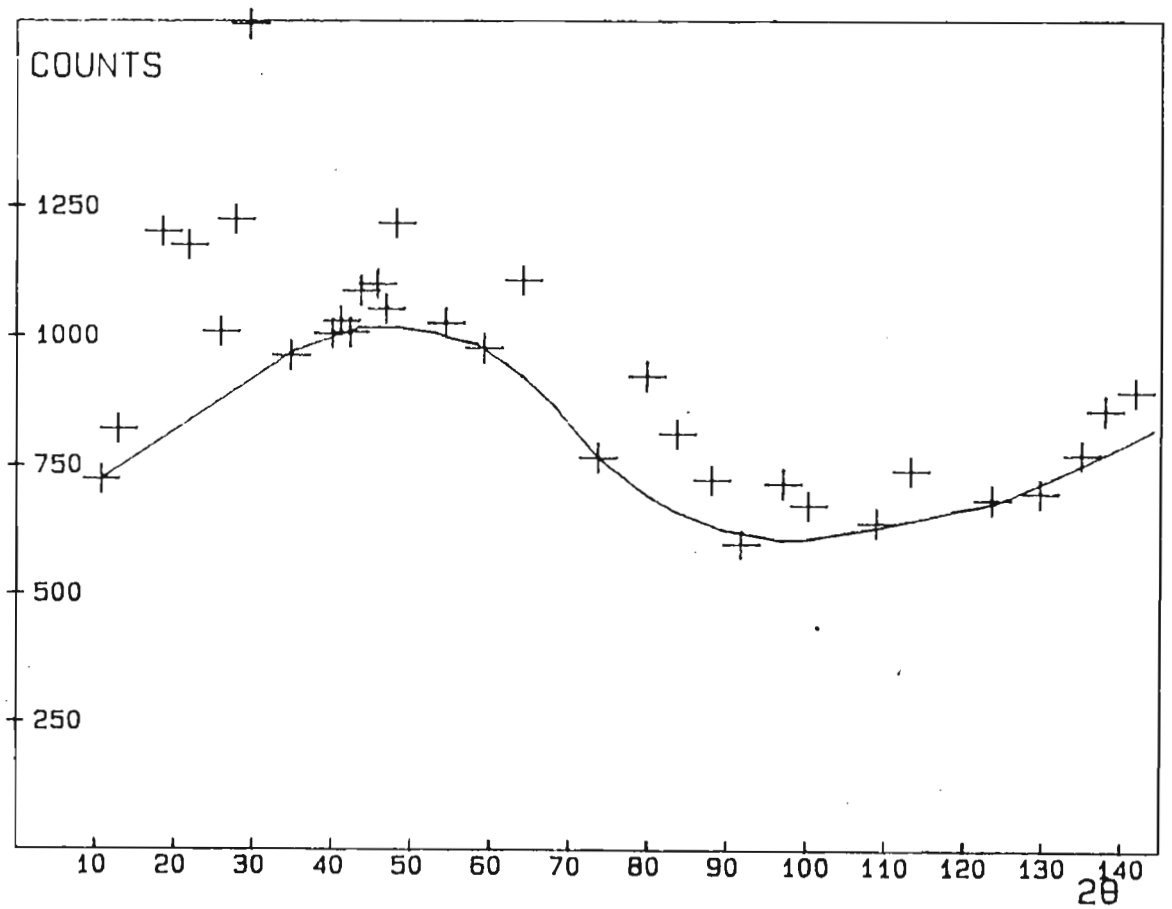

Fig 6.3 Graph of the initial global background. The individual (smoothed) intensity minima are shown as crosses.

6.4 Different forms of α_1 and α_2 components

In refining the parameters and intensities of the peaks, the profile parameters of the α_2 peak could be allowed to differ from those of the α_1 peak. To test whether such refinements were satisfactory two refinements were carried out in the akermanite range 48,20 - 49,50, one which fixed the form of the α_2 peak to that of the α_1 peak (constrained refinement), and the other which allowed the forms to differ (full refinement). The parameter values which resulted from these refinements are shown in table 6.4.

Table 6.4 Comparison of profile parameters when the form of the α_2 peak differs from that of α_1.

parameter	$\alpha_1 \neq \alpha_2$	$\alpha_1 = \alpha_2$
r_{21}	0,368 (0,045)	0,518 (0,016)
$2w_{11}$	0,115 (0,005)	0,133 (0,004)
$2w_{12}$	0,161 (0,009)	
$2w_{r1}$	0,117 (0,006)	0,085 (0,004)
$2w_{r2}$	0,071 (0,005)	
s_{11}	0,84 (0,10)	1,14 (0,06)
s_{12}	5,15 (0,34)	
s_{r1}	2,32 (0,15)	1,14 (0,10)
s_{r2}	0,37 (0,29)	

For the full refinement, we see that the parameters differ markedly, and attain unacceptable values. Especially the left hand shape parameter of α_2 (n_{12}) attains a value of 5,15. This causes the α_2 contribution to have an extremely large secondary maximum (see fig 3.6). However the fit is good and the form of the α_1/α_2 doublet is satisfactory (see fig 6.4a). The explanation for this unexpected behaviour is that the secondary maximum of the α_2 peak falls under the maximum of the α_1 peak. For this to occur the left width of α_2 ($2w_{12}$) attains the large value of 0,16. However attaining a good fit with such physically meaningless parameters is not satisfactory. The constrained refinement shows a fit that is as good (fig 6.4b) with parameters remaining within acceptable limits.

It was therefore felt best to keep the form of the α_2 peak fixed to that of the α_1 peak. This would also have the additional advantage of reducing the number of parameters refined.

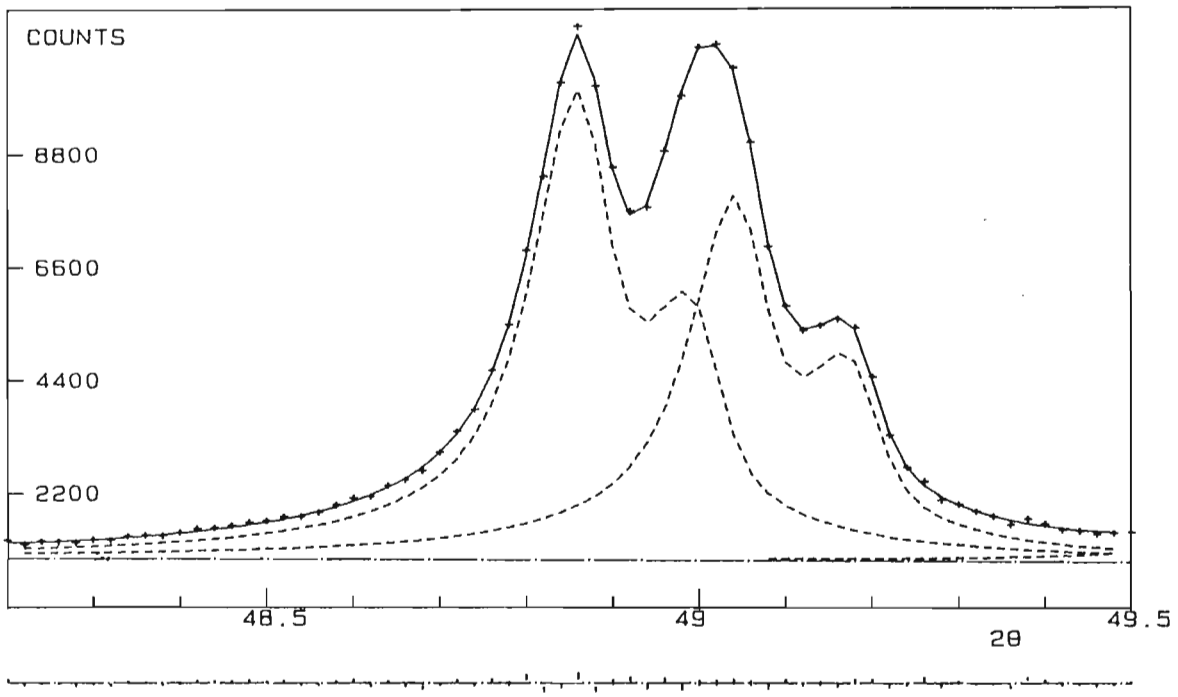

Fig 6.4a Full refinement: the form of the α_2 peak was free from that of the α_1.

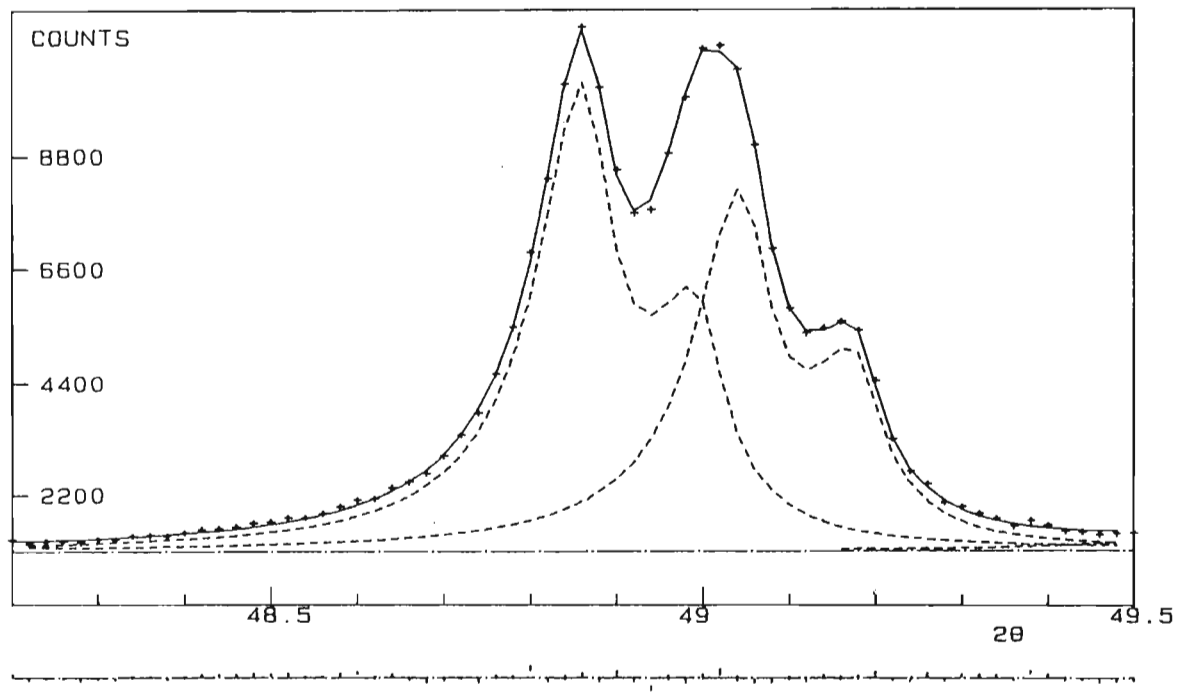

Fig 6.4b Contrained refinement: the form of the α_2 peak was fixed to that of the α_1.

6.5 Upper and lower shape parameters - tests

The option of fitting two shape parameters to each side of the peak ie, a total of four independent shape parameters has been described in section 5.8.2. The aim was to produce a better fit to the peak profile by fitting the upper part of the peak (within the halfwidth) and the tail of the peak (beyond the halfwidth) using different shape parameters. It was hoped that this would be particularly useful in the low angle range of the diffraction pattern where the asymmetric peak broadening due to instrumental factors is particularly strong. The limits for values of the shape parameters defining the upper portions of the peak could be taken a little wider, ie slightly below zero or larger than 1,5 since it is only in the lower part of the peak that these shape parameter values generate a negative region or an extra peak (see figure 3.6).

To test the effect of using the "half shapes" a (low angle) range (37.28 - 40.9) of akermanite was analysed. Table 6.5 shows the profile parameters obtained using half shapes (4 shape parameters and full shapes (2 shape parameters) compared.

Table 6.5 Comparison of refinements with two shape parameters (left column) and four shape parameters (right column). del is the difference of parameter values.

parameter	full shape parameters	half shape parameters	del	del/sig
r_{21}	0,519 (0,021)	0,521 (0,021)		
$2w_l$	0,140 (0,007)	0,134 (0,008)		
$2w_r$	0,075 (0,005)	0,085 (0,007)		
s_{ll}	1,11 (0,09)	1,17 (0,13)		
s_{lu}	1,11 (-)	1,97 (0,69)		
s_{ru}	0,74 (0,00)	-0,22 (0,84)		
s_{rl}	0,74 (-)	0,60 (0,09)		
Intensity 1	2300 (28)	2297 (28)	3	0,11
Intensity 2	2406 (28)	2403 (28)	3	0,11
Intensity 3	1044 (20)	1042 (20)	2	0,10
Intensity 4	678 (17)	676 (17)	2	0,12
R-value	0,0359	0,0362		

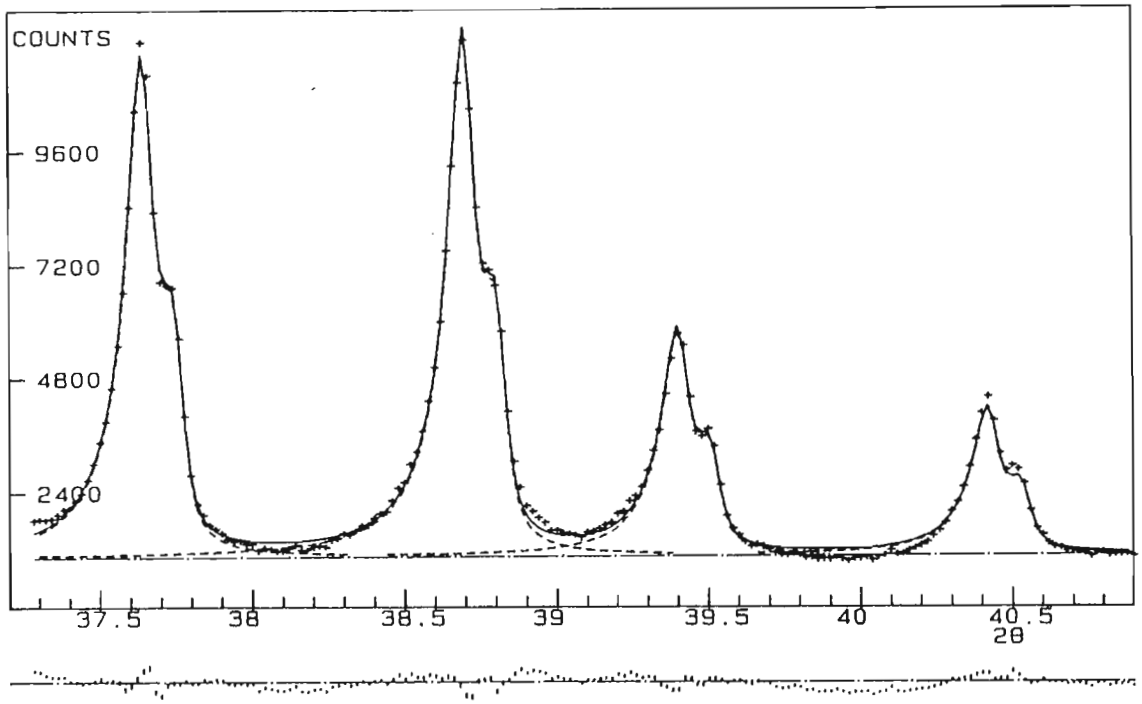

Fig 6.5a Refinement of akermanite range (37,28 - 40,90) using full shape parameters.

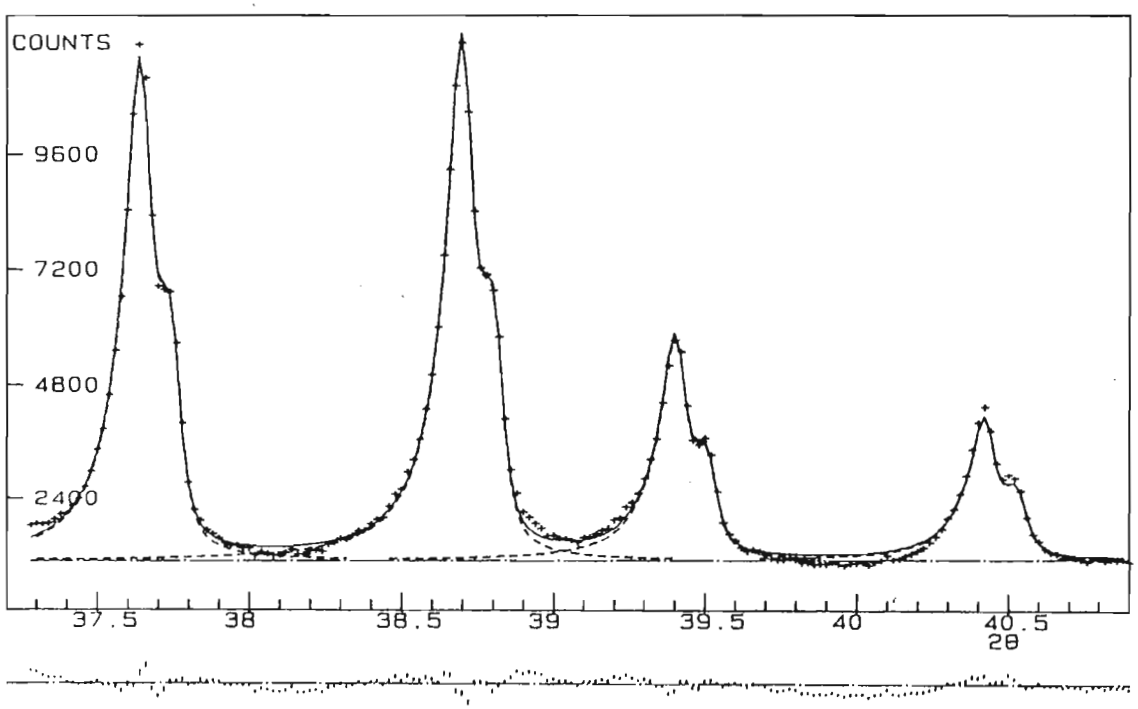

Fig 6.5b Refinement of akermanite range (37,28 - 40,90) using half shape parameters.

The plots of these two refinements are shown in figures 6.5a and b. Both appear to fit the observations equally well. In other words, no improvement was attained through increasing the number of parameters refined. In fact the R-values obtained with full shapes was lower than with half shapes (0,0359 as opposed to 0,0362). The differences between the calculated intensities obtained in the two refinements (del in table 6.5) are much smaller than the errors of the observed intensities (see del/sig in table). It can therefore be seen that this modification of fitting the peaks did not produce any improvement. The upper shape parameters are seen to be the ones that deviate far from the previous values, n_{1u} being 1,97 and n_{ru} -0,22, and their errors are very large. This can be understood as being due to the fact that the values are determined from very few observations.

The half shape parameters were tested on other ranges of akermanite and on individual silicon peaks with similar results and these parameters were therefore not used further.

6.6 Detailed analysis of individual ranges

The profile refinement strategies developed here are suitable for the stage of analysis at which the unit cell parameters of the structure are well known. If this is not the case more general methods have to be used to identify peak positions, after which a search is made for suitable cell parameters according to which the peaks are indexed. Such methods are not dealt with in this study and the evaluation of the akermanite diffraction pattern was undertaken using "known" cell parameters and space group. The chemical formula of the Fe-akermanite sample studied is $CaMg_{0,4}Fe_{0,6}Si_2O_7$. The structure was assumed to be isomorphous with Mg-akermanite $CaMgSi_2O_7$. This isomorphism has been shown by transmission electron microscope studies to exist for these mixed crystals in the range 0 to 70% replacement of Mg by Fe (Seifert, 1984, private communication). The crystal structure of Mg-akermanite was reported in a single crystal study by Kimata and Ii (1981). The space group is tetragonal $P\bar{4}2_1m$ with lattice parameters a = 7,835(1) and c = 5,010(1) Å. The lattice parameters of the Fe-akermanite powder sample were a = 7,8751(8)

and c = 5,0146(7) Å (Seifert, 1984, private communication).

6.7 Preliminary refinement

The above lattice parameters were used to determine the 2θ-positions for all hkl-reflections and these positions were used as starting values for refinements in the individual ranges chosen as described in section 6.1. The five profile parameters (w_l, w_r, n_l, n_r and r_{21}) were refined together with the positions and integrated intensities of all the peaks. As mentioned previously, after initial testing the two options of:
1) allowing the α_1 and α_2 peaks to have different forms and
2) using independent upper and lower shape parameters
were not implemented in the full analysis of the spectrum. The background parameters were held constant having been determined as described in section 6.3. In each case a graph was plotted showing the Yo and Yc values for qualitative assessment of the fit.

In many of the ranges this procedure (refinement of all parameters except background) produced a satisfactory result. In some cases the shape parameters became quite large (up to 1,6) but as this was considered a preliminary stage these values were considered acceptable. In some cases, however, the inversion of the matrix failed in the refinement. Inspection of the parameter values after the last successful iteration showed that certain peaks had been displaced a great distance from their starting positions to rather meaningless positions where the profile function could not match the observed intensities. When a large displacement occurred it was invariably the case of a very weak reflection that fell near stronger peaks. Examples of this were the starting position 89,13° which fell on the α_2 position of a stronger reflection, and 114,58 and 115,14° which fell within a cluster of stronger peaks. In these cases the values of the starting positions identified were held fixed in a subsequent refinement which ran satisfactorily. In the high angle region between 118 and 144° the refinement failed for all ranges except the range 123,6 - 129,6°. In these ranges the shape parameters took on unacceptable values, for example n_r = 4,3 for the range

137,8 - 144,0°, and the R-values (see section 5.3) remained high. The reason for this poor behaviour of the refinement is probably that at these high angles the overlap is severe and the peaks are very broad so that in no region of the pattern is the intensity due only or mainly to one peak. In the range 123,6 - 129,6° one peak, namely the one at 124,48°, is much stronger than all the others, permitting a satisfactory refinement. The only way found to obtain satisfactory preliminary refinements in this high angle range was to fix the shape parameters at some suitable values.

6.8 The case of very close peaks

In many cases the 2θ positions for different reflections are identical due to crystal symmetry, eg the 431 and 501 reflections in the tetragonal crystal system. These reflections have to be refined as one peak and the integrated intensity of the sum and not the individual reflections is later used in the structure refinement.

When reflection positions are very close but not identical the same problem arises. For example, the 0 0 4 and 6 1 1 reflections of Fe-akermanite are expected at 2θ-values of 75,82 and 75,83° respectively. When these two starting positions were used the integrated intensities refined to values of -828 and +1633, the negative value being unacceptable. This separation of only 0,01° 2θ therefore appears to be insufficient for profile refinement as individual peaks, and such pairs of reflections also have to be treated as a single peak. Relections with a separation of 0,03° were refined successfully as separate peaks. In the Fe-akermanite diffraction pattern there happened to be no separations of 0,02°. Thus the strategy required was to refine as single peaks those whose separation was less than 0,02° 2θ and as separate peaks those whose separation was greater than 0,02° 2θ.

In the case of the presence of pairs of very close and of very weak peaks, the initial refinement did not progress satisfactorily. Further refinements were therefore done in which certain constraints to be discussed in the next section were placed on the parameters. When all possible ranges had been satisfactorily refined graphs were plotted of the various profile

parameters obtained as functions of 2θ (Fig 6.10a, b and c). From these the best functional dependence on 2θ was deduced for use in a final refinement.

6.9 The case of weak peaks

If a weak reflection occurred on the flank of a strong peak it often happened that the weak peak moved an unacceptably large distance from the starting position. In this way the secondary pseudo-Voigt function placed on the flank of a primary one could "improve" the fit of the primary peak by moving to an optimum position some distance from the position of the very weak reflection. The positions of such weak peaks were therefore kept constant in further refinements.

In the high angle region with severe overlap, due to the higher density of peaks and the broadening of the profile, the shifts of unconstrained weak peaks tended to be larger. In several cases negative intensities were generated for weak peaks (whether constrained to their positions or not). In these cases the intensities were set to zero so that the should not adversely affect the intensities obtained for neighbouring stronger peaks.

6.10 Effect of peaks outside the range.

The endpoints of the ranges were chosen to lie in regions of the spectrum where there was as large a gap as possible beteen neighbouring peaks. However, for some ranges, there were large peaks present just beyond the endpoints. These peaks were therefore included in the refinement of the adjacent range but keeping their intensities constant at values obtained in previous refinements. Figures 6.6a and b show the effect that the "outside peaks" have on the fit of the two adjacent ranges (59,10° - 64,06°) and (64,10° - 68,10°). When two neighbouring peaks are included in the analysis of each range (fig 6.6b) the fit is better at the 61,10° 2Θ endpoint than when they are excluded (fig 6.6a). The differences in integrated intensities obtained are, however, not very large. These differences, "del" in table 6.6, are not larger than the estimated errors ("sig" in the table) of the intensities. Nevertheless it is important to include outside peaks to yield better fits.

Table 6.6 Effect on intensity when outside peaks are considered

2Θ position	intensity with outside peaks	intensity without outside peaks	del	del/sig
59,82	351 (10)	355 (10)	4	0,40
60,08	927 (12)	930 (14)	3	0,23
60,93	294 (9)	297 (10)	3	0,03
61,35	1828 (17)	1819 (15)	9	0,55
61,67	116 (10)	111 (11)	5	0,50
62,17	168 (7)	171 (8)	3	0,40
62,90	1684 (14)	1698 (16)	14	0,93
63,57	257 (8)	273 (8)	16	2,00
64,62	765 (11)	771 (11)	6	0,55
65,03	1353 (13)	1361 (13)	8	0,62
66,24	721 (14)	718 (14)	3	0,21
66,54	2077 (18)	2085 (18)	8	0,44
67,16	838 (13)	838 (13)	0	0,00
67,42	581 (3)	584 (3)	3	1,00

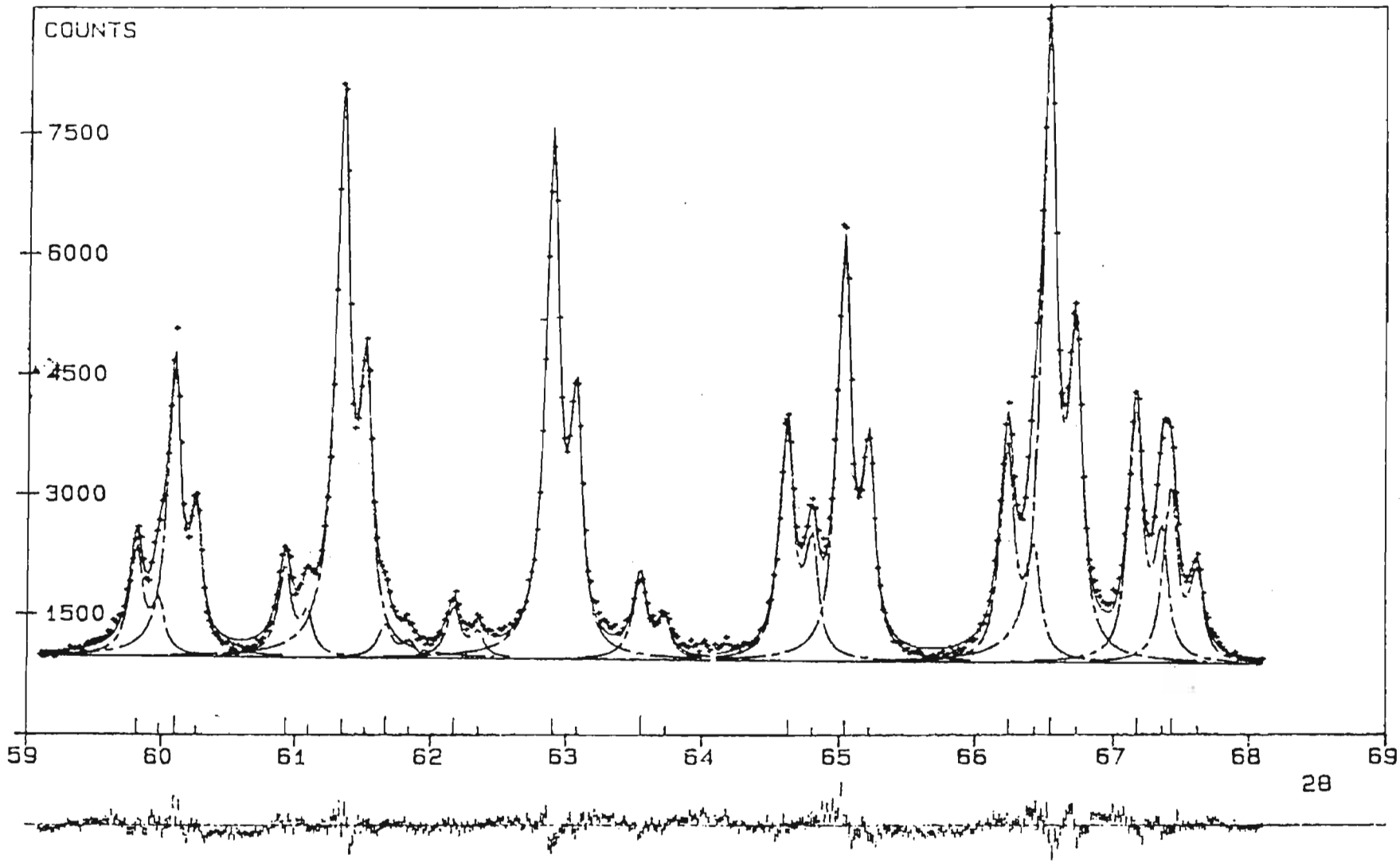

Fig 6.6a Refinement of the ranges 59,10 - 64,06 and 64,10 - 68,10 omitting "outside" peaks.

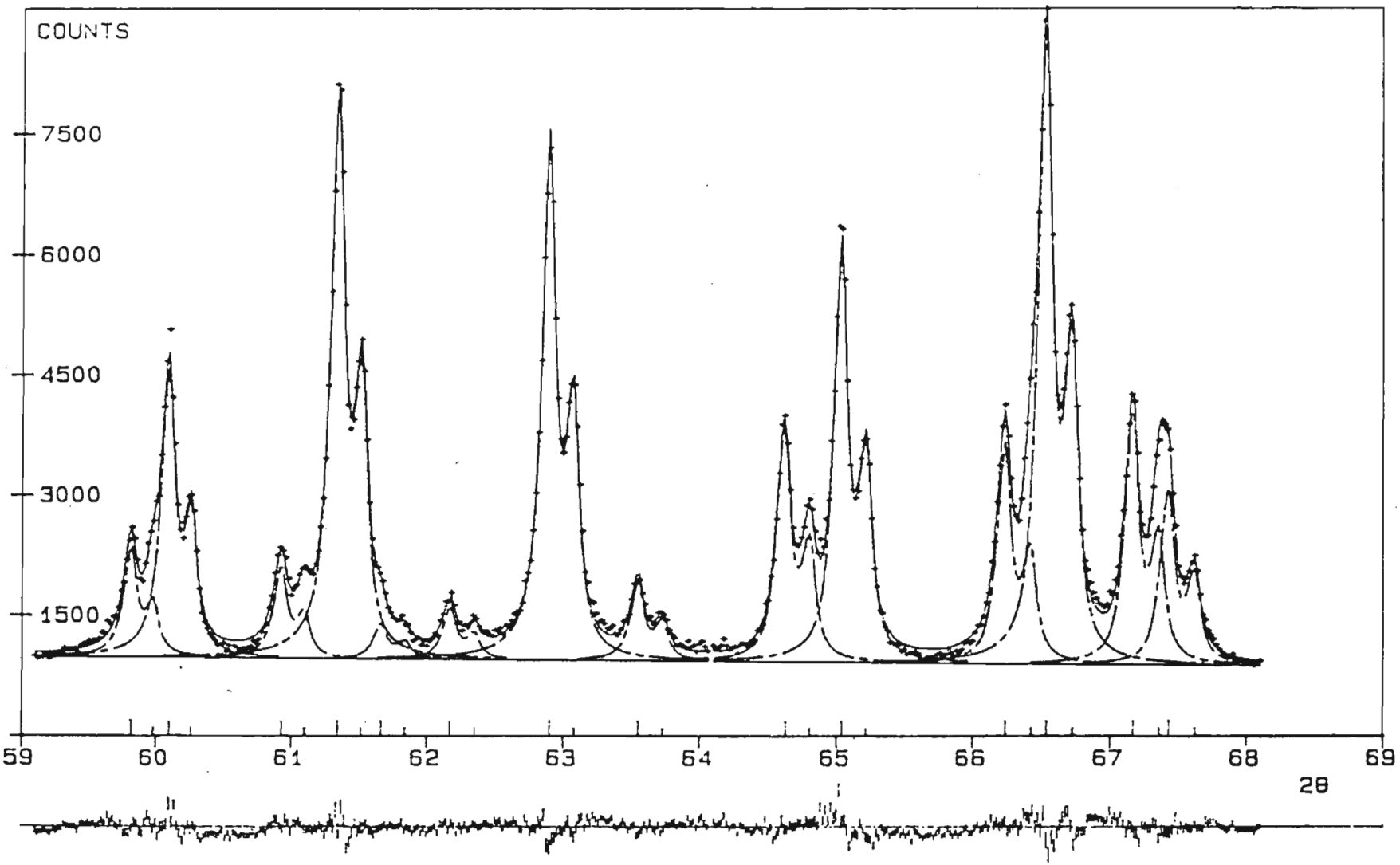

Fig 6.6b Refinement of the ranges 59,10 - 64,06 and 64,10 - 68,10 with "outside" peaks included.

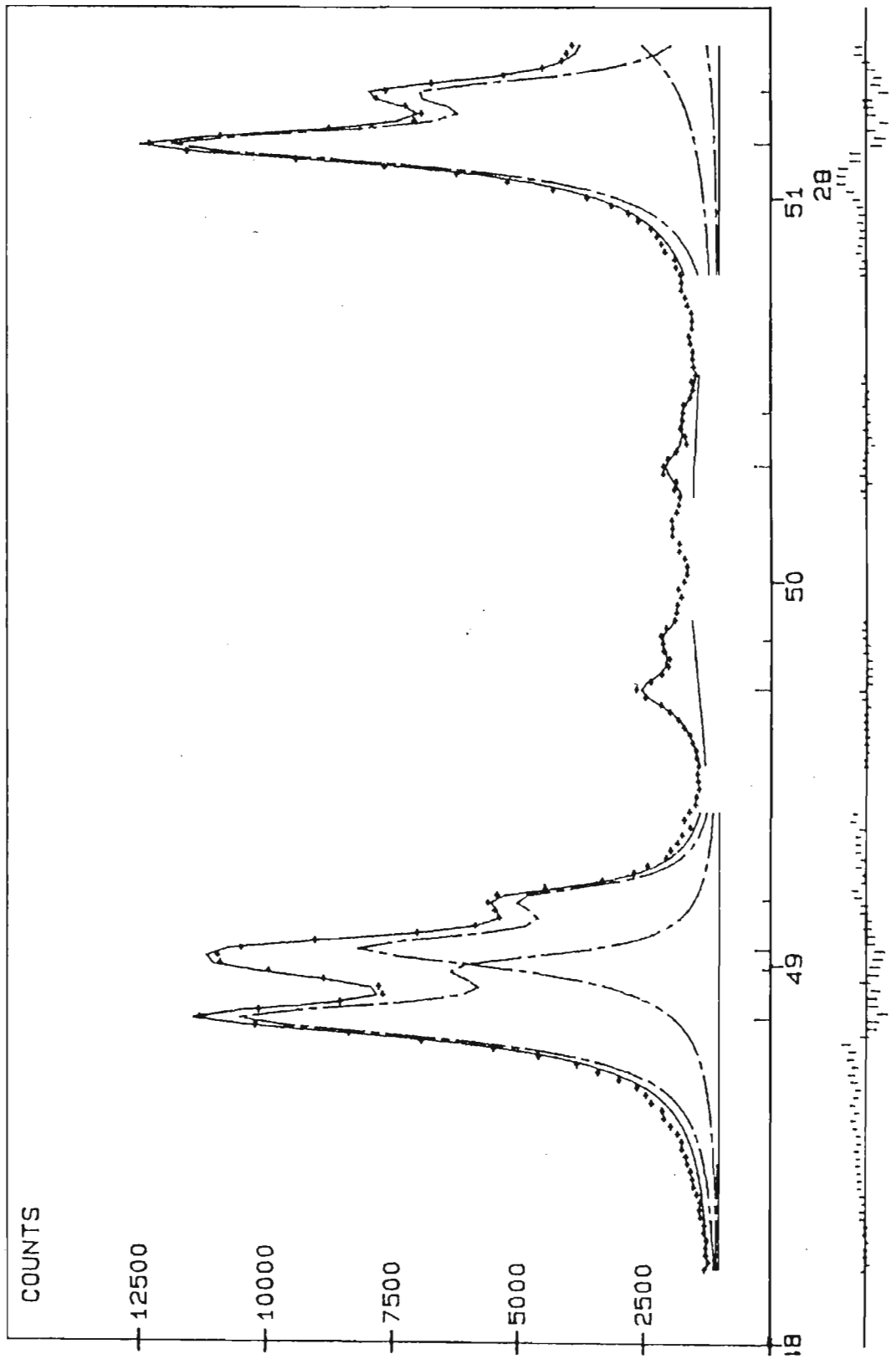

Fig 6.7 Refinement of peaks on spurious background.

6.11 Regions of spurious intensity

Several regions of spurious intensity occured. These were either sharp peaks at positions where no akermanite peaks were expected, eg, at 26,7 and 30,1° 2θ (see appendix 1). This is likely to be due to some crystalline impurity. These were in the low angle region and care was taken in determining the integrated intensity of neighbouring akermanite peaks (by numerical integration see section 6.15). It is possible but unlikely that further impurity peaks occurred at peak positions of akermanite peaks in which case they would go unnoticed and cause the intensity to be too high. A peak on the flank of an akermanite peak would not affect the intensity obtained by profile fitting too seriously. Evidence of spurious intensity on the flank of a peak is noticeable at 41,6 and 42,5° 2θ.

Broad regions of spurious intensity are also visable eg, at 19,7°; 49,4 - 50,8 and 53,0 - 54,0° 2θ (see appendix 1). These could be due to poorly crystalline impurities in the sample or regions of some stray radiation in the diffractometer geometry. The 49,4 - 50,8° region was simply omitted from the refinement of the range 48,2 - 53,0° in which it occurred.

This region however included two weak akermanite peaks at 49,71 and 50,28. As the background in this region appeared to be very uneven the two peaks were refined individually, each over a small range keeping their profile parameters and positions constant but allowing the background parameters bg1 and s1 to refine. Fig 6.7 shows the fit for these two peaks including the short sections of linear background.

6.12 Adjustments to the global background

The first approximation to the global background function obtained as described in section 6.3 did not prove to be entirely satisfactory over the whole diffraction pattern. For example the background had to be reduced slightly where the calculated intensities were found to be too far above the observations. In the region between 73 and 89° 2θ, however, it was found necessary to raise the background very sharply. Fig 6.8a shows the fit for

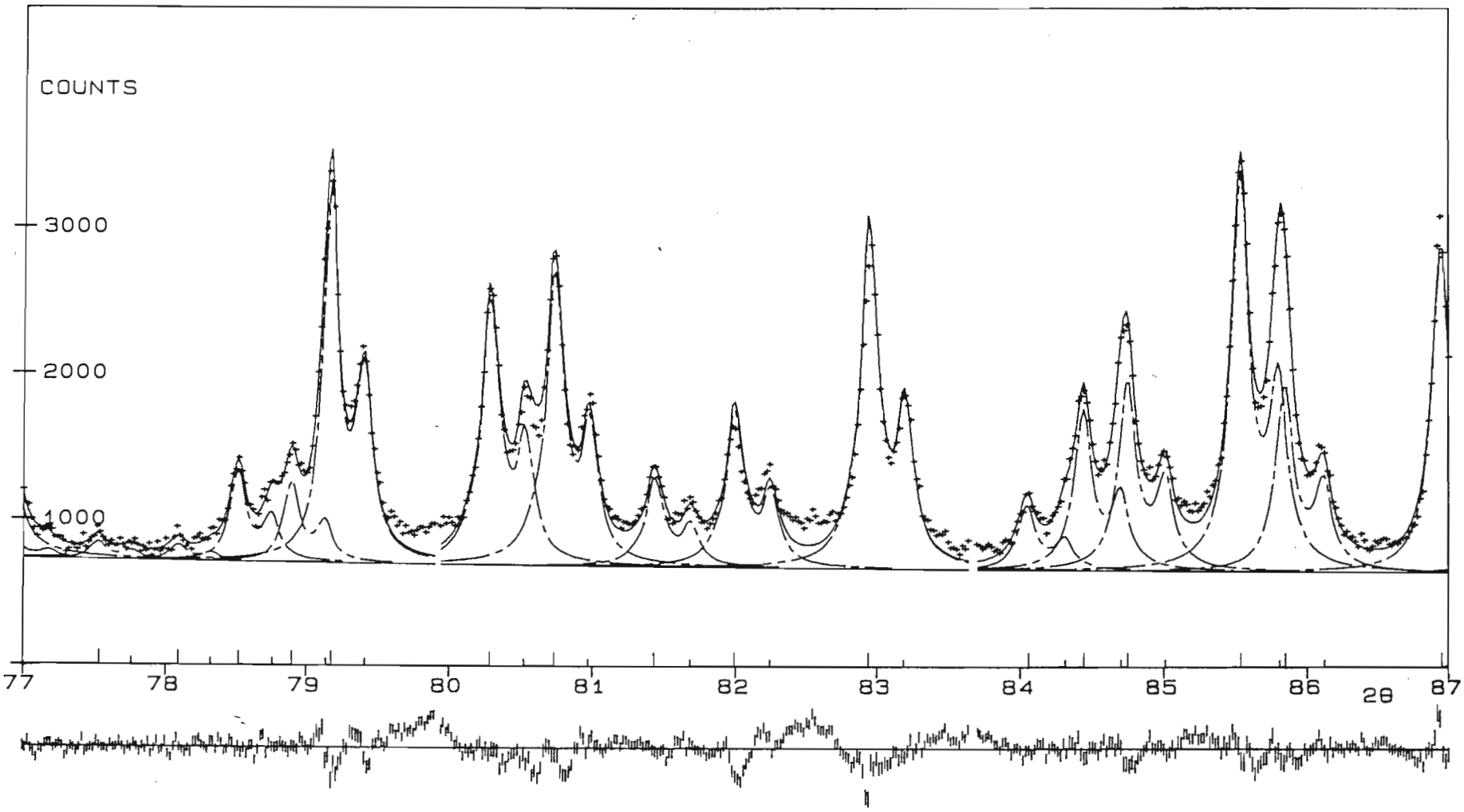

Fig 6.8a Refinement of the three ranges (73,60 - 79,90), (79,90 - 83,65) and (83,65 - 89,30) using the linear global background.

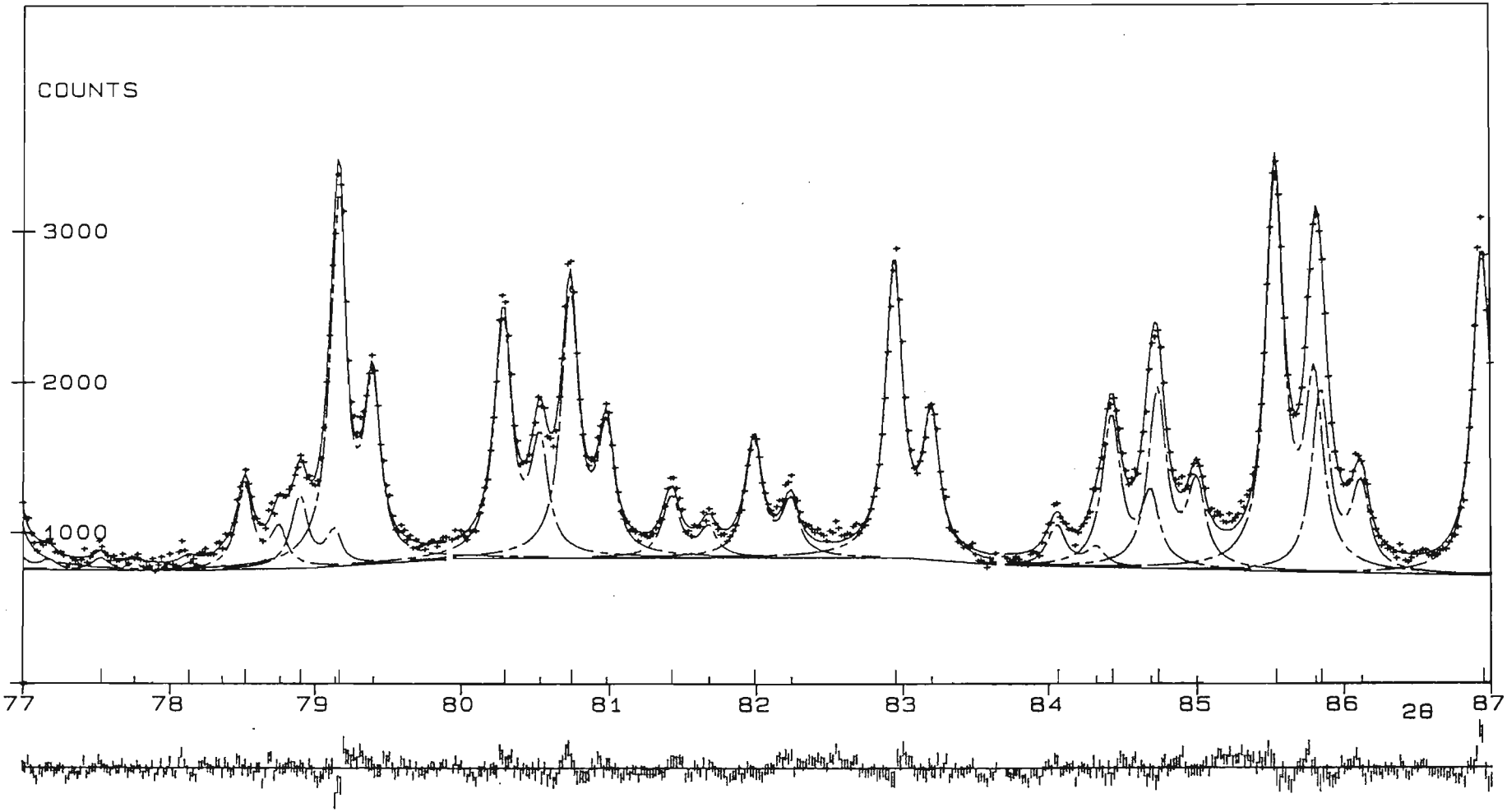

Fig 6.8b Refinement of the three ranges (73,60 - 79,90), (79,90 - 83,65) and (83,65 - 89,30) using the global background raised between 79 and 89°.

this region before modification. The fact that Yo is greater than Yc in many places between the peaks shows that the background is far too low. Fig 6.9 shows the first global background and the one obtained after the modifications including the sharp increase between 73 and 89° 2θ. Fig 6.8b shows the fit using the modified background. The marked improvement is clearly visable both in the fit itself and in the line showing Yo - Yc.

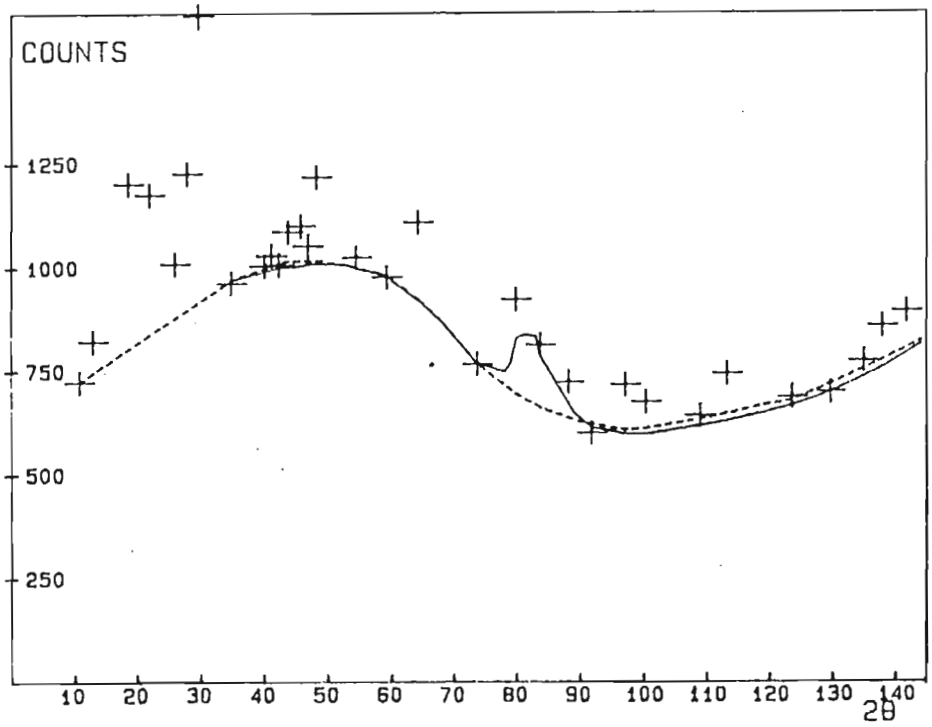

Fig 6.9 Global background curve

- - - initial estimate

——— final estimate including relatively sharp peak

\+ minima in the low level regions

6.13 The global profile parameters

The refinements described above generated a set of profile parameters which are shown plotted against 2θ in fig 6.10a, b and c. Smooth curves were drawn through these values to obtain global profile parameters for use in a final refinement. The r_{21} ratio is fairly well defined and remains close to 0,5 throughout the range. The left and right widths (the values plotted are twice the halfwidths) increase as expected from about 45° 2θ.

Fig 6.10 Profile parameters refined in individual ranges with smooth curves showing global values used in final refinements.

(a) ratio of α_2/α_1 peak height, r_{21}

(b) left and right widths (+ $2w_l$, x $2w_r$)

(c) left and right shape parameters (+ n_l, x n_r)

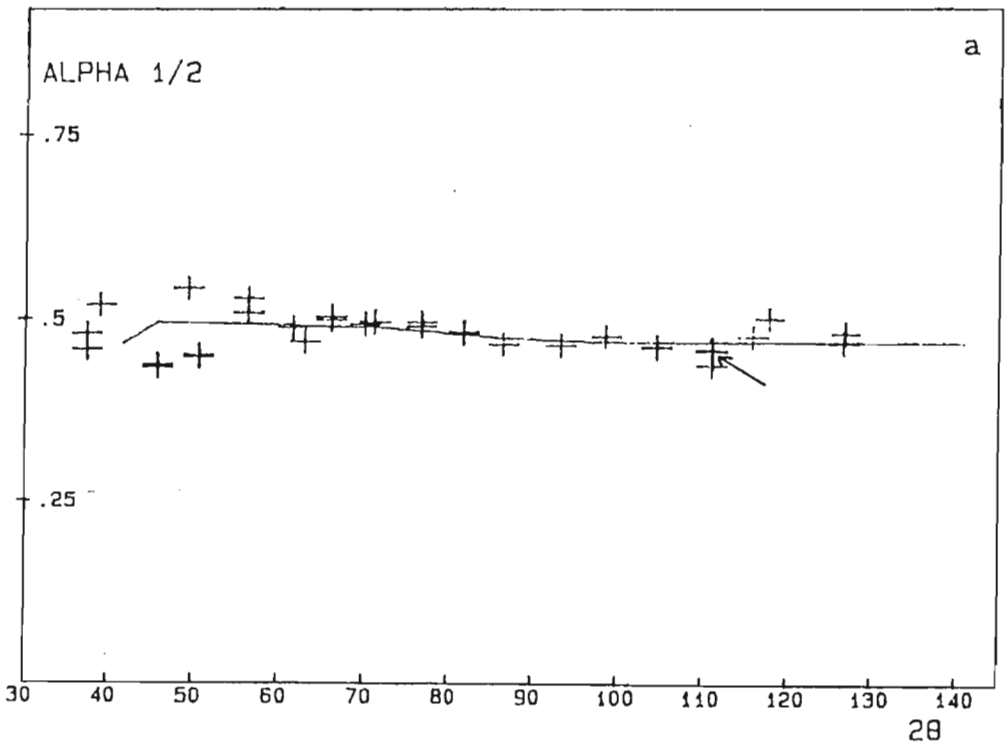

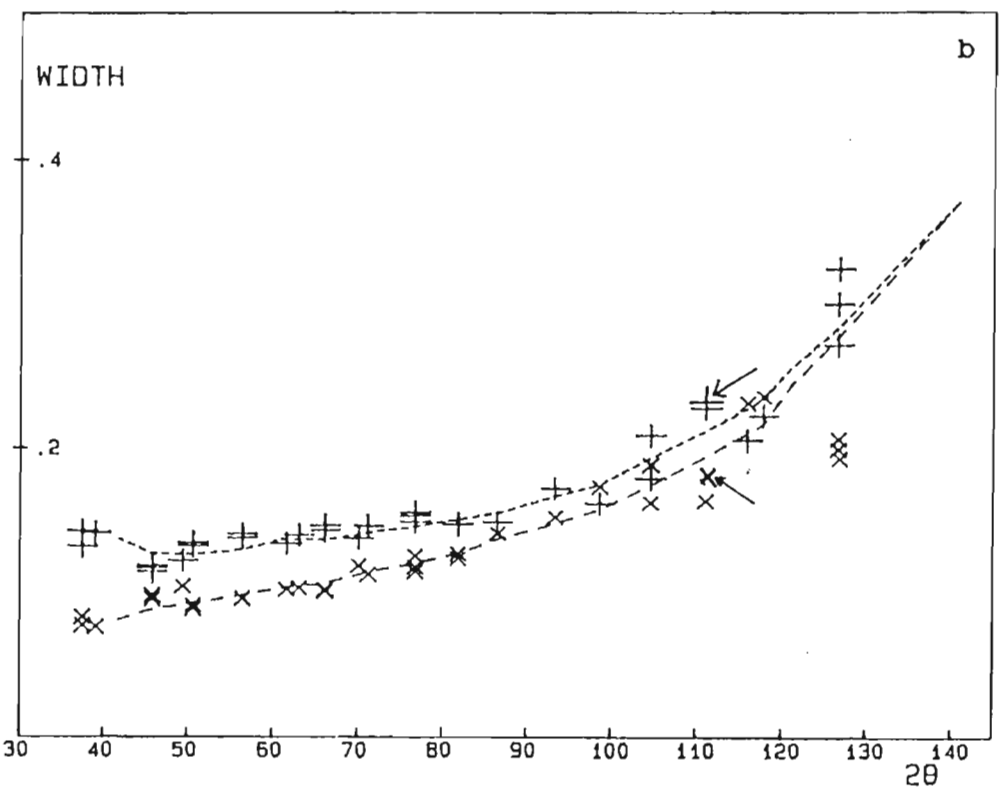

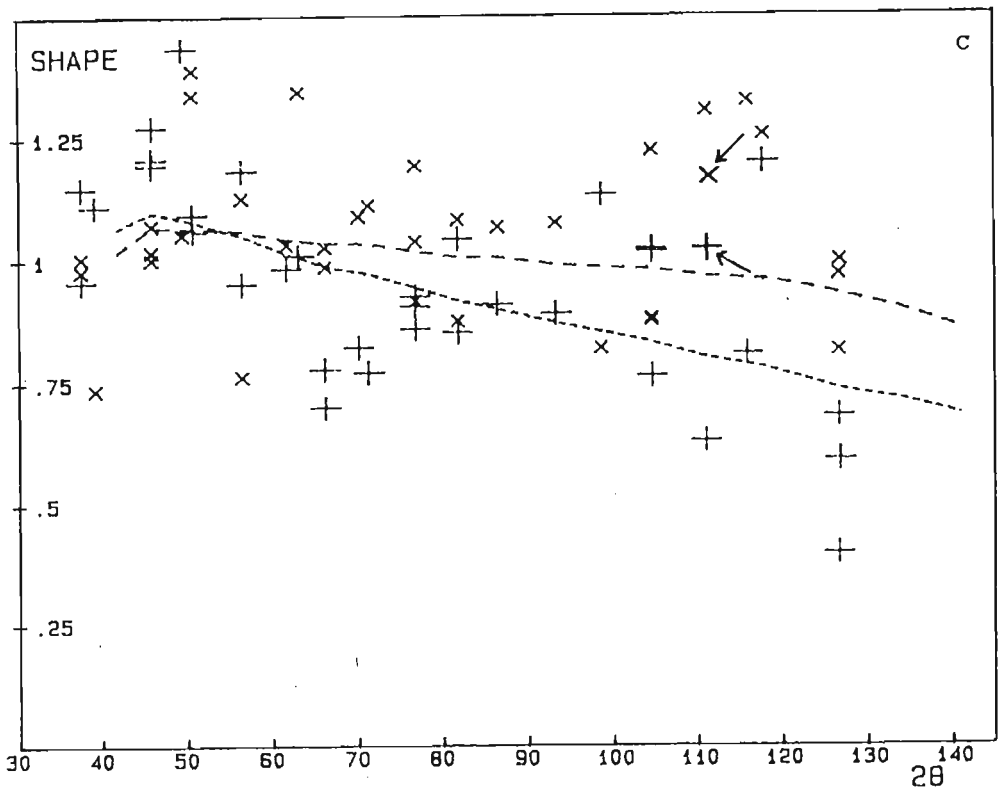

The value for w_1 is higher than w_r because of asymmetric instrumental broadening. (w_1 would increase drastically below 40° in the range where numerical integration was used to determine intensities).

As with the ratio r_{21} the widths are well determined except at high angles were a certain amount of "guessing" is required. The shape parameters, however, are very badly determined and the "best" curves drawn through the points are also very approximate. However, the obtaining of a good fit is not very sensitive to the exact values of the shape parameters. To see this, we will compare the intensities obtained using the refined profile parameters marked with arrows in fig 6.10 and those obtained using the global profile parameters (range 109;0 - 113,0°). Table 6.7 shows profile parameters and intensities obtained from both sets of refinements. In the table del is the difference in values between the two sets of refinements, and del/sig is this difference as a fraction of the error. Although the shape parameters differ quite markedly, the difference in integrated intensities obtained is only of the order of the magnitude of

their errors (see del/sig-values in table 6.7. Thus we can conclude that the curve chosen to describe the shape parameters is satisfactory since a different choice would not produce a significant change in the intensities.

Table 6.7 Integrated intensities obtained using different profile parameters (see text).

parameter	refined profile parameters	global profile parameters	del	del/sig
r_{21}	0,463 (0,024)	0,470	0,007	0,30
$2w_l$	0,232 (0,016)	0,212	-0,020	1,25
$2w_r$	0,177 (0,014)	0,194	0,017	1,22
n_l	1,02 (0,21)	0,80	-0,22	1,06
n_r	1,16 (0,18)	0,96	-0,20	1,06
I_1	96 (4)	91 (4)	-5	1,25
I_2	30 (5)	31 (5)	1	0,20
I_3	159 (9)	160 (8)	1	0,13
I_4	104 (7)	102 (6)	-2	0,33
I_5	83 (7)	87 (6)	4	0,67
I_6	90 (7)	91 (6)	1	0,17
I_7	127 (9)	134 (6)	7	0,88

6.14 The final analysis of the spectrum

A final analysis of the pattern was conducted using the global profile parameters obtained from fig 6.10. The final intensities and positions of the peaks are listed in appendix 2 which details the structure refinement. The background used was the global background shown in fig 6.9.

A plot of the entire refined spectrum is shown Appendix 1. The end points of the ranges of refinement are shown at the appropriate 2θ positions below the zero line. The positions $2\theta_1$ and $2\theta_2$ (α_1 and α_2 contributions) are shown as spikes on the zero line for each hkl-reflection - the α_1 spikes larger than those for α_2. The contributions of individual peaks (α_1/α_1 doublet) are also shown with dashed lines. The deviations Yo - Yc are shown below the spectrum with error bars equal to $\sqrt{Yo}$.

6.15 Numerical step integration of the range 10 - 35° 2θ

The peaks found in the range 10 - 35° 2θ were well separated, but they exhibited a high degree of asymmetry due to instrumental broadening. Analyses of the peaks using program PPP were done on the two peaks at 15,90 and 20,96° individually, constraining the parameters for α_1 and α_2 to be equal. The final parameter values are shown in table 6.8.

Table 6.8 Parameter values resulting from refinements of akermanite peaks at 15,90 and 20,96°

param	15,90°	20,96°
r_{21}	-0,113 (0,367)	2,691 (0,419)
$2w_1$	0,214 (0,012)	0,132 (0,005)
$2w_r$	0,112 (0,028)	0,111 (0,005)
n_1	1,28 (0,12)	2,11 (0,09)
n_r	0,38 (0,13)	0,59 (0,06)

As can been seen from fig 6.11 the program can fit the shape of the peaks, producing stable and low R-values, but the parameter values produced are unacceptable. For the peak at 15,90°, the ratio r_{21} is negative and for the peak at 20,96 the value is 2,69 whereas the correct value is ≈ 0,5. This means that the program is using the α_2 peak (which completely overlaps the α_1 peak) in a way that is not physically meaningful to fit the shape of the peak to give the required asymmetry. Also, for the refinement of the peak at 20,96° the value of the left shape parameter is too large.

Since there was no overlapping of reflections in this range it was decided to use the numerical step program (see section 5.9) to determine the integrated intensities, rather than the profile fitting program PPP. The intensity of each peak was calculated using equation 5.7. From this, the background contribution had to be subtracted. The background was determined conveniently using PPP. This involved refining the background parameters (bg1 and s1) only, while keeping the intensity of the peak at zero and omitting the region in the range which contained the peak itself. Intensities of the separated peaks of akermanite (10 - 35° 2θ) and silicon (all peaks) were determined in this way. A selection of

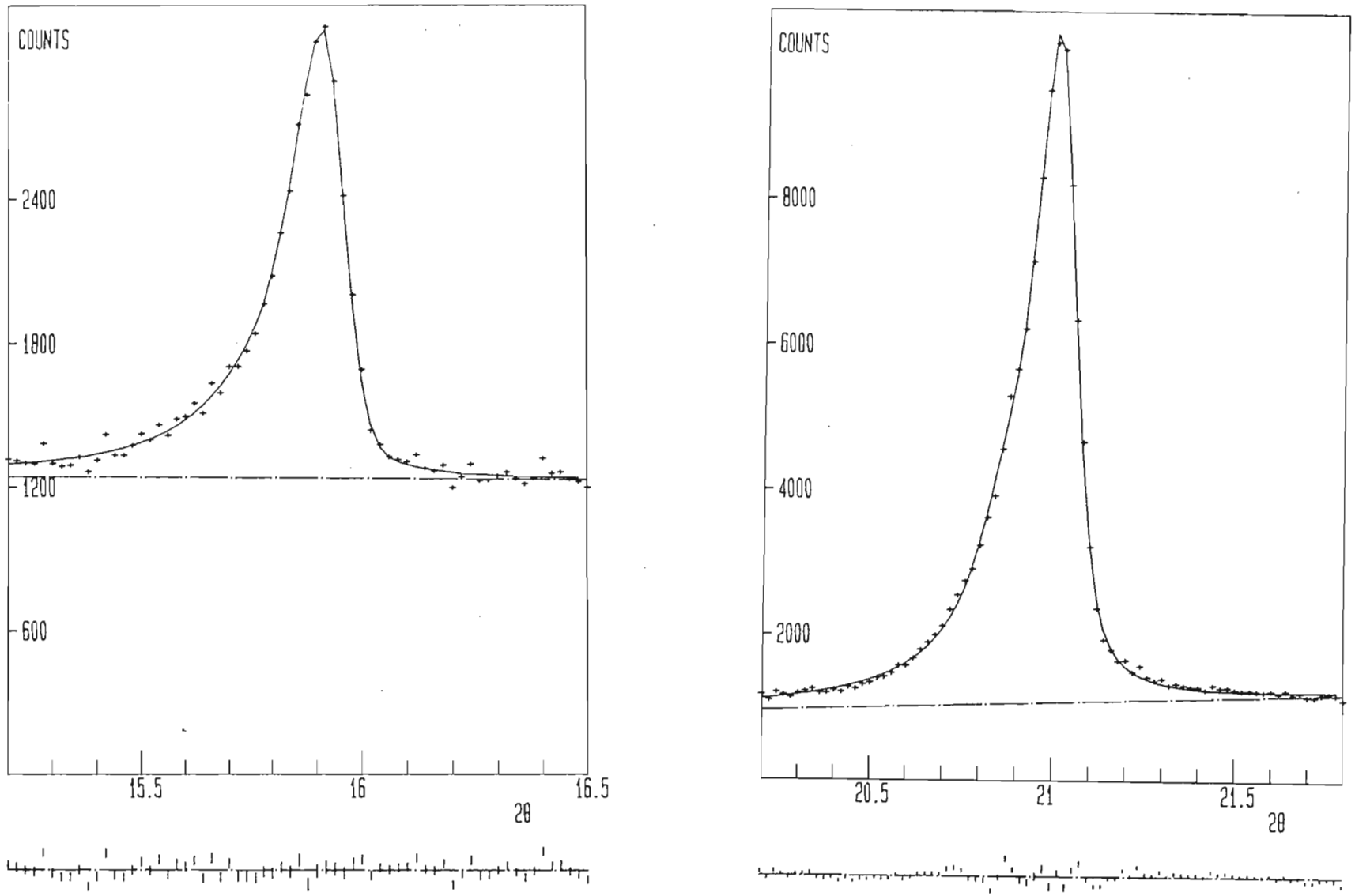

Fig 6.11 Fit of peaks using PPP refining all parameters
- profile, background and peak position and intensity.

values is shown in table 6.9 in the column labelled "linear".

Equation 5.7 was in effect joining adjacent points by straight lines and calculating the area under these lines (trapezoidal rule). It was felt that if a quadratic function was used instead of a straight line for the integration a more accurate estimate of the intensity might be obtained. The following method was investigated. For the determination of the area under the curve between the positions x(i) and x(i+1), (x ≡ 2θ) a quadratic was calculated through the observations x(i-1), x(i) and x(i+1), or through x(i), x(i+1) and x(i+2). The integral of the quadratic between x(i) and x(i+1) would be the element of area and a sum of these elements would yield the intensity of the peak. The intensities obtained using the quadratic approximation to fit the points are shown in table 6.9 in the column labelled "quadratic". As can be seen, the differences (del in table 6.9) between the intensities obtained using the linear and quadratic approximations are negligible. The quadratic approximation was only used in the actual peak region as the statistical fluctuations make its use in the background region meaningless.

Table 6.9 Intensities of peaks obtained using numerical integration.

sample	range (2θ)	quadratic	linear	del	%del
Ak	19,80 - 21,80	5938,29	5938,13	0,154	0,0026
Ak	27,50 - 29,50	10882,12	10861,06	1,061	0,0098
Ak	46,32 - 48,29	5163,27	5162,76	0,510	0,0099
Si	55,15 - 57,09	8230,42	8230,35	0,062	0,0008
Si	67,90 - 70,40	5576,40	5576,19	0,206	0,0037
Si	86,60 - 89,40	10275,24	10275,04	0,196	0,0019
Si	93,60 - 96,60	12086,01	12085,79	0,219	0,0018
Si	125,40 - 129,60	9852,97	9852,93	0,039	0,0004

All the intensities of the peaks in range 10 - 35° 2θ were evaluated using the above method. Two of the peaks, one at 23,86 and the other at 31,00 had peaks present at the bottom of their left flanks which were not reflections of akermanite. The intensities arising from these peaks had to be excluded from the integrated intensities. This was done manually. The flanks of the akermanite peaks were sketched manually and points on these curves were used to replace observed intensities from which the

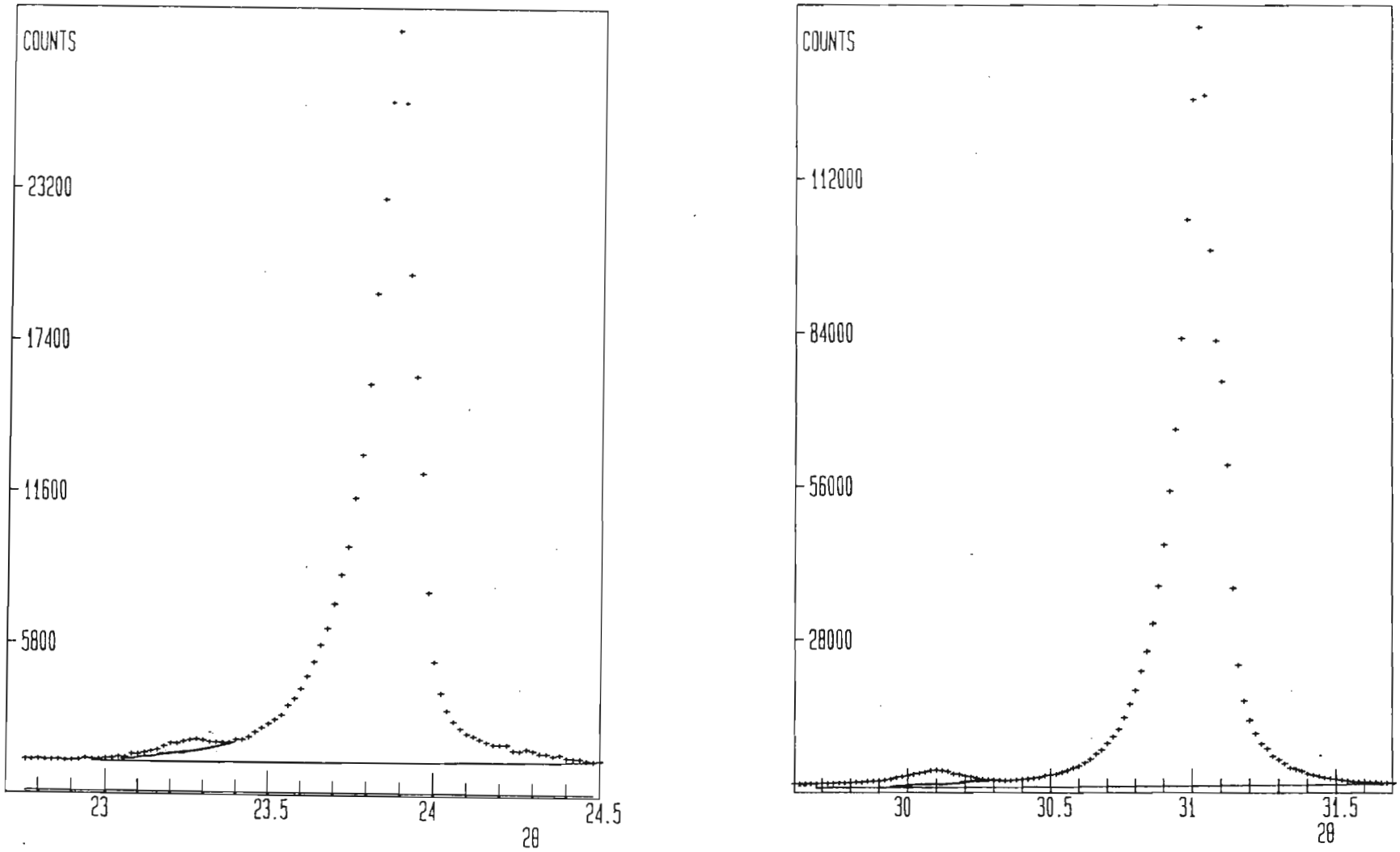

fig 6.12 Akermanite peaks with extraneous peaks on their flanks:
left diagram - peak at 23,86, right diagram - peak at 31,00·2θ

integrated intensities were determined. Figure 6.12 shows these peaks together with the extraneous peaks. A full list of the intensities of the peaks is given in appendix 2.

6.16 Summary of profile fitting step

The implementation of the strategies discussed above permits the determination of integrated intensities of as large a number of reflections as possible. The larger this number the greater the accuracy with which structural parameters can be determined from them. In the case of the akermanite diffraction pattern the number of hkl-values (unique reflections) occuring in the range $2\theta < 144°$ is 213. Of these, 187 were separated by more than $0,02° 2\theta$, the limit for identification of individual intensities, ie there were 26 cases where reflections overlapped exactly due to crystal symmetry or approximately by chance. In the diffraction pattern 173 peaks were identified at these positions with integrated intensities $I > 2\sigma(I)$. However all 187 values including zeros can be utilised as data available for the crystal structure refinement.

Chapter 7 CRYSTAL STRUCTURE REFINEMENT

Integrated intensities of reflections were used in refinement of crystal structural parameters. Sets of data from samples of SiO_2, ErB_4 and Fe-akermanite were evaluated. The program POWLS, used to perform this refinement was developed by Will, Jansen and Schäffer (1983). This program will be described in the next section.

7.1 The program POWLS

The program POWLS is a least squares program similar to PPP which fits intensities Ic calculated by using equation 2.8.

$$I = Sc.Mu(hkl).Lp(hkl).Po(hkl).\left|F_{hkl}\right|^2 \qquad [7.1]$$

to the observed values Io of the integrated intensities. The input data are observed intensities and their errors, crystal space group and cell parameters, wavelength of the radiation and starting parameters of the atoms in the cell - positions, occupancies and temperature factors. Using the space group number, symmetry information is read in from the file SYMPOS. The atomic scattering factors are read in from file FXORFL and the anomalous scattering factors for the appropriate radiation from file FXANOM. Initially the program calculates the full set of 2θ-values for all reflections in the corresponding Laue symmetry group, ie including reflections that overlap exactly due to crystal symmetry. The appropriate multiplicity values are then calculated for use in equation 7.1. The Lp factor is also calculated.

It is required of the user to assign the hkl-reflections (planes) (by reference number) to the peaks of integrated intensity in the data set, sometimes assigning two or more overlapping planes to one peak. Peaks of zero intensity (ie missing peaks) may be omitted, or included with some small intensity value just greater than zero (input of zero observed intensity causes an error in program execution).

The iterative least squares procedure then refines the

structural parameters to give the best fit of calculated and observed intensities. The temperature factor can be a common one for all atoms (overall) or the atoms can be given individual isotropic or anisotropic temperature factors. The scale factor and preferred orientation parameter can also be refined. Constraints can be placed on the parameters. This is done in the subroutine PATCH eg for anisotropic thermal parameters.

7.2 Refinement of SiO_2 structure

This data set is provided in the POWLS manual and was used as a test of the implementation of the program. The structure has space group $P3_221$ (No. 154). The Si atom is at the special position (x, 0, 1/6) and the O atom at a general position (x, y, z). Both atoms were given anisotropic temperature factors. Parameter constraints are required to be input in PATCH for the Si atom in the special position, namely

$$B_{11} = B_{22}/2$$
$$B_{23} = 2B_{13}$$

The parameters obtained for various refinement runs are shown in table 7.1. The parameter abbreviations in the second column have the following meanings: SF - scattering factor (this is not a refinable parameter, the value is merely a reference number to identify the scattering factor table); OC - site occupancy factor; X Y Z - fractional coordinates; B_{ij} - anisotropic thermal parameters; B - isotropic thermal parameters; SCALE - scale factor; OTEMP - overall temperature factor; PREFOR - preferred orientation parameter.

The program was run both with the constraints (see column labelled Si11 - WITH PATCH) and without the constraints (column labelled Si4 - NO PATCH). The results can be compared with the set of values given in the program manual (column labelled MANUAL - WITH PATCH). As could be expected the unconstrained refinement produces a better fit (a lower residual of 0,0091 as opposed to 0,0100) but does not correspond to the symmetry of the crystal.

Table 7.1 Parameter values obtained in SiO_2 refinements. Si4 - unconstrained refinement, Si11 - constrained refinement, MANUAL - quoted in program manual. The final two columns give the difference between the parameter values from the constrained refinements as a percentage: a) the parameter value itself and b) the parameter error.

Parameter	Starting Value	Si4 NO PATCH	MANUAL WITH PATCH	Si11 WITH PATCH	%DIFF Si11-MANUAL
1 SF (Si)	2.0000	2.00000	2.00000	2.00000	
2 OC (Si)	3.0000	3.00000	3.00000	3.00000	
3 X (Si)	.4697	.47258 (71)	.47275 (77)	.47276 (77)	.002 (.00)
4 Y (Si)	.0000	.00000	.00000	.00000	
5 Z (Si)	.1667	.16667	.16667	.16667	
6 B11 (Si)	.0093	.02040 (269)	.01904 (218)	.01905 (217)	.053 (.46)
7 B22 (Si)	.0078	.00684 (238)	.00597 (251)	.00598 (251)	.167 (.00)
8 B33 (Si)	.0049	.00625 (186)	.00435 (156)	.00435 (156)	.461 (.64)
9 B12 (Si)	.0039	.00390	.00300	.00300	
10 B13 (Si)	.0000	.01888 (540)	-.00021 (76)	-.00019 (76)	10.000 (.00)
11 B23 (Si)	.0000	-.00002	-.00042	-.00038	
12 SF (O)	1.0000	1.00000	1.00000	1.00000	
13 OC (O)	6.0000	6.00000	6.00000	6.00000	
14 X (O)	.4135	.41609 (85)	.41615 (89)	.41615 (89)	.000 (.00)
15 Y (O)	.2669	.26671 (88)	.26658 (94)	.26658 (94)	.000 (.00)
16 Z (O)	.2858	.28626 (63)	.28641 (68)	.28640 (68)	.003 (.00)
17 B11 (O)	.0190	.01680 (446)	.01592 (502)	.01600 (501)	.250 (.20)
18 B22 (O)	.0144	.00791 (245)	.00672 (251)	.00672 (250)	.000 (.40)
19 B33 (O)	.0083	.00572 (412)	.00580 (444)	.00581 (443)	.172 (.22)
20 B12 (O)	.0106	.00835 (297)	.00719 (337)	.00723 (336)	.550 (.30)
21 B13 (O)	-.0025	.00011 (195)	.00038 (211)	.00037 (210)	2.700 (.48)
22 B23 (O)	-.0035	.00339 (184)	.00444 (188)	.00448 (18)	.897 (.53)
23 SCALE	1.0000	.03232 (51)	.03221 (56)	.03221 (56)	.000 (.00)
24 OTEMP	.0000	.00000	.00000	.00000	
25 PREFOR	.0000	.10976(3956)	.11728(4317)	.11785(4302)	.488 (.35)
R-Weighted		.00910	.01000	.01000	.000
R-cor		.00950	.01020	.01020	.000
RWR		1.89491	2.19981	2.18773	.552

The constrained refinement agrees well with that reported in the manual. For the coordinates (x, y, z) there are differences of 1 in the fifth and final figure. The oxygen temperature parameters show a somewhat larger difference up to 8 in the fourth significant figure. This may be due to the limited precision of the computer (PC-XT) and it is to be expected that the difference should be most apparent in the temperature factors of the lighter atom. The preferred orientation parameter shows a difference of 5 in the fourth figure. However, all differences are far less than

the estimated errors of the parameters ($\approx 0,005\sigma$). A computer quirk was noted in that two intensity values input as 556 and 946 appeared in the printout of the calculation as 557 and 947. This slight difference in input values may also have contributed to the small difference in final parameters.

7.3 Refinement of ErB_4 structure

The structure has tetragonal space group P4/mbm (No. 127). The Er atom is at special position (x, x + ½, 0) and the B atoms at special positions (0, 0, z) (x, x + ½, ½) and (x, y, ½). The last position has multiplicity 8 and the others 4 giving the stoichiometry ErB_4. The PATCH subroutine is therefore required to set y = x + ½ for the atoms Er and B(2).

Table 7.2 Comparison of parameter values for ErB_4 obtained using overall and individual B's. (NR = not refined).

Parameter	Starting Value	Overall	Individual
1 SF (Er)	2.0000	NR	NR
2 OC (Er)	4.0000	NR	NR
3 X (Er)	.3183	.31777 (.00036)	.31778 (.00037)
4 Y (Er)	.8183	.81777	.81778
5 Z (Er)	.0000	NR	NR
6 B (Er)	.0000	NR	.30175 (.00158)
7 SF (B1)	1.0000	NR	NR
8 OC (B1)	4.0000	NR	NR
9 X (B1)	.0000	NR	NR
10 Y (B1)	.0000	NR	NR
11 Z (B1)	.2031	.21172 (.01325)	.21562 (.00383)
12 B (B1)	.0000	NR	.19592(1.64608)
13 SF (B2)	1.0000	NR	NR
14 OC (B2)	4.0000	NR	NR
15 X (B2)	.0859	.09458 (.00518)	.09438 (.00601)
16 Y (B2)	.5859	.59458	.59440
17 Z (B2)	.5000	NR	NR
18 B (B2)	.0000	NR	1.16417(1.77580)
19 SF (B3)	1.0000	NR	NR
20 OC (B3)	8.0000	NR	NR
21 X (B3)	.1767	.17752 (.00846)	.17860 (.00970)
22 Y (B3)	.0382	.04790 (.00689)	.04926 (.00809)
23 Z (B3)	.5000	NR	NR
24 B (B3)	.0000	NR	1.22973(1.13383)
25 SCALE	.0023	.00259 (.00003)	.00259 (.00003)
26 OTEMP	1.0300	.32129 (.04890)	.00000
27 PREFOR	.0000	-.30205 (.00865)	-.30160 (.00877)
R-Weighted		.0437	.0432
R-Cor		.0437	.0432
RWR		.168E+07	.164E+07

Two refinements are compared in table 7.2, one using an overall temperature factor and one using individual isotropic temperature factors. While the residual obtained using individual temperature factors is significantly lower (R = 0,0432 as opposed to 0,0437) the temperature factors for the B-atoms have very large errors owing to the fact that these atoms scatter very much less than Er. The temperature factors for the B-atoms would be expected to be higher than for Er but the values are not found to be higher than their errors and so their determination is not significant.

It is interesting to note that the error in the x coordinate for atom B2, (0,00518), where x and y are related to each other by a constant, is less than for atom B3 (0,00846) where x and y are independent. Clearly a change in the value of x affects more reflections in the constrained case, because y changes with x, and this results in more accurate refinement.

7.4 Refinement of Fe-akermanite

The structure has tetragonal spacegroup $P\bar{4}2_1m$ (No. 113). The structure of Mg-akermanite has the positional parameters shown in table 7.3.

Table 7.3 Atom positions in Mg-akermanite (Kimata and Ii, 1981).

Atom	OC	X	Y	Z
Ca	4	0,3318	½-X	0,5067
Mg	2	0	0	0
Si	4	0,1397	½-X	0,9352
O1	2	0	0	0,1974
O2	4	0,1410	½-X	0,2536
O3	8	0,0803	0,1867	0,7877

While both the Mg and Si sites (0,0,0) and (x, ½ - x, z) are tetrahedrally coordinated the two atomic types appear to be completely segregated between the two positions. In the case of Fe-akermanite with 60% replacement of Mg by Fe, Mössbauer spectroscopy suggested that the Fe^{2+}-ions were distributed between two different tetrahedrally coordinated sites (Seifert, 1984, private communication). A possible explanation for this would be that Fe replaces not only Mg at the site (0,0,0) but

also some Si at the site (x, ½ - x, z) and that some of the Si therefore is found at the (0, 0, 0) site. The identification by X-ray diffraction of a small replacement of atoms differing by not too much in their scattering factors would require very accurate intensities. It was for this reason that great care was taken in the generation of as many separated integrated intensities as possible.

Table 7.4 Starting values for refinement of Fe-akermanite.

Atom	OC	X	Y	Z
Ca	4,0	0,3318	½-X	0,5067
Mg	0,8	0	0	0
Fe	1.2	0	0	0
Si	4,0	0,1397	½-X	0,9352
Si	0	0	0	0
Fe	0	0,1397	½-X	0,9352
O1	2,0	½	0	0,1974
O2	4,0	0,1410	½-X	0,2536
O3	8,0	0,0803	0,1867	0,7877

The starting values used for the atomic coordinates of Fe-akermanite are shown in table 7.4. Both Fe and Mg are placed at the site (0, 0, 0) (with 60% Fe) with occupancy 1,2 and 0,8, the total multiplicity of the site in the cell being 2. Si was placed at site (x, ½ - x, z) with occupancy 4. However, both Si and Fe were given a component at the other tetrahedral site starting with occupancy zero. In the PATCH subroutine the total Fe occupancy was constrained to be 1,2 and the total Si occupancy 4. Further the occupancies of the individual sites had to have the correct totals. The following relationships between the occupancies (OC) were therefore set in PATCH:

$$OC\ [Si(x, ½ - x, z)] = 2,8 + OC\ [Fe(0, 0, 0)]$$

$$OC\ [Si(0, 0, 0)] = 1,2 - OC\ [Fe(0, 0, 0)]$$

$$OC\ [Fe(x, ½ - x, z)] = 1,2 - OC\ [Fe(0, 0, 0)]$$

Finally, for the Ca site and the one Fe/Si site the relationship $y = ½ - x$ was set. It is important to note that if the

occupancies are refined, then the individual temperature factors of the atoms should not be refined, since the changing of these parameters would in effect be the changing of the electron densities at the respective positions, and this is the same as changing the occupancy of the atoms at these positions. Table 7.5 shows such a refinement which converged to a residual of R = 0,1035. The change in occupancy of Fe at (0,0,0) from a value of 1,2 is -0,0394, with an error of 0,0387. The change as a fraction of the parameter error (DEL/SIG) is thus only 1, and should be much greater than 1 for the change to be considered significant. The value therefore neither confirms nor refutes the theory of Fe distribution between the tetrahedral sites. Some of the parameters differ significantly in the two structures. The parameters Ca(x), Si(x), Si(z) and O3(y) change by a value greater than 1,5σ. It should however be noted that the Mg-akermanite structure was refined using individual anisotropic temperature factors while the Fe-akermanite refinement was done with an overall temperature factor. Thus the two refinements are not directly comparable.

In determining the error of the observed intensities no account had been taken of possible fluctuations in the primary beam intensity. If these fluctuations are estimated at 1% the errors should be increased to

$$\sigma(I) = [(\sigma_{ppp})^2 + (0,01 \times Io)^2]^{\frac{1}{2}}$$

The errors influence the refinement in that the observations are given weight $1/\sigma^2$. A further refinement was done using these errors. The result is shown in table 7.6. The residual has increased to 0,1149. The estimated errors of the parameters increase. Of interest is the Fe occupancy which now drops by only 0,0190 with a parameter error of 0,0468. The change thus appears even less significant than in the refinement shown in table 7.5.

The program POWLS allows the option of using correlation coefficients between observations. This option was tested by introducing the correlations obtained in PPP for a number of the ranges. Correlations of up to 20% were noted. The result of the POWLS refinement (table 7.7) was not significantly changed, the

residual is R = 0,1030. However, the calculation time increased markedly by about 50%.

Finally, a refinement for comparison was done keeping the occupancies constant (zero occupancy of the Fe on the Si site). This refinement generated a residual of 0,1059 which does seem significantly above the value of 0,1035 obtained with refined occupancy. However the comparison of the weighted squared residual (which is more closely related to the quantity refined) shows a less significant difference 0,1477 as opposed to 0,1473.

For record purposes Appendix 2 shows the observed and calculated intensities obtained from the refinement of table 7.5.

Table 7.5 Refinement of Fe-akermanite using starting values from Mg-akermanite. DEL is the change and SIGMA the error of the parameter.

REF\	PARAMETER			OLD VALUE (BEFORE CYCLE 1)	NEW VALUE (AFTER CYCLE 6)	SIGMA	DEL	DEL/SIG
YES	3	X	CA	.33180	.32907	.00054	-.00273	5.1
NO	4	Y	CA (½-X)	.16820	.17093	.00000		
YES	5	Z	CA	.50670	.50756	.00123	.00086	.7
YES	14	OC	FE (0,0,0)	1.20000	1.16063	.03869	-.03937	1.0
NO	20	OC	SI (X,½-X,Z)	4.00000	3.96064	.00000		
YES	21	X	SI	.13970	.13819	.00080	-.00151	1.9
NO	22	Y	SI (½-X)	.36030	.36181	.00000		
YES	23	Z	SI	.93520	.94228	.00133	.00708	5.3
NO	26	OC	SI (0,0,0)	.00000	.03936	.00000		
NO	32	OC	FE (X,½-X,Z)	.00000	.03936	.00000		
YES	41	Z	O1 (¼,0,Z)	.17890	.17740	.00469	-.00150	.3
YES	45	X	O2	.14100	.13898	.00159	-.00202	1.3
NO	46	Y	O2 (½-X)	.35900	.36102	.00000		
YES	47	Z	O2	.25360	.25384	.00304	.00024	.1
YES	51	X	O3 (X,Y,Z)	.08050	.07961	.00184	-.00089	.5
YES	52	Y	O3	.18670	.19067	.00167	.00397	2.4
YES	53	Z	O3	.78770	.78867	.00213	.00097	.5
YES	55	SKALA		.01338	.01169	.00028	-.00169	6.0
YES	56	TEMP.FAK		1.00000	1.72426	.07247	.72426	10.0
YES	57	PREF. OR		.00000	-.25777	.02326	-.25777	11.1

RWR/(N-M) OF LINEARIZED EQUATIONS = 92.0014

RWR/(N-M) OF NONLINEAR EQUATIONS = 92.0014

R - VALUE = .1035 (BASED ON UNWEIGHTED ABSOLUTE RESIDUALS)

R - VALUE = .1473 (BASED ON WEIGHTED SQUARED RESIDUALS, WITHOUT CORRELATIONS)

R - VALUE = .1473 (CORRELATIONS INCLUDED)

RWR = 15364.2 (CORRELATIONS INCLUDED)

Table 7.6 Refinement of Fe-akermanite. As for table 7.5 but using increased error estimates for the observations.

REF\		PARAMETER		OLD VALUE (BEFORE CYCLE 1)	NEW VALUE (AFTER CYCLE 6)	SIGMA	DEL	DEL/SIG
YES	3	X	CA	.33180	.32874	.00056	-.00306	5.5
NO	4	Y	CA (½-X)	.16820	.17126	.00000		
YES	5	Z	CA	.50670	.50720	.00137	.00050	.4
YES	14	OC	FE (0,0,0)	1.20000	1.18104	.04679	-.01896	.4
NO	20	OC	SI (X,½-X,Z)	4.00000	3.98103	.00000		
YES	21	X	SI	.13970	.13877	.00084	-.00093	1.1
NO	22	Y	SI (½-X)	.36030	.36123	.00000		
YES	23	Z	SI	.93520	.94090	.00145	.00570	3.9
NO	26	OC	SI (0,0,0)	.00000	.01897	.00000		
NO	32	OC	FE (X,½-X,Z)	.00000	.01897	.00000		
YES	41	Z	O1 (¼,0,Z)	.17890	.18082	.00564	.00192	.3
YES	45	X	O2	.14100	.13716	.00173	-.00384	2.2
NO	46	Y	O2 (½-X)	.35900	.36284	.00000		
YES	47	Z	O2	.25360	.25650	.00356	.00290	.8
YES	51	X	O3 (X,Y,Z)	.08050	.08039	.00199	-.00011	.1
YES	52	Y	O3	.18670	.19187	.00179	.00517	2.9
YES	53	Z	O3	.78770	.78807	.00277	.00037	.1
YES	55	SKALA		.01338	.01137	.00045	-.00210	4.7
YES	56	TEMP.FAK		1.00000	1.75464	.09455	.75464	7.8
YES	57	PREF. OR		.00000	-.29623	.03131	-.29623	9.5

RWR/(N-M) OF LINEARIZED EQUATIONS = 44.0876

RWR/(N-M) OF NONLINEAR EQUATIONS = 44.0876

R - VALUE = .1149 (BASED ON UNWEIGHTED ABSOLUTE RESIDUALS)

R - VALUE = .2243 (BASED ON WEIGHTED SQUARED RESIDUALS, WITHOUT CORRELATIONS)

R - VALUE = .2243 (CORRELATIONS INCLUDED)

RWR = 7362.63 (CORRELATIONS INCLUDED)

Table 7.7 Refinement of Fe-akermanite. As for table 7.5 but with correlations included between 35 peaks.

REF\		PARAMETER		OLD VALUE (BEFORE CYCLE 1)	NEW VALUE (AFTER CYCLE 6)	SIGMA	DEL	DEL/SIG
YES	3	X	CA	.33180	.32906	.00054	-.00274	5.1
NO	4	Y	CA (½-X)	.16820	.17094	.00000		
YES	5	Z	CA	.50670	.50759	.00122	.00089	.7
YES	14	OC	FE (0,0,0)	1.20000	1.16138	.03836	-.03862	1.0
NO	20	OC	SI (X,½-X,Z)	4.00000	3.96137	.00000		
YES	21	X	SI	.13970	.13820	.00079	-.00150	1.9
NO	22	Y	SI (½-X)	.36030	.36180	.00000		
YES	23	Z	SI	.93520	.94236	.00132	.00716	5.4
NO	26	OC	SI (0,0,0)	.00000	.03863	.00000		
NO	32	OC	FE (X,½-X,Z)	.00000	.03863	.00000		
YES	41	Z	O1 (¼,0,Z)	.17890	.17746	.00464	-.00144	.3
YES	45	X	O2	.14100	.13902	.00158	-.00198	1.3
NO	46	Y	O2 (½-X)	.35900	.36098	.00000		
YES	47	Z	O2	.25360	.25377	.00300	.00017	.1
YES	51	X	O3 (X,Y,Z)	.08050	.07960	.00181	-.00090	.5
YES	52	Y	O3	.18670	.19069	.00165	.00399	2.4
YES	53	Z	O3	.78770	.78872	.00211	.00102	.5
YES	55	SKALA		.01338	.01172	.00028	-.00166	6.0
YES	56	TEMP.FAK		1.00000	1.73078	.07176	.73078	10.2
YES	57	PREF. OR		.00000	-.25633	.02305	-.25633	11.1

RWR/(N-M) OF LINEARIZED EQUATIONS = 90.0013

RWR/(N-M) OF NONLINEAR EQUATIONS = 90.0013

R - VALUE = .1030 (BASED ON UNWEIGHTED ABSOLUTE RESIDUALS)

R - VALUE = .1465 (BASED ON WEIGHTED SQUARED RESIDUALS, WITHOUT CORRELATIONS)

R - VALUE = .1461 (CORRELATIONS INCLUDED)

RWR = 15210.2 (CORRELATIONS INCLUDED)

Table 7.8 Refinement of Fe-akermanite. As for table 7.5 but keeping Fe occupancy constant.

REF\		PARAMETER		OLD VALUE (BEFORE CYCLE 1)	NEW VALUE (AFTER CYCLE 6)	SIGMA	DEL	DEL/SIG
YES	3	X	CA	.33180	.32912	.00054	-.00268	5.0
NO	4	Y	CA (½-X)	.16820	.17088	.00000		
YES	5	Z	CA	.50670	.50746	.00123	.00076	.6
YES	14	OC	FE (0,0,0)	1.20000	1.20000	.00000		
NO	20	OC	SI (X,½-X,Z)	4.00000	4.00000	.00000		
YES	21	X	SI	.13970	.13813	.00080	-.00157	2.0
NO	22	Y	SI (½-X)	.36030	.36187	.00000		
YES	23	Z	SI	.93520	.94284	.00133	.00764	5.7
NO	26	OC	SI (0,0,0)	.00000	.00000	.00000		
NO	32	OC	FE (X,½-X,Z)	.00000	.00000	.00000		
YES	41	Z	O1 (¼,0,Z)	.17890	.17690	.00468	-.00200	.4
YES	45	X	O2	.14100	.13900	.00161	-.00200	1.2
NO	46	Y	O2 (½-X)	.35900	.36100	.00000		
YES	47	Z	O2	.25360	.25323	.00300	-.00037	.1
YES	51	X	O3 (X,Y,Z)	.08050	.07974	.00184	-.00076	.4
YES	52	Y	O3	.18670	.19160	.00143	.00490	3.4
YES	53	Z	O3	.78770	.78840	.00212	.00070	.3
YES	55	SKALA		.01338	.01165	.00028	-.00173	6.2
YES	56	TEMP.FAK		1.00000	1.71785	.07212	.71785	10.0
YES	57	PREF. OR		.00000	-.25554	.02318	-.25554	11.0

RWR/(N-M) OF LINEARIZED EQUATIONS = 91.9956

RWR/(N-M) OF NONLINEAR EQUATIONS = 91.9956

R - VALUE = .1059 (BASED ON UNWEIGHTED ABSOLUTE RESIDUALS)

R - VALUE = .1477 (BASED ON WEIGHTED SQUARED RESIDUALS, WITHOUT CORRELATIONS)

R - VALUE = .1477 (CORRELATIONS INCLUDED)

RWR = 15455.30 (CORRELATIONS INCLUDED)

Chapter 8 CONCLUSIONS

The main part of this study has been the optimisation of the profile fitting stage of the so-called two-step method of crystal structure refinement from powder data. The main elements of the strategy employed for the case where the lattice parameters are already known were the following.

1) The pattern was split into suitable ranges.
2) A global background function was determined from the minima in the diffraction pattern and this was later modified during the fitting process.
3) The profile parameters were refined in individual ranges and subsequently the 2θ-dependence of these parameters was determined.
4) The profile function was the pseudo-Voigt function made asymmetric by the use of different parameter values on the left and right flanks, but with the form of the α_2 component fixed to that of α_1.
5) It was attempted to identify intensity at every expected position and positions of peaks that appeared weak were fixed.
6) The intensities of those peaks which became negative during the refinement were fixed at zero.
7) Reflections whose 2θ-values were separated by less than 0,02° were refined as single peaks, those further apart were refined as separate peaks.
8) In the region below 35° 2θ where peaks are very asymmetric but well separated integrated intensities were determined by numerical step integration rather than by profile fitting.

With reference to point 5. it may be asked why, if the lattice parameters are known, the positions of even the strong peaks are refined at all. The reasons are that the lattice parameters may be slightly inaccurate or that there may be systematic errors in the diffractometer geometry such as sample height displacement, non-regularity of gear wheels of the diffractometer circles. These effects could cause peaks to shift by small amounts and allowing the strong peaks with steep flanks to move slightly gives much better fits.

Further improvements to the technique could be the subject of further study.

1) The profile parameters were set to be constant in each range. However, once the 2Θ-dependence has been determined the parameters should be allowed to vary across the individual ranges. This would entail a small modification to the program and would allow the refinement of larger ranges to be undertaken, in principle the whole diffraction pattern in one range.

2) The profile function could be improved. The so-called α_3 component on the left flank should be fitted. Further, the shape of the profile function near the peak shows systematic deviations which are difficult to match.

The integrated intensities thus obtained are used in a second step to refine the atomic structure of the crystal. This two-step method is in competition with the easily automated and popular Rietveld refinement. The Rietveld procedure and the programs available to implement it should now be tested in the light of the experience gained in the careful application of the profile fitting procedures.

References

Abramowitz M and Stegun I A (1972). "Handbook of Mathematical Functions", Dover, New York.

Ahtee M, Unonius L, Nurmela M and Suortti P (1984). J. Appl. Cryst., 17, 352-357.

Bolzenius B H, Engel D W, Elf F, Heiba Z and Will G (1985). Z. Krist., 170, 19-21.

Dent Glasser L S (1977). "Crystallography and its Applications", Van Nostrand Reinhold, England.

Gradshteyn I S and Ryzhik I M (1980). "Table of Integrals, Series and Products", Academic Press, New York.

Hall M M (1977). J. Appl. Cryst., 10, 66-68.

International Tables for X-ray Crystallography (1974). Vol IV, Kynoch Press, Birmingham.

James R W (1967). "The Optical Principles of the Diffraction of X-rays", Bell and Sons, Northampton, Great Britian.

Kimata M and Ii N (1981). N. Jb. Miner. Mh., 1981, 1-10.

Kittel C (1976). "Introduction to Solid State Physics", Wiley, New York.

Klug P and Alexander L (1974). "X-ray Diffraction Procedures", Wiley, New York.

Martin B R (1971). "Statistics for Physicists", Academic Press, London.

Pugh E M and Winslow G H (1966). "The Analysis of Physical Measurements", Addison-Wesley, London.

Retief J J and Engel D W (1985). J. Appl. Cryst., 18, 150-155.

Stout G H and Jensen L H (1968). "X-ray Structure Determination", Macmillan, New York.

Toraya H, Yoshimura M and Somiya S (1983). J. Appl. Cryst., 16, 653-657.

Will G, Jansen E and Schäfer W (1983). "POWLS80 Program Manual", KFA, Jülich.

Will G, Parrish W and Huang T C (1983). J. Appl. Cryst., 16, 611-622.

Wilson A J C (1963). "Mathematical Theory of X-ray Powder Diffractometry", Philips Technical Library, Eindhoven.

APPENDIX 1

Observed and calculated point intensities, Yo and Yc, of Fe-akermanite.

(+) - Yo

continuous line - Yc.

dashed line - contribution from individual peaks.

calculated hkl-positions (α_1 larger than α_2) marked on dashed line.

(Yo - Yc) with error bars shown below scale.

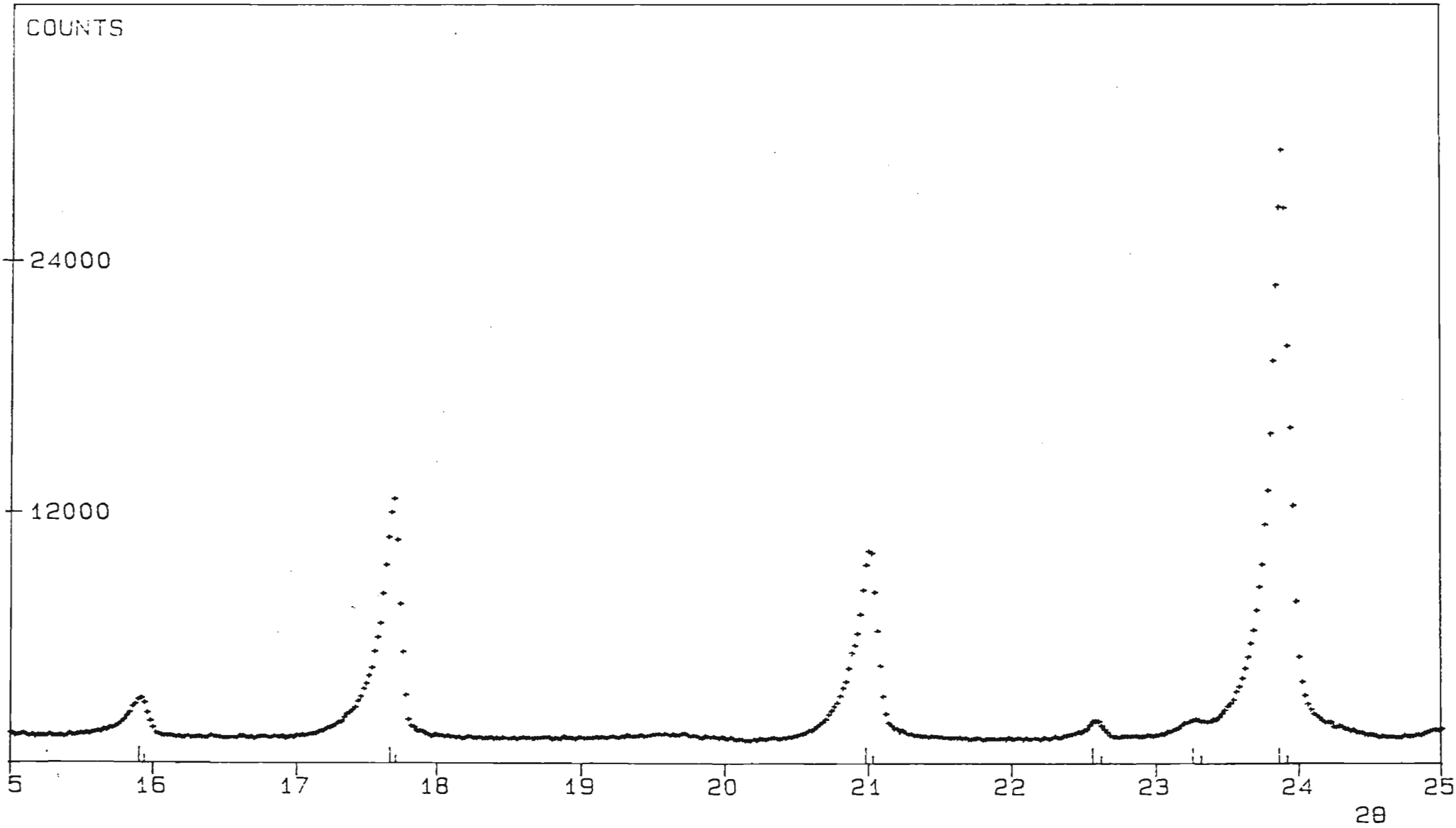
COUNTS
24000
12000
5
16
17
18
19
20
21
22
23
24
25
2θ

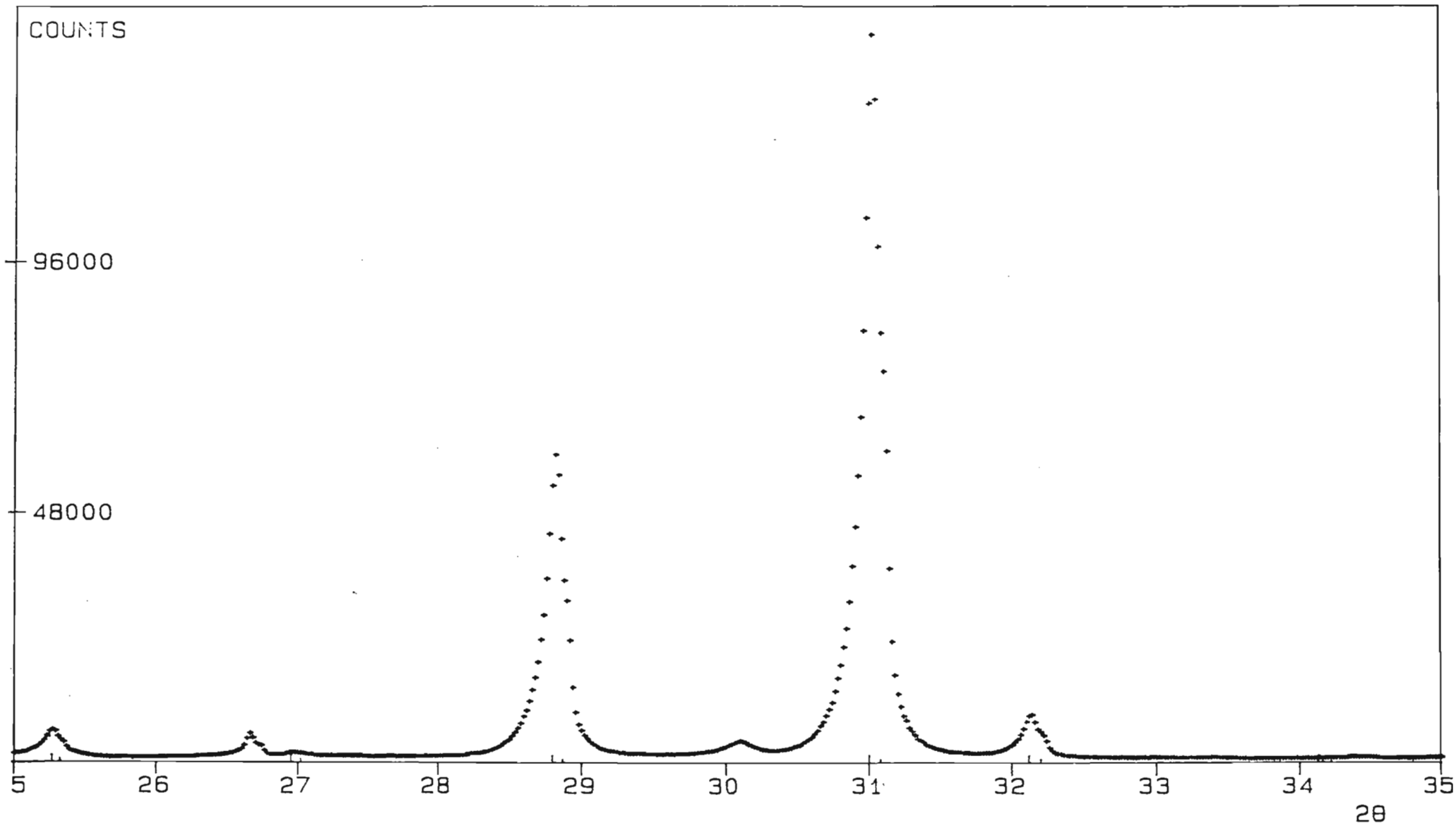
COUNTS
96000
48000
5
26
27
28
29
30
31
32
33
34
35
2θ

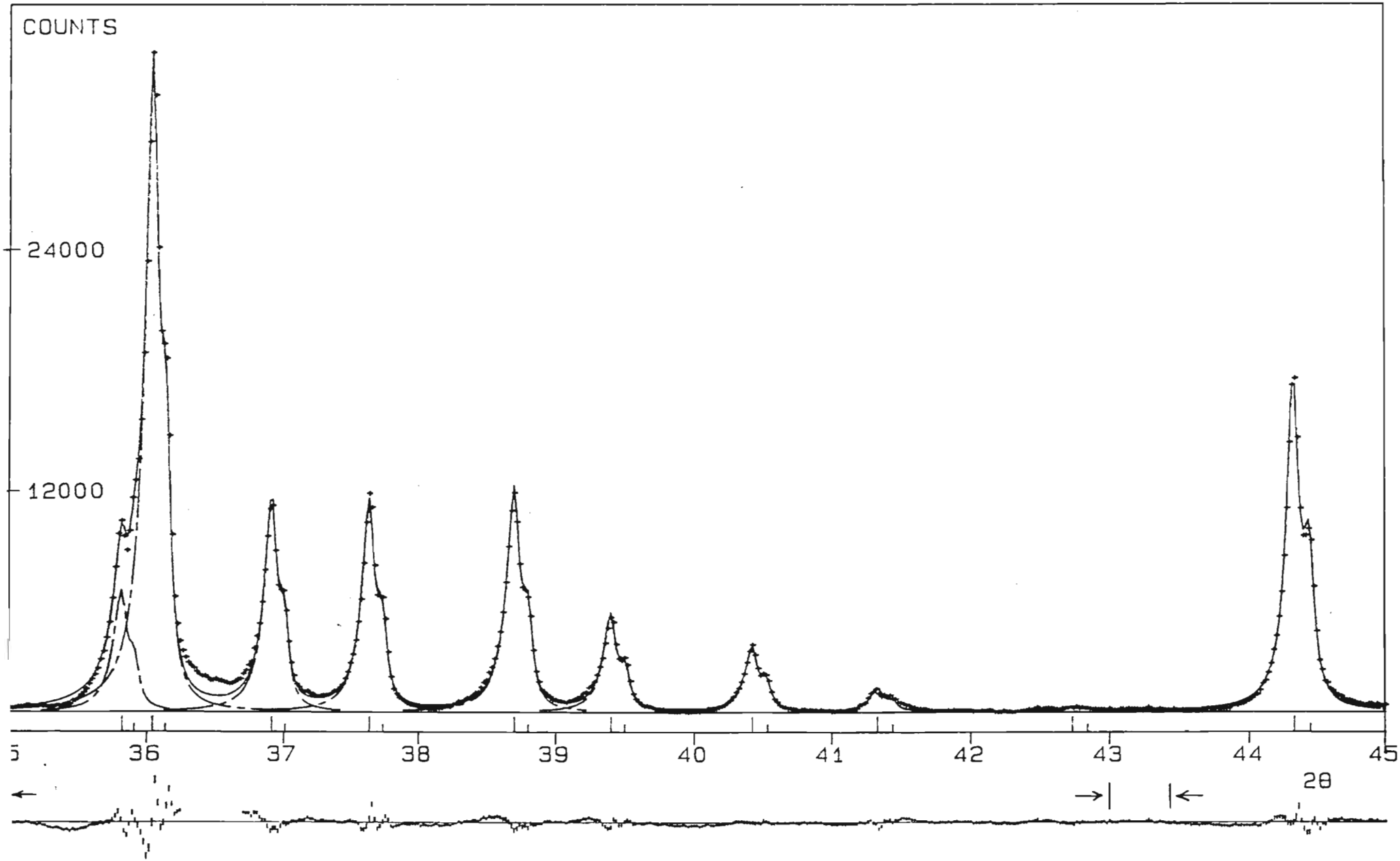
COUNTS
24000
12000
5
36
37
38
39
40
41
42
43
44
45
2θ

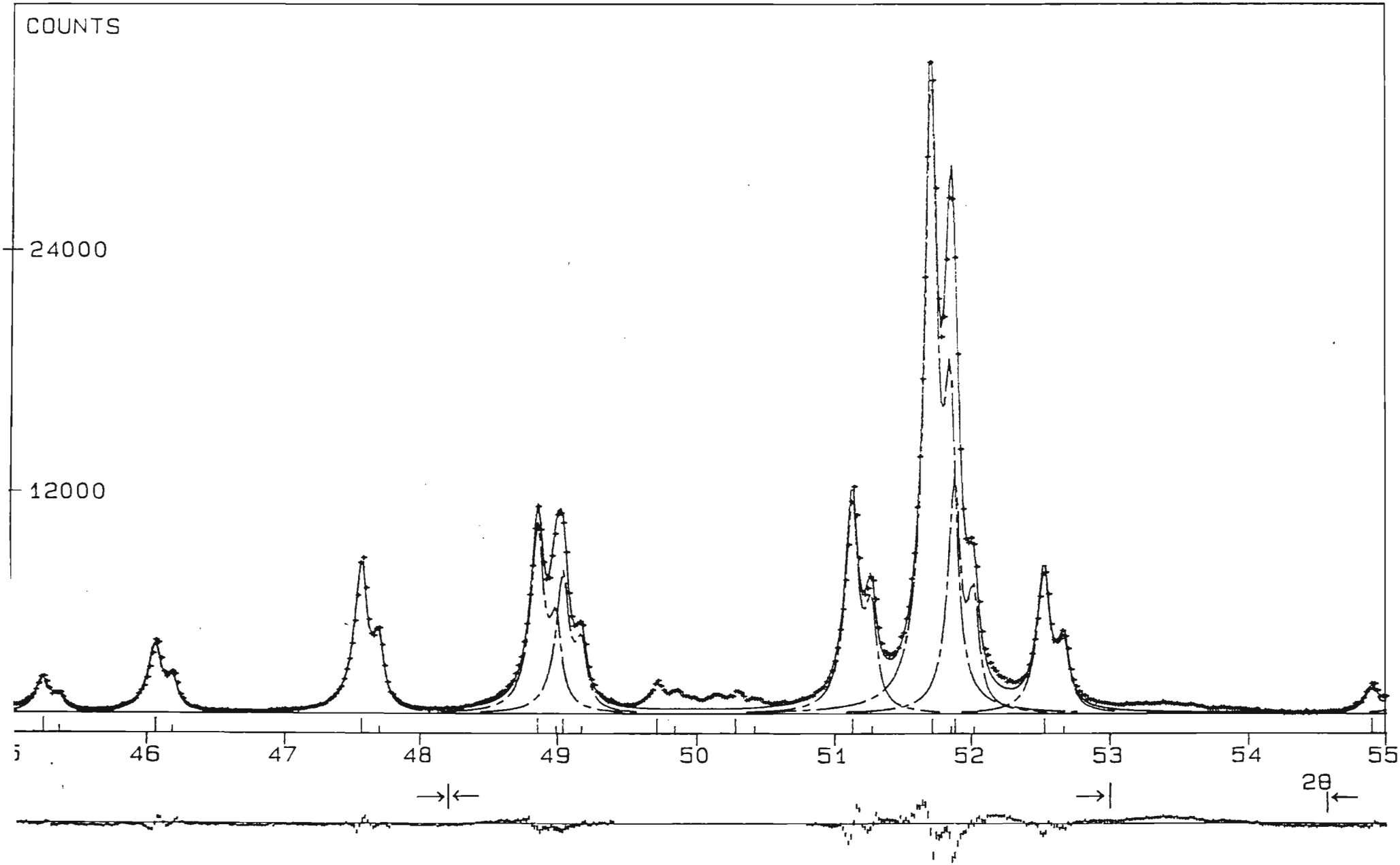
COUNTS
24000
12000
46
47
48
49
50
51
52
53
54
55
2θ

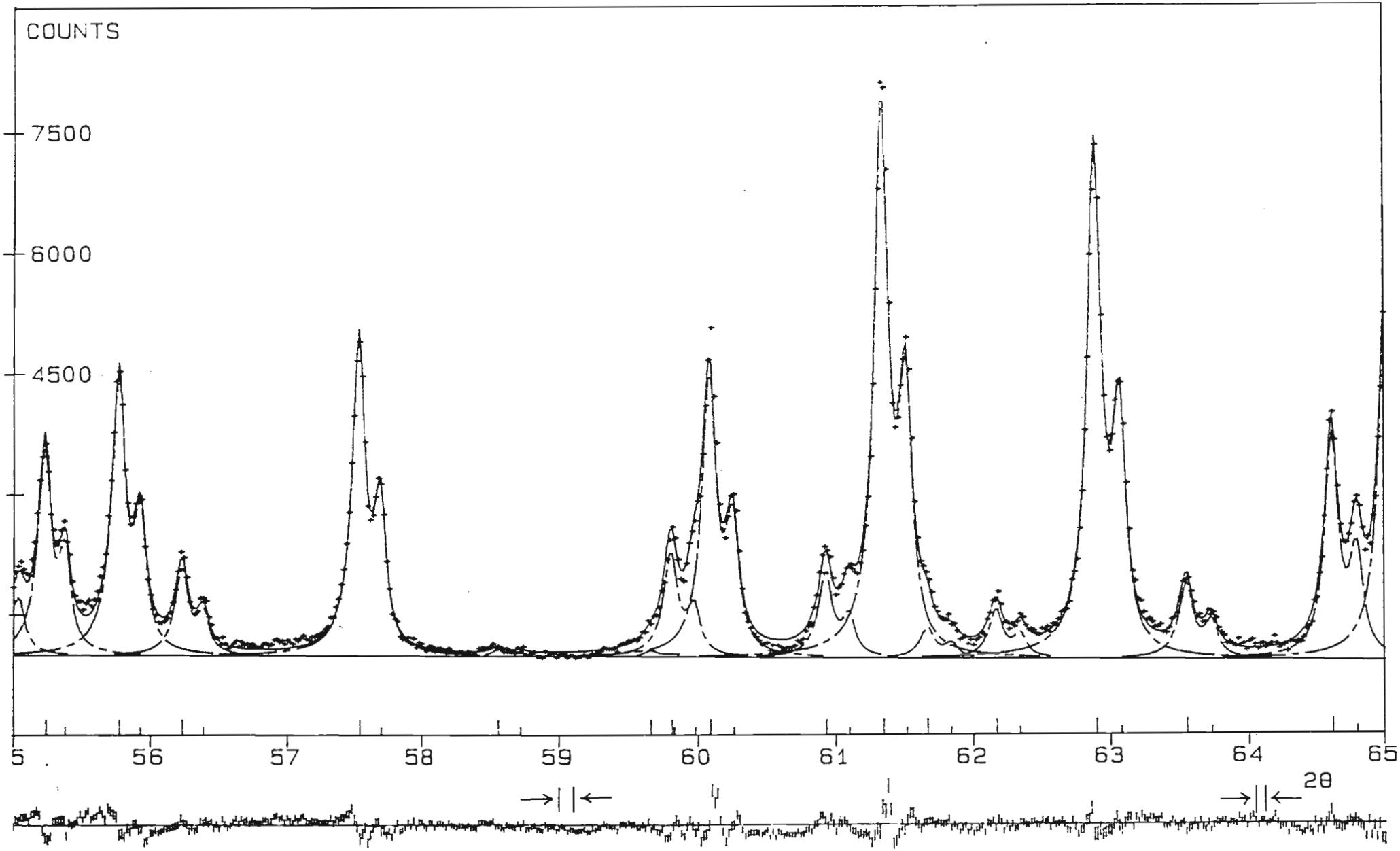
COUNTS
7500
6000
4500
5
56
57
58
59
60
61
62
63
64
65
2θ

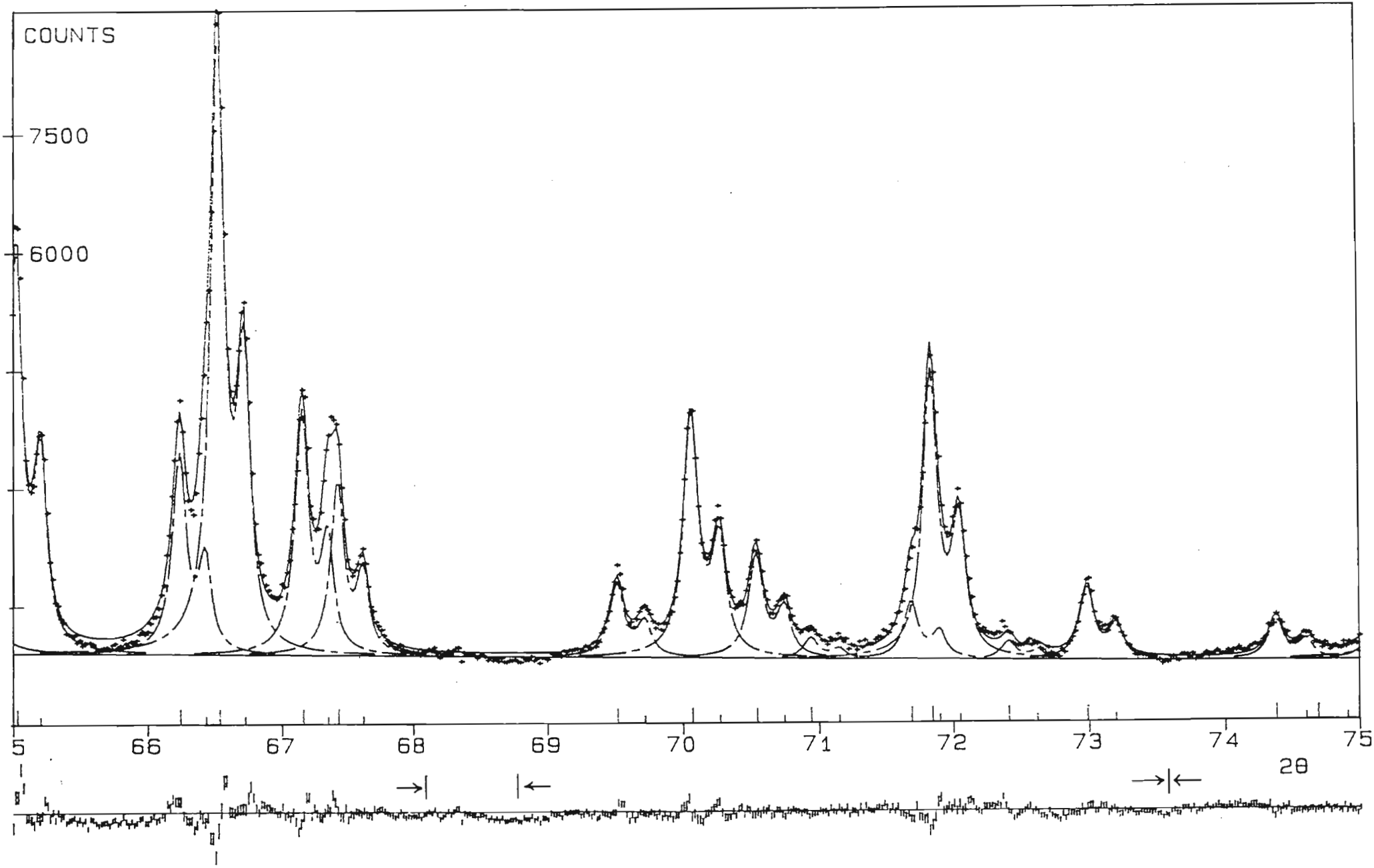
COUNTS
7500
6000
65
66
67
68
69
70
71
72
73
74
75
2θ

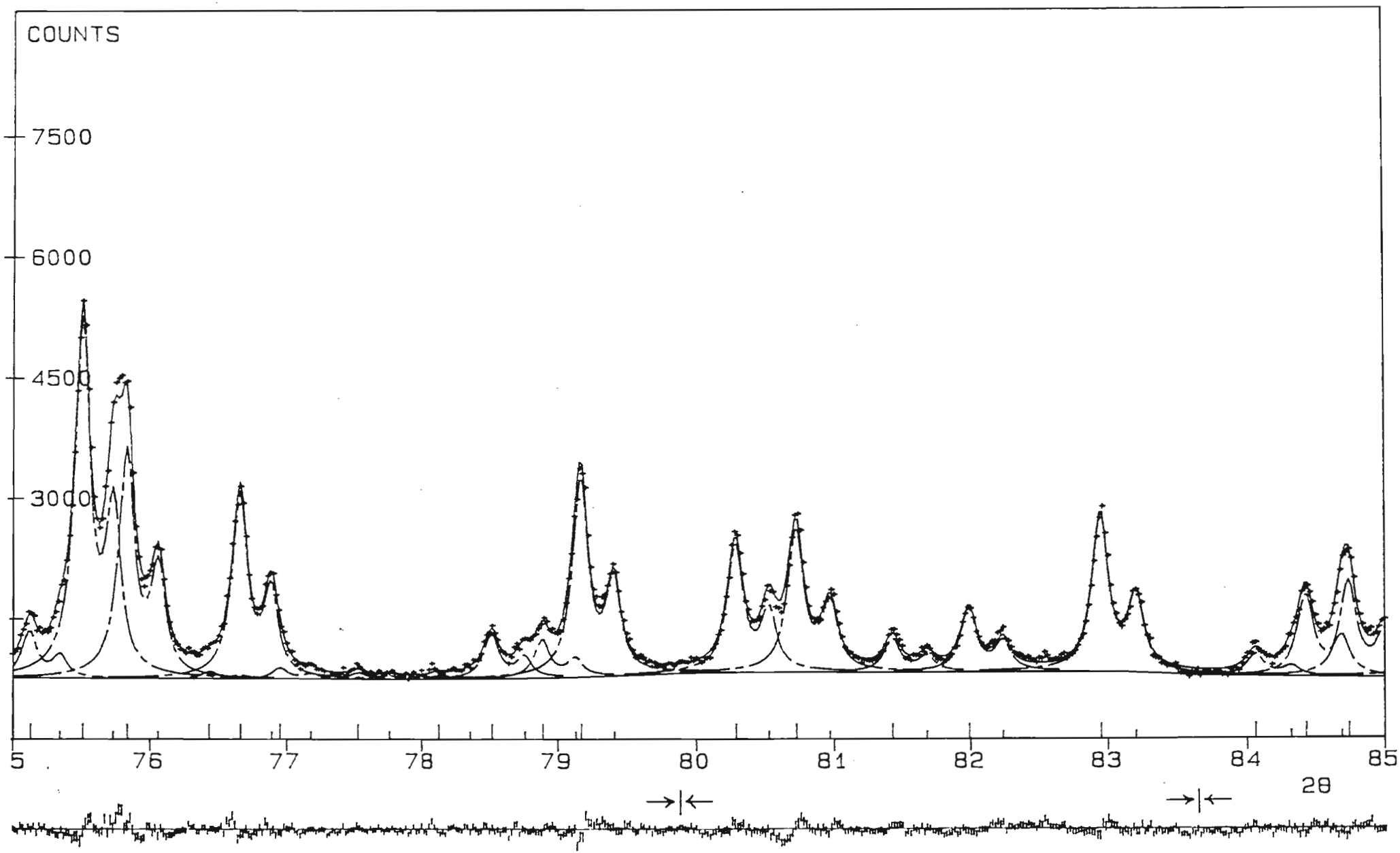
COUNTS
7500
6000
4500
3000
5
76
77
78
79
80
81
82
83
84
85
2θ

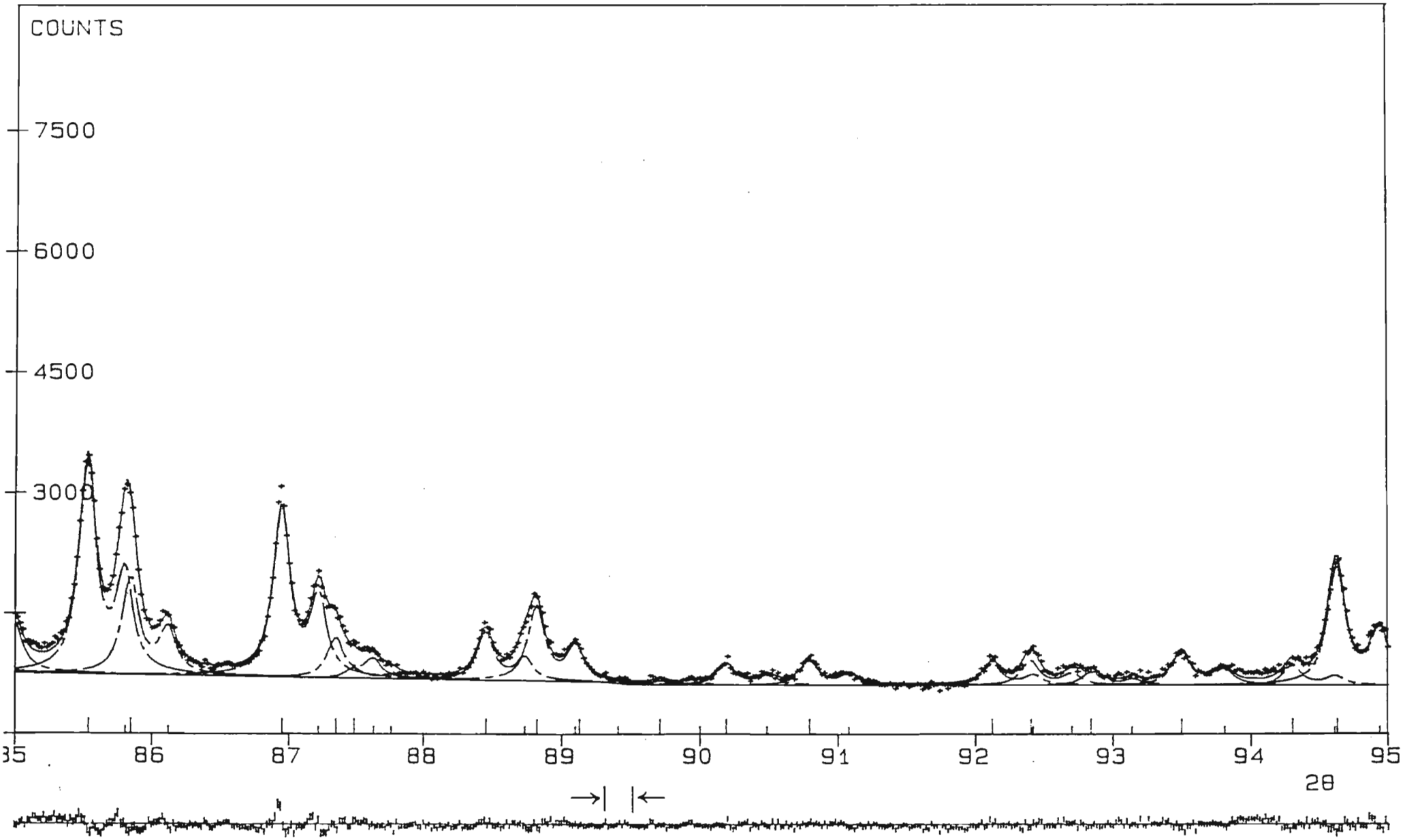
COUNTS
7500
6000
4500
3000
85
86
87
88
89
90
91
92
93
94
95
2θ

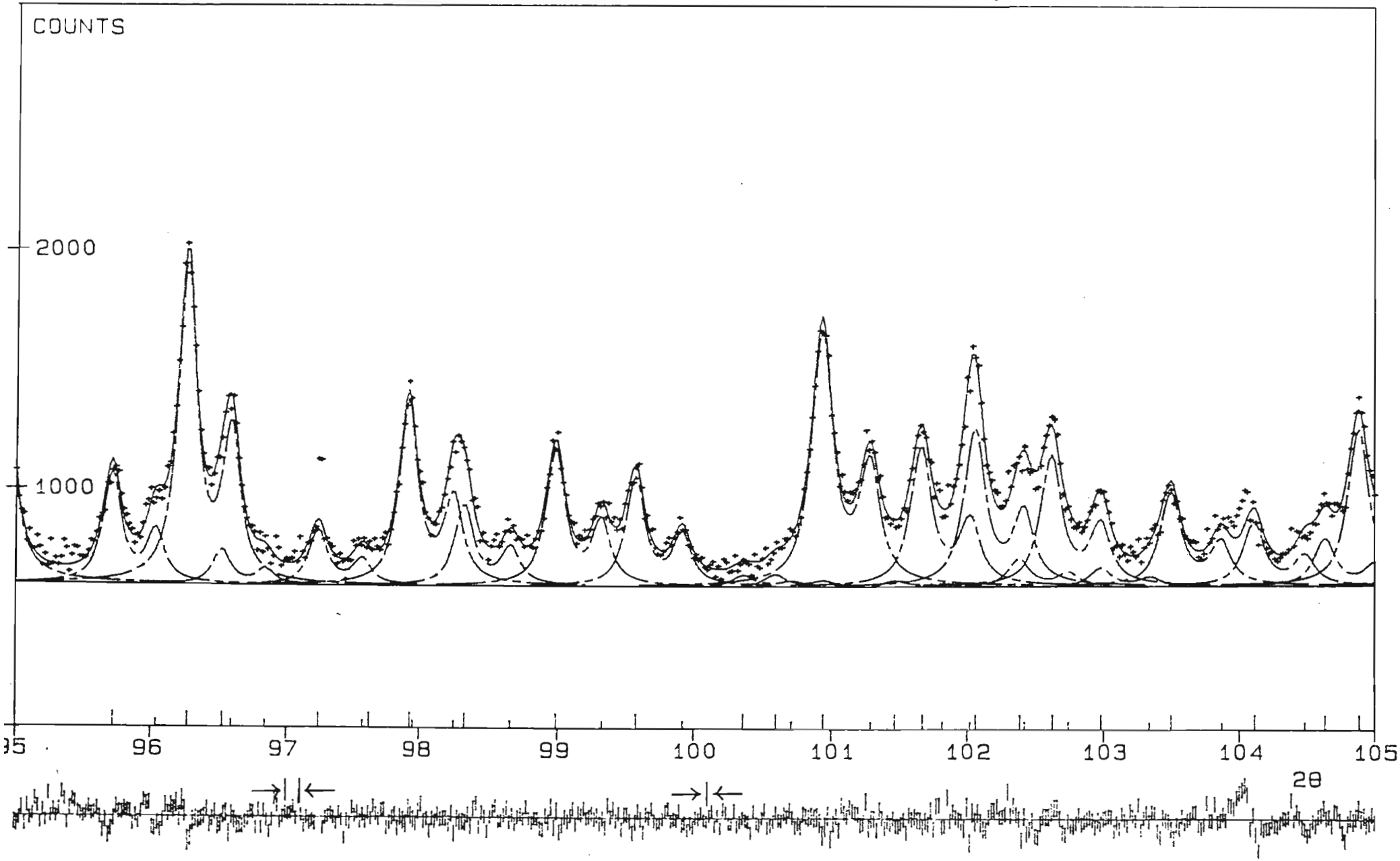
COUNTS
2000
1000
95
96
97
98
99
100
101
102
103
104
105
2θ

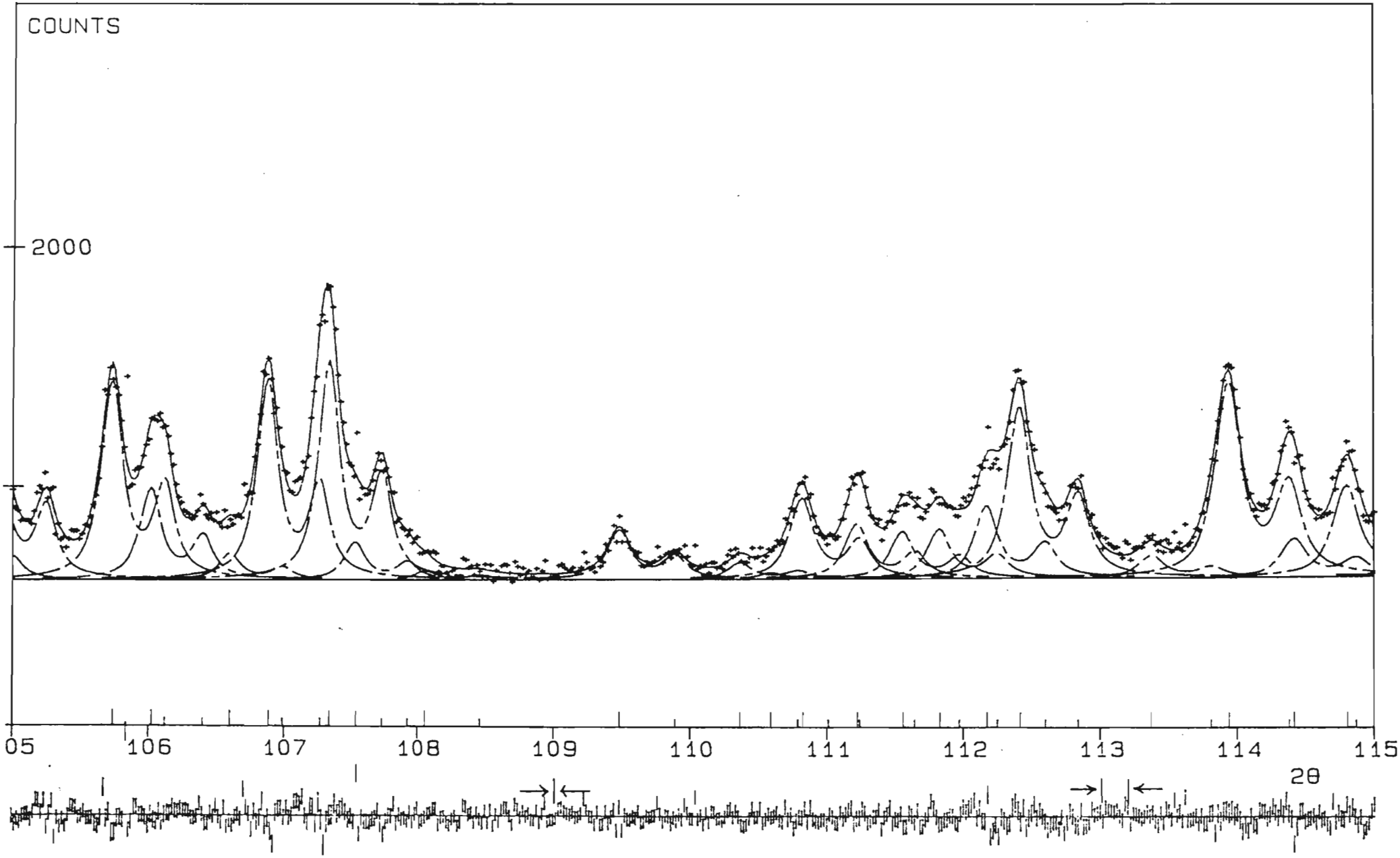
COUNTS
2000
05
106
107
108
109
110
111
112
113
114
115
2θ

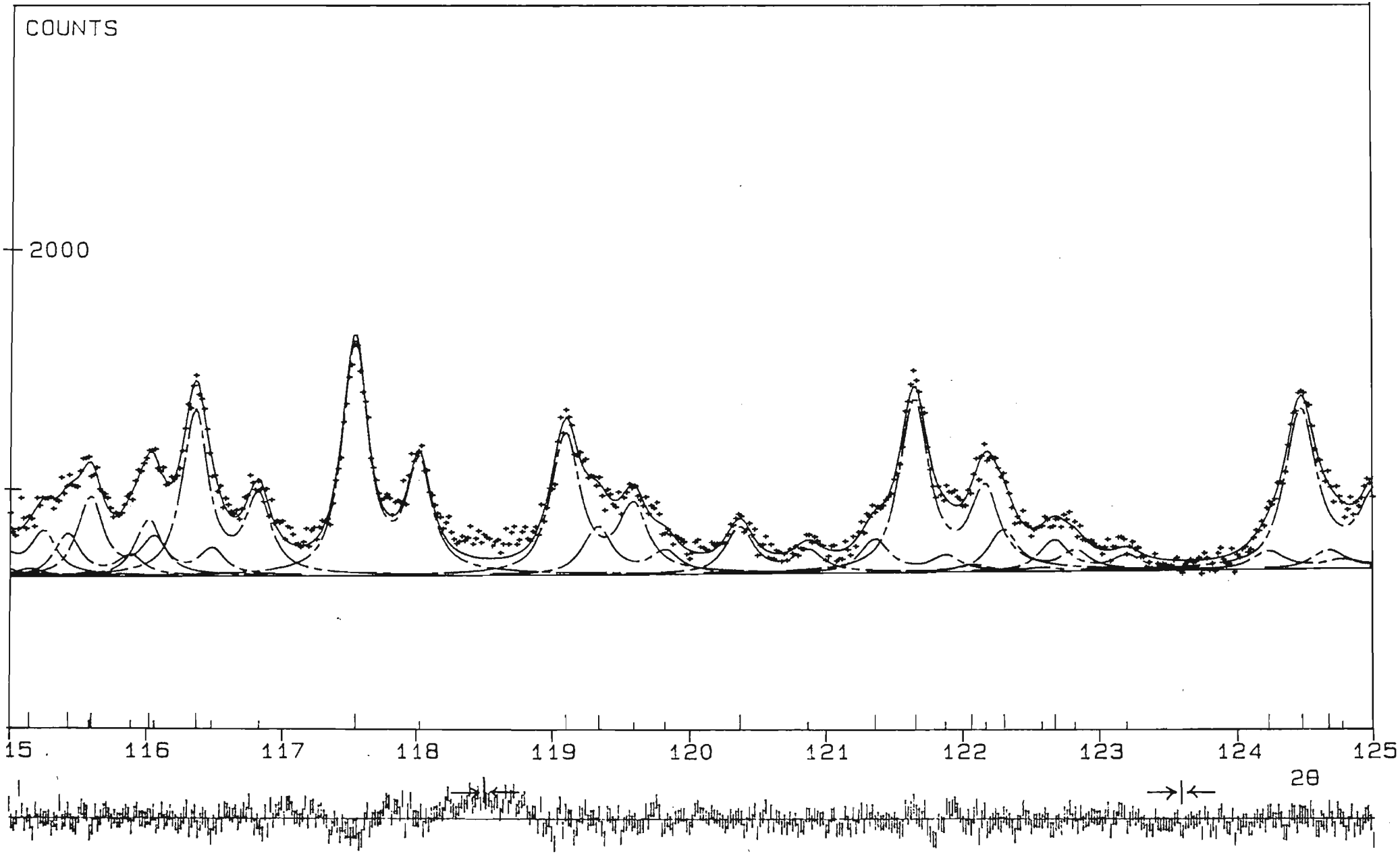
COUNTS
2000
15
116
117
118
119
120
121
122
123
124
125
2θ

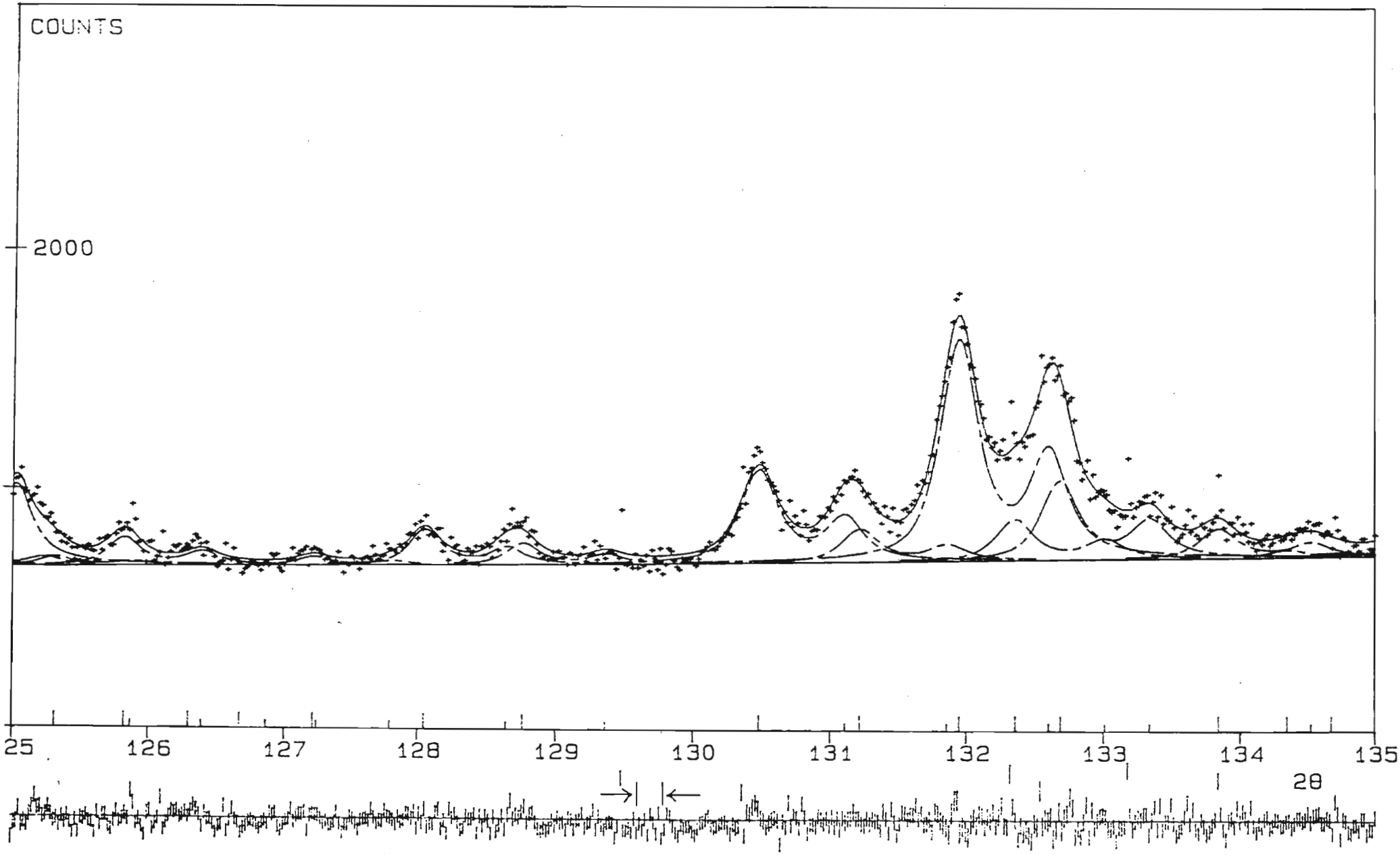
COUNTS
2000
25
126
127
128
129
130
131
132
133
134
135
2θ

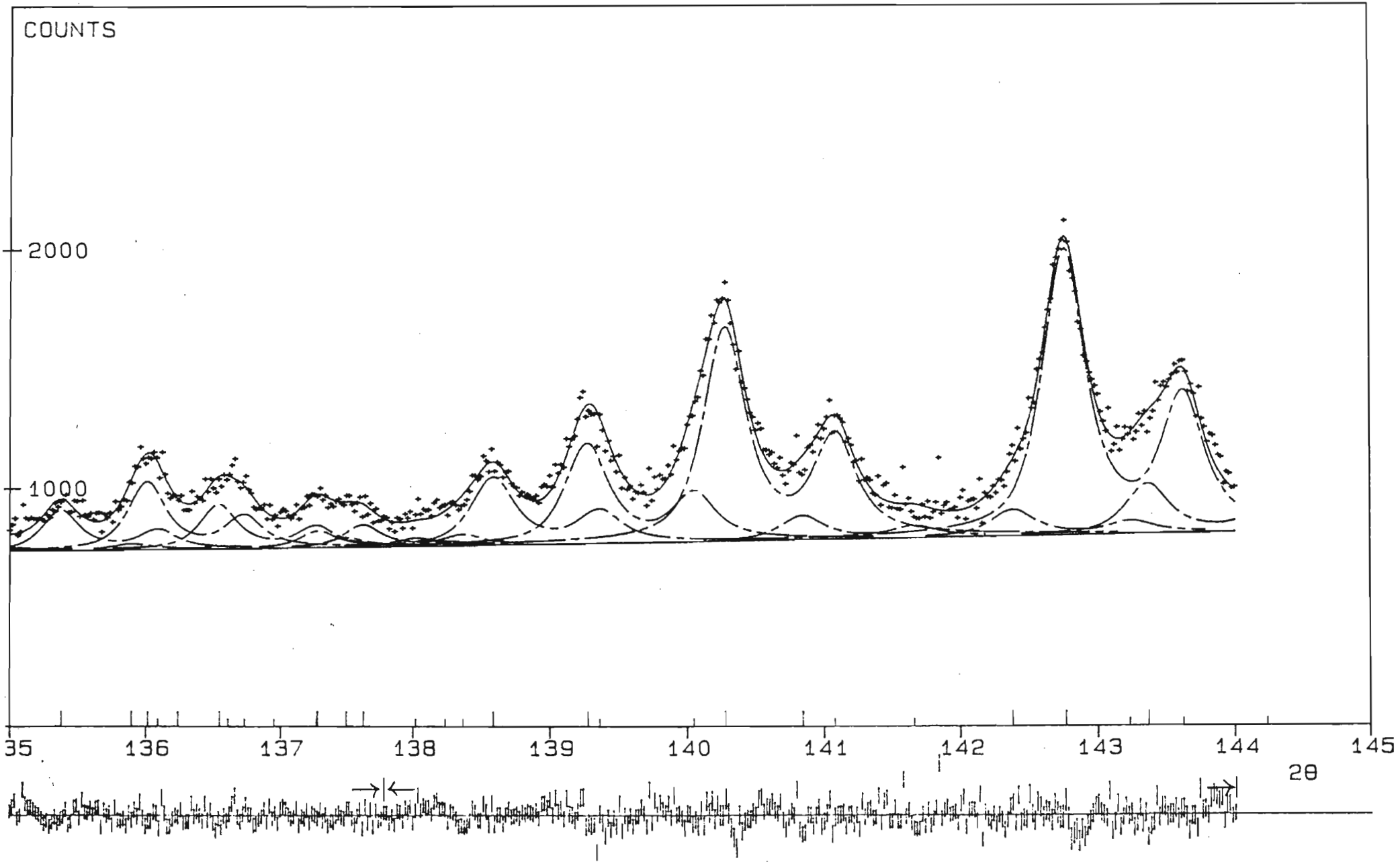
COUNTS
2000
1000
35
136
137
138
139
140
141
142
143
144
145
2θ

APPENDIX 2

Observed and calculated integrated intensities Io and Ic of Fe-akermanite. The columns are peak ref no., reflection ref no., Miller index, 2θ, structure factor, observed and calculated intensities (sum if reflections overlap), Io - Ic, (Io - Ic)/σ(Io), (Io - Ic)/Io

PEAK	PLANE	H	K	L	2THETA	F	SUM(OBS)	SUM(CALC)	DELTA	DEL/SIG	DELTA%
1	1	1	1	0	15.90	8.85	360.00	373.59	-13.59	-1.70	-3.77
2	2	0	0	1	17.67	25.06	2291.00	2281.50	9.50	.95	.41
3	3	1	0	1	20.98	17.09	2021.00	2047.31	-26.31	-2.63	-1.30
4	4	2	0	0	22.56	6.08	137.00	86.08	50.92	10.18	37.17
5	5	1	1	1	23.86	32.75	5821.00	5980.42	-159.42	-5.31	-2.74
6	6	2	1	0	25.27	17.67	1137.00	1147.94	-10.94	-1.09	-.96
7	7	2	0	1	28.80	61.85	11614.00	11982.87	-368.87	-7.38	-3.18
8	8	2	1	1	31.00	71.52	27863.00	27270.61	592.39	5.92	2.13
9	9	2	2	0	32.12	40.91	1381.00	1856.72	-475.72	-15.86	-34.45
10	10	0	0	2	35.78	41.61	1327.10	1439.55	-112.45	-3.27	-8.47
11	11	3	1	0	36.04	58.06	7010.20	5845.73	1164.47	22.22	16.61
12	12	2	2	1	36.90	31.33	2331.10	1987.88	343.22	11.84	14.72
13	13	1	0	2	37.62	31.67	2307.10	2391.57	-84.47	-2.98	-3.66
14	14	3	0	1	38.68	38.71	2465.30	2367.14	98.16	3.41	3.98
15	15	1	1	2	39.38	17.96	1078.50	800.09	278.41	13.26	25.81
16	16	3	1	1	40.41	14.37	735.00	698.32	36.68	1.99	4.99
17	17	3	2	0	41.30	9.83	272.90	124.82	148.08	10.58	54.26
18	18	2	0	2	42.72	5.24	56.30	42.64	13.66	1.92	24.26
19	19	2	1	2	44.31	38.25	3860.80	4078.43	-217.63	-9.46	-5.64
20	20	3	2	1	45.25	15.35	389.80	505.56	-115.76	-11.13	-29.70
21	21	4	0	0	46.06	39.19	819.00	780.29	38.71	3.02	4.73
22	22	4	1	0	47.57	47.03	1785.00	2094.61	-309.61	-18.32	-17.35
23	23	2	2	2	48.84	45.03	2253.30	2115.89	137.41	3.61	6.10
24	24	3	3	0	49.04	67.33	1697.40	2007.70	-310.30	-8.57	-18.28
25	25	4	0	1	49.71	16.35	269.40	238.16	31.24	3.19	11.60
26	26	3	0	2	50.28	9.41	138.20	87.86	50.34	2.26	36.43
27	27	4	1	1	51.13	38.40	2589.90	2645.58	-55.68	-1.89	-2.15
28	28	3	1	2	51.69	62.77	7648.80	7492.76	156.04	2.42	2.04
29	29	4	2	0	51.88	51.94	2825.00	2111.32	713.68	13.07	25.26
30	30	3	3	1	52.53	44.88	1754.80	1439.50	315.30	13.03	17.97
31	31	0	0	3	54.88	30.49	327.30	303.83	23.47	3.35	7.17
32	32	4	2	1	55.24	21.43	656.90	611.00	45.90	5.60	6.99
33	33	3	2	2	55.77	23.88	884.10	862.38	21.72	2.53	2.46
34	34	1	0	3	56.21	16.13	272.90	275.68	-2.78	-.43	-1.02
35	35	1	1	3	57.52	28.94	1001.20	886.80	114.40	13.00	11.43
36	36	4	3	0	58.56	2.17	19.60	2.84	16.76	2.84	85.50
37	37	4	0	2	59.66	4.03	23.30	10.53	12.77	1.37	54.80
38	38	5	1	0	59.83	18.53	349.20	197.17	152.03	15.05	43.54
39	39	2	0	3	60.08	33.85	936.60	927.68	8.92	.73	.95
40	40	4	1	2	60.93	14.75	288.10	297.94	-9.84	-1.11	-3.41
41	41	2	1	3	61.34	34.61	1841.60	1780.05	61.55	4.10	3.34
42	42	5	0	1	61.68	15.68					
42	43	4	3	1	61.68	1.36	103.80	138.18	-34.38	-3.86	-33.12
43	44	3	3	2	62.17	18.73	165.30	209.79	-44.49	-5.85	-26.91
44	45	5	1	1	62.91	33.90	1700.20	1288.42	411.78	30.73	24.22
45	46	5	2	0	63.57	18.92	256.60	180.93	75.67	9.58	29.49
46	47	4	2	2	64.62	20.43	756.80	470.29	286.51	23.88	37.86
47	48	2	2	3	65.03	49.07	1378.90	1429.72	-50.82	-3.55	-3.69
48	49	3	0	3	66.23	33.33	688.00	669.06	18.94	1.36	2.75

49	50	5	2	1	66.55	46.88	2126.00	2095.90	30.10	1.65	1.42
50	51	4	4	0	67.19	60.42	837.60	824.07	13.53	.93	1.61
51	52	3	1	3	67.42	20.11	598.50	474.26	124.24	9.20	20.76
52	53	5	3	0	69.55	29.67	269.90	371.41	-101.51	-15.38	-37.61
53	54	4	4	1	70.09	40.25	889.30	643.50	245.80	27.31	27.64
54	55	5	0	2	70.56	8.47					
54	56	4	3	2	70.56	19.38	381.30	368.20	13.10	1.79	3.44
55	57	3	2	3	70.94	11.23	78.50	123.36	-44.86	-7.73	-57.14
56	58	5	1	2	71.72	12.16	211.90	103.42	108.48	9.95	51.19
57	59	6	0	0	71.87	66.07	1042.20	865.64	176.56	13.69	16.94
58	60	5	3	1	72.41	11.70	69.00	104.08	-35.08	-6.38	-50.84
59	61	6	1	0	73.02	29.20	268.50	328.57	-60.07	-9.53	-22.37
60	62	4	0	3	74.39	15.15	155.50	103.84	51.66	10.33	33.22
61	63	6	0	1	74.69	3.22	9.80	3.91	5.89	1.23	60.07
62	64	5	2	2	75.15	18.84	174.60	266.01	-91.41	-16.32	-52.36
63	65	4	1	3	75.52	41.46	1317.20	1426.14	-108.94	-10.89	-8.27
64	66	0	0	4	75.82	66.30					
64	67	6	1	1	75.83	15.24	845.50	919.52	-74.02	-8.41	-8.75
65	68	6	2	0	76.43	10.39	27.60	38.42	-10.82	-1.83	-39.22
66	69	3	3	3	76.65	42.32	683.50	821.27	-137.77	-16.60	-20.16
67	70	1	0	4	76.95	8.78	42.20	45.45	-3.25	-.56	-7.71
68	71	5	4	0	77.56	9.15	25.40	29.09	-3.69	-.92	-14.54
69	72	1	1	4	78.07	7.76	15.60	37.23	-21.63	-5.28	-138.67
70	73	4	4	2	78.53	27.09	165.10	244.77	-79.67	-15.32	-48.26
71	74	4	2	3	78.90	12.63	143.50	169.14	-25.64	-3.95	-17.87
72	75	6	2	1	79.20	32.98	734.70	768.24	-33.54	-4.41	-4.57
73	76	2	0	4	80.30	4.96					
73	77	5	4	1	80.31	29.07	495.60	557.99	-62.39	-9.31	-12.59
74	78	5	3	2	80.75	29.04	550.20	536.95	13.25	1.92	2.41
75	79	2	1	4	81.41	10.82	128.70	108.20	20.50	4.02	15.93
76	80	6	3	0	82.01	19.74	244.00	124.75	119.25	21.68	48.87
77	81	6	0	2	82.97	45.28	609.70	686.38	-76.68	-11.62	-12.58
78	82	6	1	2	84.07	13.60	89.90	132.52	-42.62	-7.75	-47.40
79	83	5	0	3	84.44	2.24					
79	84	4	3	3	84.44	21.62	330.30	328.95	1.35	.17	.41
80	85	2	2	4	84.73	31.62					
80	86	6	3	1	84.74	10.74	387.70	434.68	-46.98	-6.35	-12.12
81	87	5	1	3	85.54	36.02	855.30	817.60	37.70	4.14	4.41
82	88	3	0	4	85.83	31.79	395.50	424.13	-28.63	-3.49	-7.24
83	89	3	1	4	86.93	28.97	686.80	694.23	-7.43	-.99	-1.08
84	90	6	2	2	87.37	17.60	164.80	215.44	-50.64	-5.82	-30.73
85	91	7	1	0	87.52	18.34					
85	92	5	5	0	87.52	15.71	44.10	136.46	-92.36	-11.54	-209.42
86	93	5	4	2	88.47	19.76	198.60	261.93	-63.33	-10.73	-31.89
87	94	5	2	3	88.83	22.90	305.80	350.14	-44.34	-5.83	-14.50
###	95	7	0	1	89.13	.57	######	######	######	######	######
88	96	6	4	0	89.71	8.77	19.80	22.31	-2.51	-.57	-12.68
89	97	3	2	4	90.22	1.77					
89	98	7	1	1	90.22	2.47					
89	99	5	5	1	90.22	16.61	89.00	85.44	3.56	.74	4.00
90	100	7	2	0	90.81	18.34	106.90	96.72	10.18	2.12	9.52
91	101	4	4	3	92.12	12.87	94.70	62.94	31.76	5.48	33.53
92	102	6	4	1	92.42	14.88	107.40	144.93	-37.53	-5.86	-34.95
93	103	6	3	2	92.86	8.15	58.50	36.52	21.98	4.40	37.57
94	104	4	0	4	93.51	8.52	148.70	26.60	122.10	24.92	82.11
###	105	7	2	1	93.52	21.12	######	######	######	######	######
95	106	5	3	3	94.32	10.43	87.50	62.29	25.21	4.35	28.81
96	107	4	1	4	94.61	26.01	514.50	529.47	-14.97	-2.05	-2.91
97	108	3	3	4	95.71	20.24	163.30	144.48	18.82	3.55	11.53
98	109	7	3	0	96.30	41.87	471.50	489.67	-18.17	-2.30	-3.85

99	110	6	0	3	96.52	9.03	51.60	25.50	26.10	4.02	50.59
100	111	7	0	2	97.26	13.81	85.00	55.67	29.33	7.33	34.50
***	112	6	1	3	97.62	1.64	******	******	******	******	******
101	113	4	2	4	97.92	17.66	283.40	238.90	44.50	9.08	15.70
102	114	7	1	2	98.37	10.33					
102	115	5	5	2	98.37	13.89	124.10	119.39	4.71	1.02	3.79
103	116	7	3	1	99.03	17.20	209.90	180.01	29.89	7.29	14.24
104	117	6	5	0	99.62	18.89	167.00	99.21	67.79	16.95	40.59
105	118	0	0	5	100.36	2.36	19.10	.73	18.37	3.22	96.16
106	119	6	4	2	100.59	3.23	20.50	3.67	16.83	2.47	82.09
107	120	6	2	3	100.96	18.31	428.40	269.08	159.32	21.53	37.19
108	121	1	0	5	101.47	3.37	10.20	5.43	4.77	.66	46.79
109	122	7	2	2	101.71	23.98	234.60	346.34	-111.74	-12.99	-47.63
110	123	5	4	3	102.08	18.47	264.90	201.99	62.91	6.99	23.75
111	124	6	5	1	102.38	10.45	47.20	59.46	-12.26	-1.44	-25.97
112	125	1	1	5	102.59	21.32	219.80	226.82	-7.02	-.82	-3.19
113	126	8	0	0	102.98	6.51	31.10	5.93	25.17	3.65	80.93
114	127	5	0	4	103.50	2.47					
114	128	4	3	4	103.50	13.32	157.30	127.83	29.47	5.26	18.74
115	129	8	1	0	104.11	7.36					
115	130	7	4	0	104.11	22.80	107.40	161.17	-53.77	-9.78	-50.07
116	131	5	1	4	104.63	14.28	80.30	120.66	-40.36	-6.02	-50.26
117	132	2	0	5	104.85	23.74	260.30	249.03	11.27	1.63	4.33
118	133	8	0	1	105.77	35.36	337.40	357.56	-20.16	-2.72	-5.97
119	134	2	1	5	105.99	14.21	154.30	190.22	-35.92	-5.06	-23.28
120	135	6	3	3	106.60	2.56	44.60	3.49	41.11	6.32	92.18
121	136	7	4	1	106.91	16.47					
121	137	8	1	1	106.91	19.64	337.10	390.16	-53.06	-6.39	-15.74
122	138	7	3	2	107.37	19.58	368.30	236.09	132.21	14.37	35.90
123	139	8	2	0	107.53	17.49	63.00	87.53	-24.53	-3.19	-38.94
124	140	5	2	4	108.06	5.09	14.60	25.78	-11.18	-2.24	-76.60
125	141	2	2	5	109.44	11.90	91.30	49.25	42.05	10.78	46.06
126	142	8	2	1	110.39	5.06	30.70	10.42	20.28	4.22	66.06
127	143	3	0	5	110.61	3.19	11.30	4.34	6.96	1.31	61.56
128	144	6	5	2	110.85	10.40	149.50	64.61	84.89	13.47	56.78
129	145	7	0	3	111.24	18.62	102.20	112.03	-9.83	-1.56	-9.62
130	146	4	4	4	111.55	19.65	87.10	151.03	-63.93	-10.84	-73.40
131	147	3	1	5	111.78	8.89	91.00	76.87	14.13	2.32	15.53
132	148	6	6	0	112.19	30.13	134.10	135.22	-1.12	-.18	-.84
133	149	7	1	3	112.42	13.72					
133	150	5	5	3	112.42	29.27	316.70	425.00	-108.30	-17.75	-34.20
134	151	8	3	0	113.38	10.09	45.70	30.74	14.96	2.49	32.74
135	152	5	3	4	113.93	23.03	397.60	368.67	28.93	3.33	7.28
136	153	8	0	2	114.42	6.47	78.20	13.26	64.94	7.14	83.04
***	154	7	5	0	114.58	7.06	******	******	******	******	******
137	155	6	4	3	114.82	15.74	185.70	137.91	47.79	5.25	25.74
138	156	6	6	1	115.14	7.70	17.70	17.37	.33	.04	1.87
139	157	3	2	5	115.37	8.46	88.50	64.64	23.86	1.72	26.96
140	158	7	4	2	115.63	16.56					
140	159	8	1	2	115.63	8.07	163.30	242.93	-79.63	-5.31	-48.76
141	160	7	2	3	116.03	11.44	115.80	107.33	8.47	.96	7.32
142	161	6	0	4	116.35	29.60					
142	162	8	3	1	116.36	4.18	339.60	334.24	5.36	.69	1.58
143	163	6	1	4	117.58	8.25					
143	164	7	5	1	117.59	15.42	480.80	208.61	272.19	40.03	56.61
144	165	4	0	5	119.07	20.24	320.50	181.77	138.73	16.32	43.29
145	166	8	2	2	119.33	16.17	109.40	152.96	-43.56	-5.25	-39.81
146	167	4	1	5	120.33	10.57	106.10	83.05	23.05	4.19	21.72
147	168	6	2	4	121.36	8.10	76.90	60.79	16.11	2.21	20.95
148	169	3	3	5	121.61	26.99	395.50	331.46	64.04	7.04	16.19

149	170	8	4	0	122.06	4.56	17.30	7.08	10.22	1.05	59.10
150	171	7	3	3	122.31	10.19	103.60	66.02	37.58	4.58	36.28
151	172	5	4	4	122.65	10.35	74.30	84.44	-10.14	-1.54	-13.65
152	173	4	2	5	124.23	8.53	45.80	75.00	-29.20	-3.32	-63.75
153	174	6	6	2	124.50	31.86	401.60	357.13	44.47	4.24	11.07
154	175	9	1	0	124.68	12.89	46.20	59.22	-13.02	-1.05	-28.19
155	176	8	4	1	125.31	4.92	23.10	22.73	.37	.05	1.59
156	177	8	3	2	125.84	4.20	71.60	15.16	56.44	8.96	78.82
***	178	6	5	3	126.29	8.00	******	******	******	******	******
***	179	9	0	1	126.66	3.08	******	******	******	******	******
157	180	7	5	2	127.21	10.10	21.70	85.79	-64.09	-12.09	-295.33
158	181	6	3	4	128.03	8.21					
158	182	9	1	1	128.04	7.27	90.20	98.08	-7.88	-1.25	-8.73
159	183	9	2	0	128.79	19.65					
159	184	7	6	0	128.79	2.09	54.50	150.67	-96.17	-15.77	-176.46
160	185	8	0	3	130.49	26.75	270.10	307.94	-37.84	-4.67	-14.01
161	186	4	3	5	131.16	4.91					
161	187	5	0	5	131.16	9.46	96.40	73.37	23.03	2.48	23.89
162	188	7	4	3	131.95	21.49					
162	189	8	1	3	131.95	19.27	644.00	679.73	-35.73	-3.11	-5.55
163	190	9	2	1	132.35	8.12					
163	191	7	6	1	132.35	5.55	118.60	83.15	35.45	3.48	29.89
164	192	5	1	5	132.63	15.09	229.20	224.50	4.70	.47	2.05
165	193	7	0	4	133.84	11.84	85.40	69.40	16.00	2.08	18.73
166	194	0	0	6	134.34	13.90	21.10	39.79	-18.69	-2.31	-88.58
167	195	8	5	0	134.67	1.99	11.90	1.75	10.15	1.15	85.33
168	196	5	5	4	135.38	8.50					
168	197	7	1	4	135.38	6.27	118.40	72.55	45.85	5.04	38.72
169	198	1	0	6	135.89	11.93	17.70	112.07	-94.37	-5.62	-533.19
170	199	8	4	2	136.01	5.41	199.50	35.90	163.60	8.35	82.01
171	200	9	3	0	136.23	9.80	2.60	43.89	-41.29	-3.59	-1588.16
172	201	8	2	3	136.54	9.67	129.70	73.86	55.84	5.27	43.05
173	202	5	2	5	137.28	10.35	47.90	124.17	-76.27	-6.05	-159.22
174	203	1	1	6	137.49	7.21	27.90	58.72	-30.82	-1.56	-110.47
175	204	9	0	2	137.62	.50	65.30	.12	65.18	4.00	99.81
176	205	6	4	4	138.59	7.40					
176	206	8	5	1	138.60	16.54	222.90	341.37	-118.47	-11.50	-53.15
177	207	9	1	2	139.27	16.86	330.90	300.50	30.40	2.55	9.19
178	208	7	2	4	140.28	14.60					
178	209	9	3	1	140.29	23.24	700.70	746.38	-45.68	-3.60	-6.52
179	210	2	0	6	140.84	2.40	84.60	4.77	79.83	7.75	94.36
***	211	4	4	5	142.38	8.11	******	******	******	******	******
180	212	2	1	6	142.61	20.29	980.70	690.38	290.32	23.04	29.60
181	213	6	6	3	143.36	12.72	182.90	98.05	84.85	6.73	46.39